NASA Contractor Report CR-154626

RCA SERVICE COMPANY

LDAR Observations of a Developing Thunderstorm Correlated With Field Mill, Ground Strike Location, and Weather Radar Data Including the First Report of the Design and Capabilities of a New, Time-of-Arrival Ground-Strike Location System (GSLS)

Dr. Horst A. Poehler

CONTRACT NAS10-9130

National Aeronautics and Space Administration

John F. Kennedy Space Center

STANDARD TITLE PAGE

1. Report No.	2. Government Accession No.	3. Recipient's Catalog No.

4. Title and Subtitle LDAR OBSERVATIONS OF A DEVELOPING THUNDERSTORM CORRELATED WITH FIELD MILL, GROUND STRIKE LOCATION, AND WEATHER RADAR DATA INCLUDING THE FIRST REPORT OF THE DESIGN AND CAPABILITIES OF A NEW, TIME-OF-ARRIVAL GROUND-STRIKE LOCATION SYSTEM (GSLS)

5. Report Date September 20, 1978

6. Performing Organization Code

7. Author(s) Dr. Horst A. Poehler

Performing Organization Report No. RCA 620-5002

9. Performing Organization Name and Address

RCA Service Company
RCA 620
KSC, Florida, 32899

10. Work Unit No.

11. Contract or Grant No. NAS10-9130

12. Sponsoring Agency Name and Address

National Aeronautics and Space Administration
Kennedy Space Center, Florida, 32899

13. Type of Report and Period Covered Contractor Report

14. Sponsoring Agency Code

15. Abstract

An experiment designed to observe and measure a thunderstorm prior to, during, and after its development over the Kennedy Space Center was successful. Correlated measurements of airborne field strength, ground-based field strength, LDAR lightning discharge location in the clouds, weather radar percipitation echoes, plus ground strike location with the new KSC Ground Strike Location System (GSLS) were gathered, and reported. This test marks the first operational use of the GSLS System, and this report contains the first report of its design and capabilities.

16. Key Words

Lightning, Atmospheric Electricity, Thunderstorms, Measurement, Precipitation, Radar

17. Bibliographic Control	18. Distribution
May be announced in Star	Publicly available

19. Security Classif.(of this report)	20. Security Classif.(of this page)	21. No. of Pages	22. Price
Unclassified	Unclassified	135	

KSC FORM 16-27BNS (REV. 7/78)

LDAR OBSERVATIONS OF A DEVELOPING THUNDERSTORM CORRELATED WITH FIELD MILL, GROUND STRIKE LOCATION, AND WEATHER RADAR DATA, INCLUDING THE FIRST REPORT OF THE DESIGN AND CAPABILITIES OF A NEW TIME-OF-ARRIVAL GROUND-STRIKE LOCATION SYSTEM (GSLS)

RCA 620-5002

Prepared for

NATIONAL AERONAUTICS AND SPACE ADMINISTRATION

JOHN F. KENNEDY SPACE CENTER

By

RCA SERVICE COMPANY

ORIGINATOR:

Horst A. Poehler

Dr. Horst A. Poehler
Staff Scientist

APPROVED:

J. W. Taylor

J. W. Taylor, Manager
RCA 620

CONCURRENCE:

Carl L. Lennon

Carl L. Lennon, Chief
TI-INS-32

September 20, 1978

SUMMARY

An experiment designed to observe and measure a thunderstorm prior to, during, and after its development over the Kennedy Space Center was successful. Correlated measurements of airborne field strength, ground-based field strength, LDAR lightning discharge location in the clouds, weather radar precipitation echoes, plus ground strike location with the new KSC Ground Strike Location System (GSLS) were gathered, and reported. This test marks the first operational use of the GSLS System, and this report contains the first report of its design and capabilities.

OUTLINE

LIST OF ILLUSTRATIONS

LIST OF ILLUSTRATIONS (CONTINUED)

LIST OF ILLUSTRATIONS (CONTINUED)

LIST OF ILLUSTRATIONS (CONTINUED)

LIST OF ILLUSTRATIONS (CONTINUED)

APPENDIX

LIST OF TABLES

APPENDIX

ACKNOWLEDGEMENT

The author wishes to acknowledge the contributions of several co-workers and people associated with other organizations whose contributions helped to make this report possible.

James Nicholson of NOAA for his meteorological expertise in selecting the cloud to be tracked, and his meteorological guidance of the pilot during the flight.

John Pruett, Aircraft Commander, NASA Research and Development, Kennedy Space Center, for his skilled piloting of NASA-6 through and around the thundercloud under study.

Ernest Eulitz, Senior System Engineer, TI-INS-11, NASA, Kennedy Space Center, for his reduction of the flash field-mill contours.

Marvin Tucker, NASA COOP Student, Kennedy Space Center, for reducing the ground strike data.

Carl Lennon, Chief Electromagnetic Analysis Section, NASA, Kennedy Space Center for helpful discussions and comments, and for his pioneering work in the development of the LDAR and the GSLS systems.

I. INTRODUCTION

Combined LDAR/airborne field mill data[1] was available for only one, already-developed, thunderstorm, that was located outside the primary coverage area of LDAR, and outside the ground-based, KSC field mill system.

When the NASA-6 airplane became available to us for several test flights, it was decided to attempt to obtain data during the complete cycle of a developing thunderstorm, hopefully starting at a time prior to any thunderstorm activity, and preferable over the Kennedy Space Center, that is, within the prime coverage area of the LDAR System and over the KSC ground-based field mill network. The desired data was obtained on our first try, September 6, 1977.

In addition, the test marks the first operational use of the new time-of-arrival Ground Strike Location System (GSLS), providing data correlating the positions of electrical discharges in the cloud with the positions of associated ground strikes.

The detailed report of this test, including correlated weather-radar data, will be presented in this report.

II. DESCRIPTION OF THE EXPERIMENT

Five separate data systems were used to collect thunderstorm data, the Airborne Field Mill System, the Ground-Based Field Mill System, the Lightning Detection and Ranging System (LDAR), the new Ground Strike Location (GSLS), and the KSC Weather Radar. For reference, the salient features of these systems are given in the Appendix.

The plan of operation called for the NASA-6 to take off from Patrick Air Force Base at 1700 GMT, and fly to KSC to study isolated clouds - preferably

clouds producing noticeable perturbations of the KSC ground-based field mills. The clouds to be studied were to be specified by James Nicholson, Assistant Staff Meteorologist, KSC Weather Office, on the basis of meteorological and field mill data. Once a cloud was selected, the airplane was to fly a rectangular pattern around and through the cloud, as shown in Figure 1. The plans called for the flight to continue until the cloud subsides, or a new cloud develops for study, or until the thunderstorm develops to such an intensity that the pattern of Figure 1 becomes dangerous. Flights through the cloud were scheduled to be terminated on observing abrupt changes in airborne field mills.

In addition to the airborne field mills and the S-band radar transponder, NASA-6 was equipped to carry a lightning simulator so that we could conveniently locate the plane relative to the cloud electrical discharges, since both would be registered by the LDAR System. Differentiating between the lightning simulator discharges and cloud discharges should not be a problem, since the altitude of the lightning simulator would correspond to the plane's altitude, and since lightning simulator discharges occur at a regular rate, approximately one per 0.7 seconds. The design and characteristics of the lightning simulator mounted on NASA-6 have already been described in the LDAR calibration report[2].

The three components* of the airborne ambient electric field F_X, F_Y, and F_Z that were measured by the airborne field mills were recorded on the plane, and also telemetered to the ground station.

---

* See Appendix A for definition.

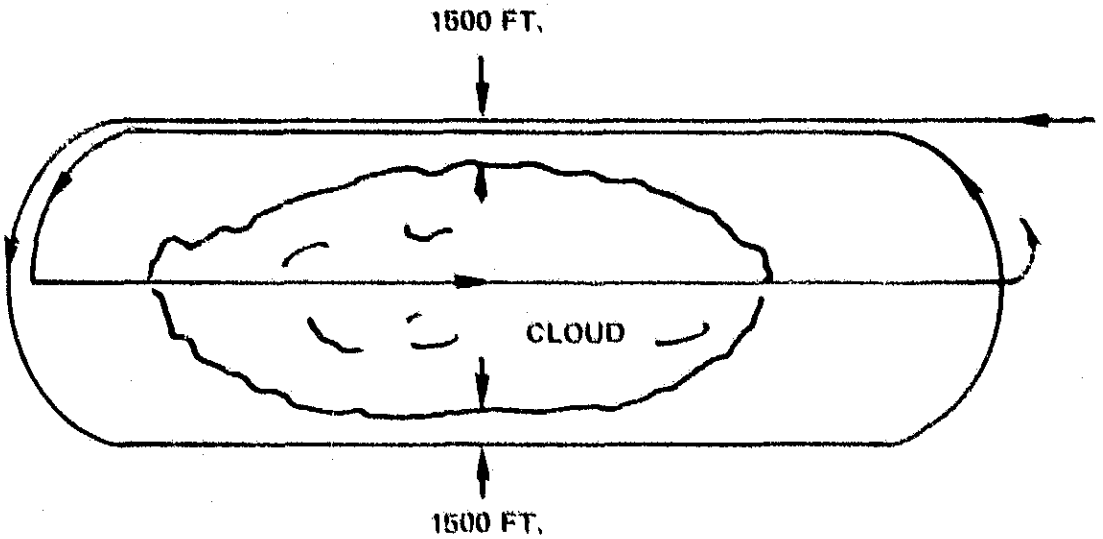

VIEWED FROM ABOVE

FIRST PASS AROUND THE CLOUD. SECOND PASS THROUGH THE CLOUD. PATTERN TO BE REPEATED UNTIL CALLED OFF. ALTITUDE - 10,500 FT.

FIGURE 1. FLIGHT PLAN

III. DISCUSSION OF THE TEST RESULTS

III A. OVERVIEW

The NASA-6 airplane left Patrick Air Force Base at 1712 GMT and flew to KSC. There Jim Nicholson selected a cloud that registered a 15,000 foot radar top, and that appeared to hold promise of further development.

The airplane made twenty-six runs that afternoon operating until 1956 GMT, when the storm started to subside.

We will discuss the general outline of the storm development, dividing the time into four phases:

Phase 1 - Pre-storm	1735-1813 Cloud #1, 1813-1847 GMT Cloud #2
Phase 2 - Initial development	1847-1903 GMT, Runs #8-10
Phase 3 - Peak of storm	1903-1947 GMT, Runs #11-17
Phase 4 - Storm subsides	1947-2202 GMT, Runs #18-19

III B. DISCUSSION OF THE FOUR PHASES OF THE STORM

Phase 1, Pre-Storm, 1735-1813 GMT, Cloud #1

The airplane started Run #1, Cloud #1 about the selected cloud at 1735 GMT and continued to follow a flight pattern similar to that shown in Figure 1 for seven passes, back and forth.

From 1735 to 1811 GMT, the NASA-6 airplane made seven passes around, and through, the cloud. As Figure 2 shows, the radar top of the cloud grew slowly, reaching a peak value of 29,000 feet at approximately 1800 GMT. Thereafter the radar tops declined rapidly. The ground field mill readings were not unusual, registering from +0.1 to +0.4 kV/m, except for the period 1735 to 1758 GMT during which period the field at Station #14 rose from +0.4 to +1.0 kV/m. By 1804 GMT the reading had fallen back to +0.4 kV/m.

The airborne field mill readings remained below 0.2 kV/m except for Run #5 (1759-1801 GMT) and Run #6 (1802-1805 GMT), both of which went through the cloud at 10,500 feet altitude. On Run #5 maximum values of F_Z of -0.6 kV/m, and maximum values of F_X of +0.85 kV/m were reached. On

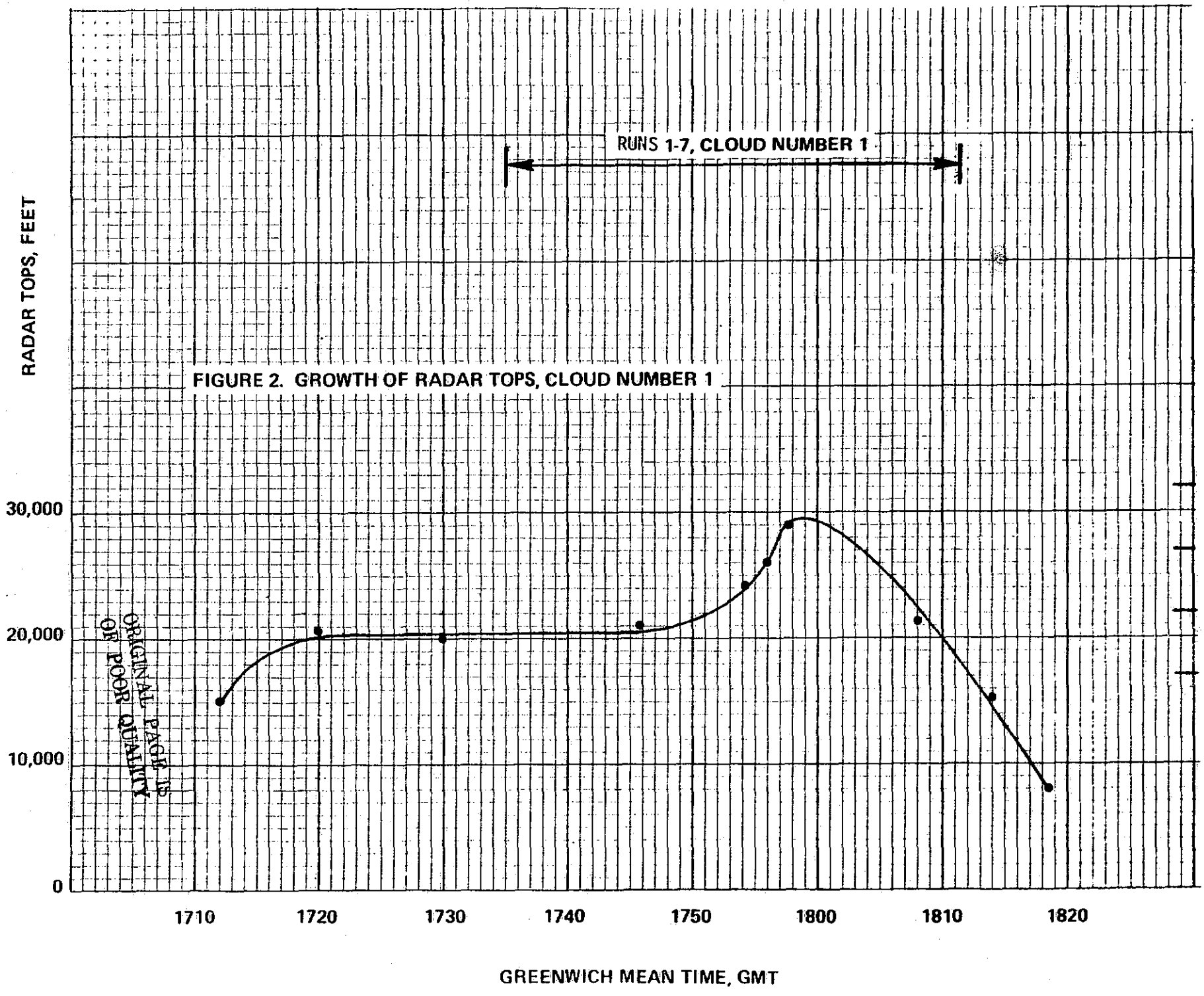

FIGURE 2. GROWTH OF RADAR TOPS, CLOUD NUMBER 1

Run #6, the maximum values for F_Z and for F_X were -0.78 kV/m and +0.56 kV/m, respectively.

The cloud did not evidence any electrical discharge activity whatever. During the period 1735 to 1813 GMT, not a single LDAR data point was observed.

Phase 1, Pre Storm, 1813-1903 GMT, Cloud #2

When the first cloud subsided, a second cloud, a few kilometers to the south, appeared to give promise of further growth. The growth of the radar tops of this second cloud is illustrated in Figure 3. Cloud #2 continued developing and providing us with the thunderstorm cloud that we had been looking for. The NASA-6 airplane made some nineteen passes around, and through, the Cloud #2 tracking it until 1956 GMT. We were thus able to observe a growing thundercloud at close range through all its stages of development and decay. The detailed study of this thundercloud forms the basis of this report.

The location of Cloud #2 is indicated by the 1840 GMT radar precipation echo shown superimposed on the LDAR plot for the period 1813-1847 GMT in Figure 4.

All the weather precipitation echo plots shown in this report were collected by the Kennedy Space Center weather radar, and supplied for our use by James Nicholson, Assistant Staff Meteorologist.

In Figure 4, as well as in subsequent LDAR plots, the location of the center of the LDAR System at

X = 613,593.0 Feet East, and Y = 1,528,943.5 Feet North

in the Florida East System, will be denoted by a "+" symbol. In subsequent plots in which LDAR is superimposed on field mill contour plots, the location of the center of the LDAR System will not be marked, so as to avoid confusion with the + and - sign of the electric field contours. Also,

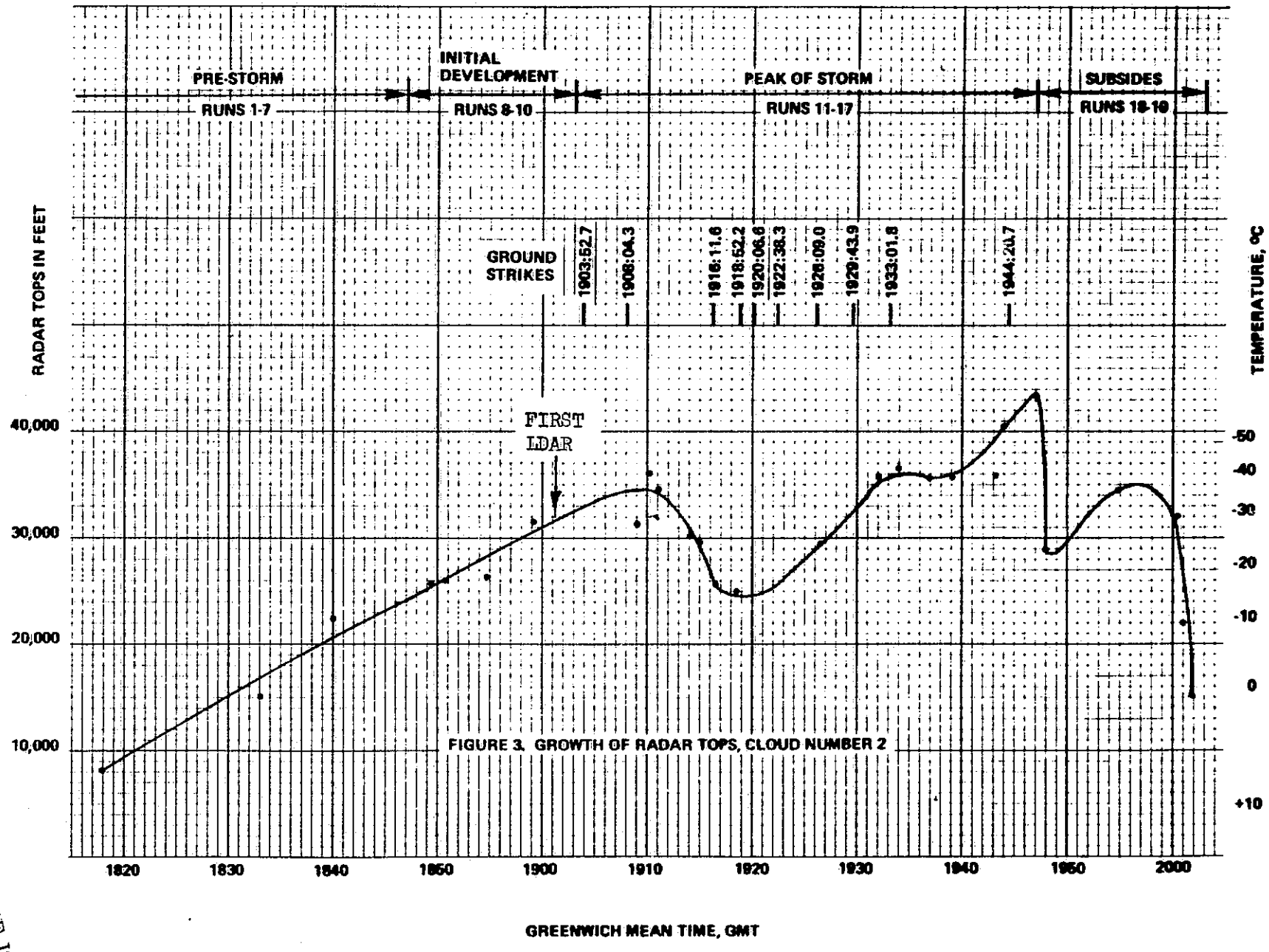

FIGURE 3. GROWTH OF RADAR TOPS, CLOUD NUMBER 2

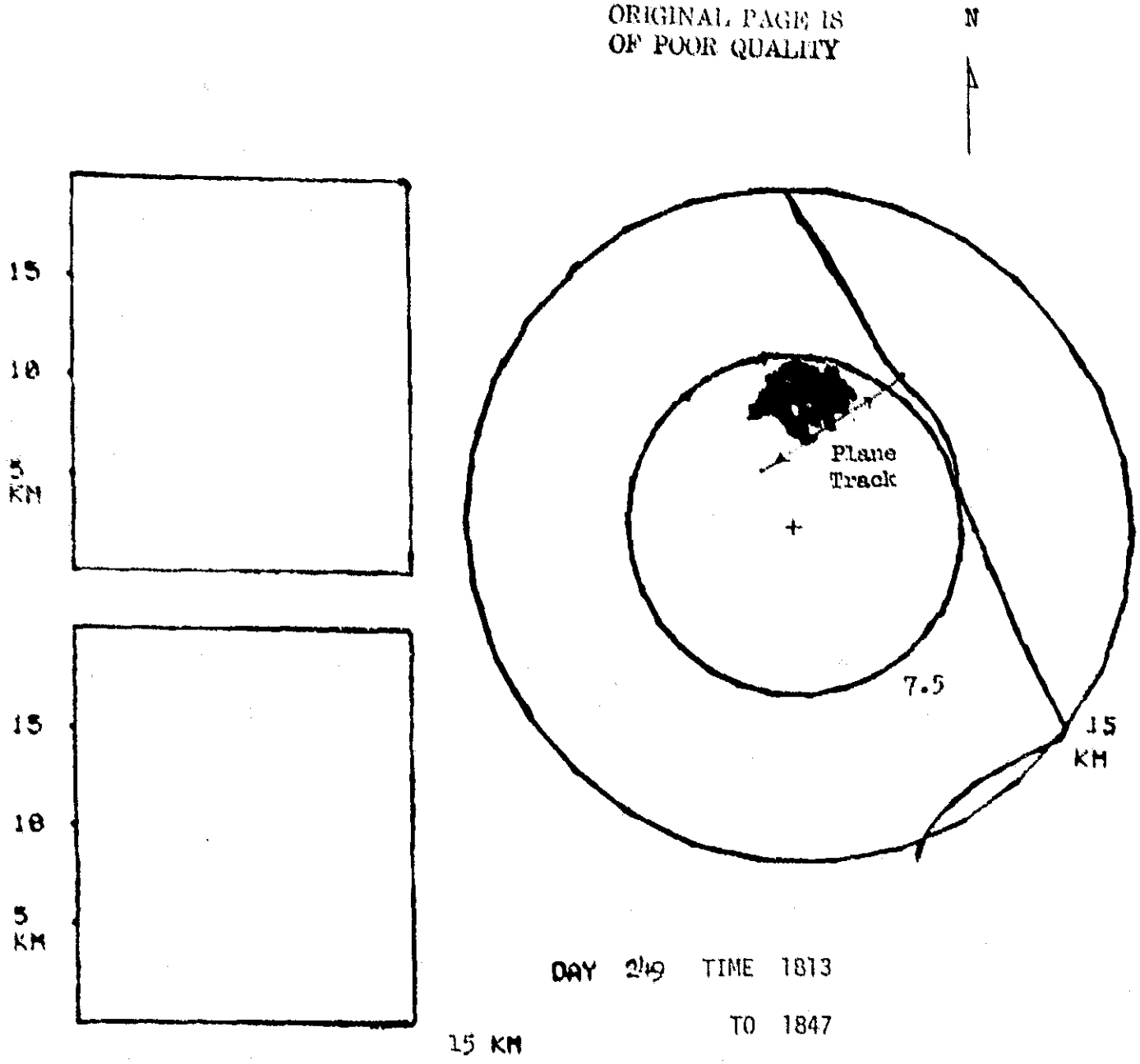

FIG. 4 RADAR PRECIPITATION ECHO, CLOUD NUMBER 2, 1840 GMT ADDED TO LDAR PLOT 1813-1847 GMT

superimposed is the flight path for its first seven passes, 1813-1847 GMT. Note that no LDAR response is shown in the plot for this time period, showing that the cloud was not electrically active. The absence of LDAR response is in accord with past observations, since LDAR responses generally are not observed until radar tops exceed 30,000 feet. During the period 1813-1847 GMT the radar tops had only reached the altitude of 24,000 feet, as Figure 3 indicates.

During Runs #1 to #7 (Cloud #2) 1813-1847 GMT, the ground field mill readings generally were not unusual (0.1 to 0.4 kV/m) except for 1813 GMT, when the first negative field readings were obtained and for 1822 GMT. Small negative fields of -0.047 kV/m were noted at site #12 at 1813 GMT. At 1822 GMT a negative field of -0.139 kV/m was observed at site #14. The contoured field mill plot for 1822 GMT is shown in Figure 5. The location of Cloud #2 is shown by the superposition of the radar precipitation echo of 1840 GMT. Note that the field mill readings for each site are given at the right. For reference the location of the field mill sites is shown in Figure 6, which is drawn approximately to the same scale as Figure 5.

During the period 1813 to 1847 GMT (Runs #1 to #7), no airborne field mill reading greater than 0.1 kV/m was recorded. This means that the plane did not encounter any significant charge centers in its passes, and is in accord with the known fact that, in the absence of charges aloft, the electric field is maximum at the ground and decreases as the elevation increases.

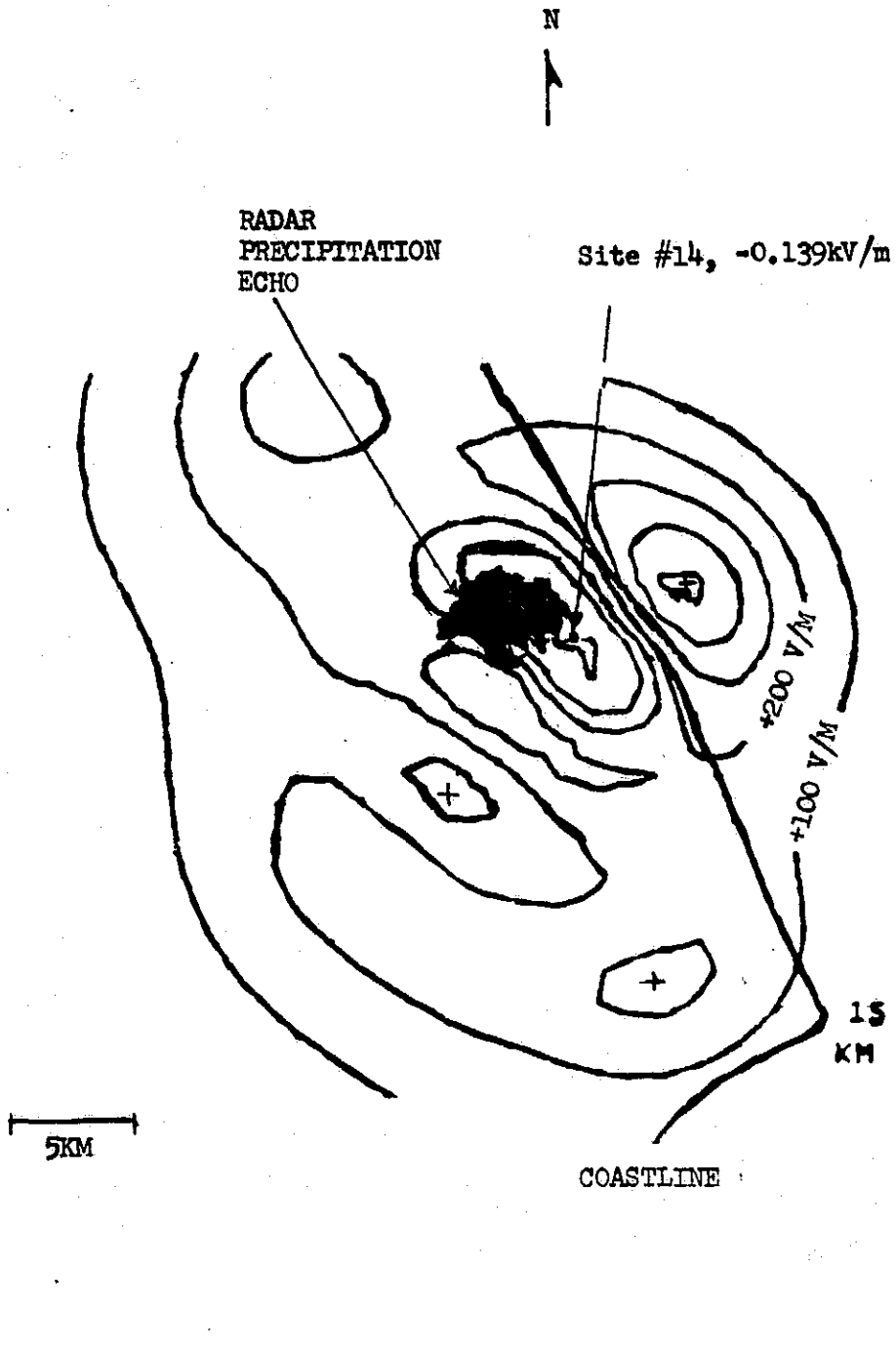

KSC EQUIPOTENTIAL
GRADIENT CONTOURS

09/06/77 GMT 1822:8.178

Line Scale - 100 V/M

Site #	Volts/M
1	292
2	353
3	261
4	292
5	292
6	261
7	230
8	323
9	292
10	328
11	199
12	-47
13	415
14	-139
15	353
16	329
17	290
18	160
19	323
20	199
21	290

FIG. 5 FIELD MILL CONTOUR PLOT
OF 1822 GMT, WITH SUPERIMPOSED
RADAR PRECIPITATION ECHO OF 1840 GMT
(PHASE 1, PRE-STORM (1815-1847 GMT))

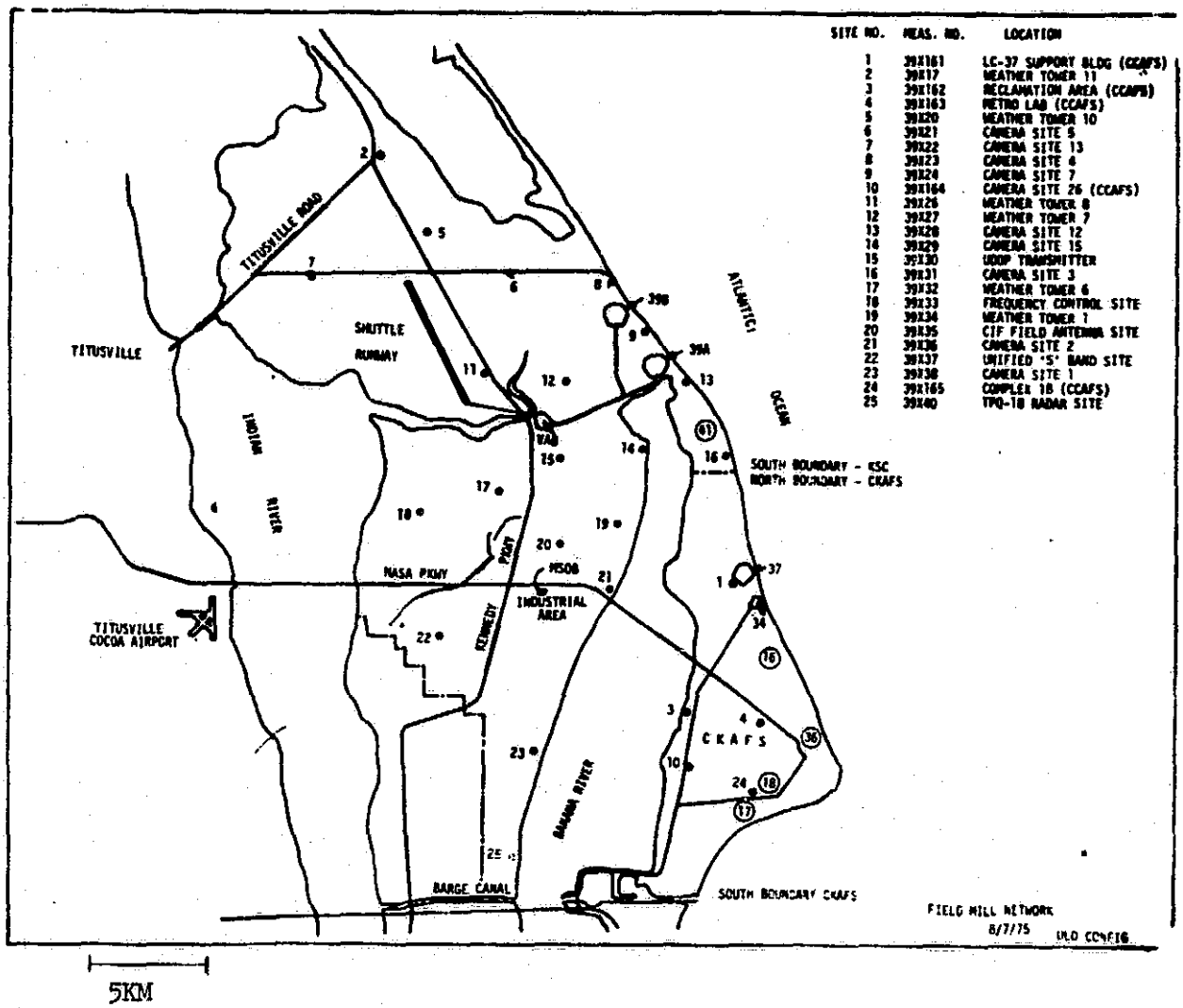

FIG. 6 FIELD MILL SITE LOCATION

Phase 2, Initial Development, 1847-1903 GMT

During the period 1847 to 1903 GMT (Runs #8 to #10), the radar tops increased from 24,000 to 32,000 feet (see Figure 3) and the first visual signs of electrical activity in the cloud made their appearance.

In Figure 7 the PPI radar precipitation echo of 1848 GMT is shown superimposed on the LDAR plot of 1848-1858 GMT. Note the growth since 1840 GMT, Figure 4. In Figure 8 the vertical extent of the precipitation echo is shown in the radar RHI plot of 1849 GMT. It should be pointed out that all RHI plots are centered at the radar, whose location is indicated in Figure 7. The radar is located at

X = 600,572 Feet East, and Y = 1,559,707 Feet North

in the Florida East System, some 6 miles northwest of the LDAR. In LDAR coordinates, the radar (x,y) position in meters is (-3969,+9380). The orientation of the x,y coordinate system is show in Figure 40.

In all the radar plots isocontouring was used. The lighter portion of the radar echo corresponds to a return approximately 25 db stronger than the dark portion of the precipitation echo, in both the PPI and the RHI plots. In some cases, especially where the lighter portion is internal to the precipitation echo, the lighter portion appears white.

The first LDAR response occurred at 1901:21.172 GMT, as determined from a printout of the LDAR data. It occurred at the (x,y,z) coordinate (1.2, 4.5, 7.6) km. (see Figure 9). At that time the radar tops were 31,000 feet (see Figure 3), in accord with our past observations the LDAR responds generally do not appear until radar tops reach 30,000 feet.

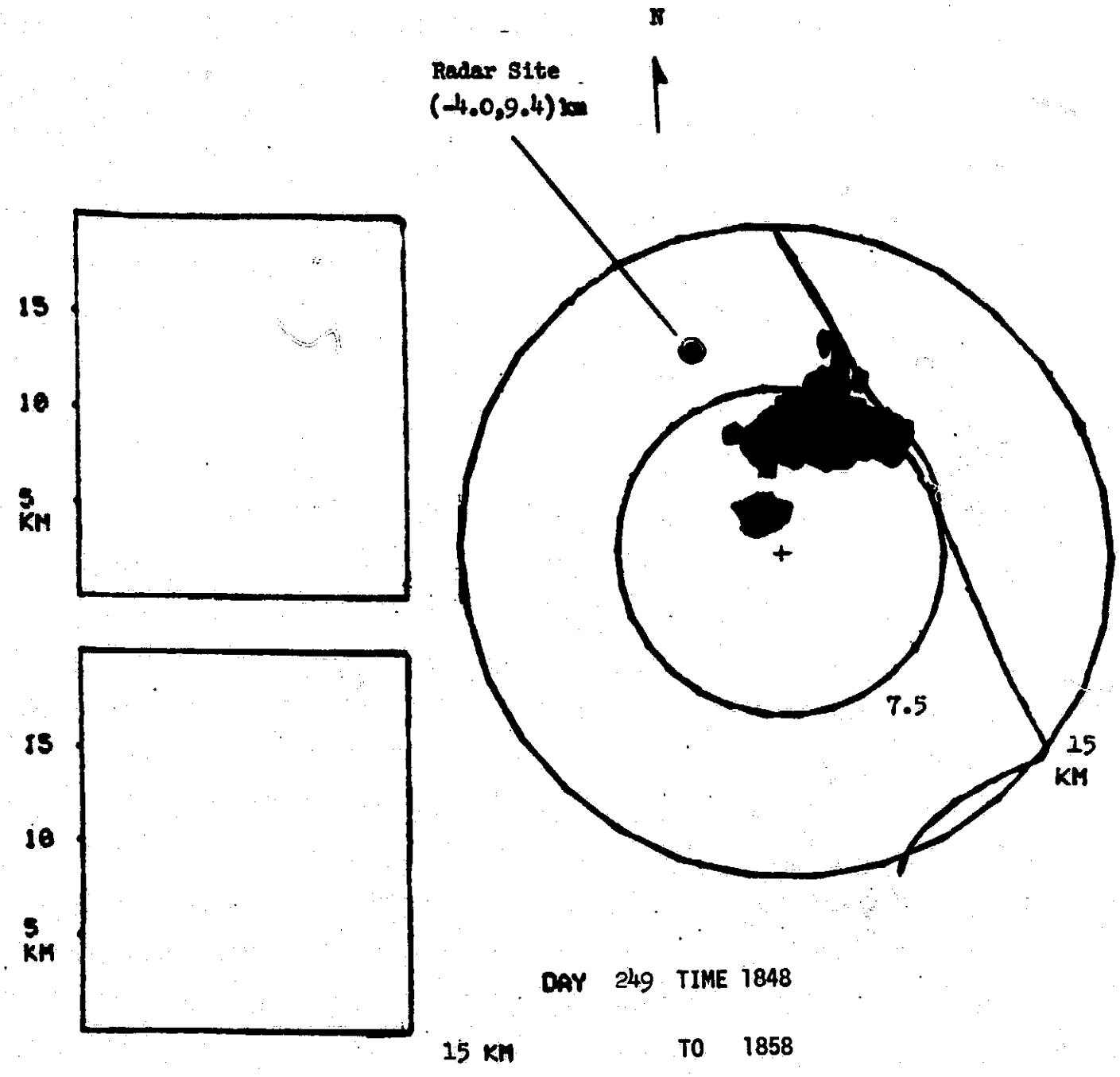

FIG. 7 RADAR PRECIPITATION ECHO OF 1848 GMT SUPERIMPOSED ON LDAR PLOT OF 1848-1858 GMT

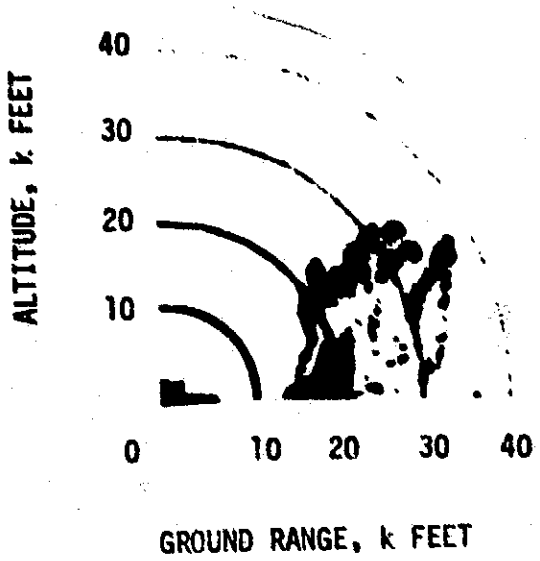

FIG. 8 RADAR RHI PLOT OF 1849 GMT
AZIMUTH 119°

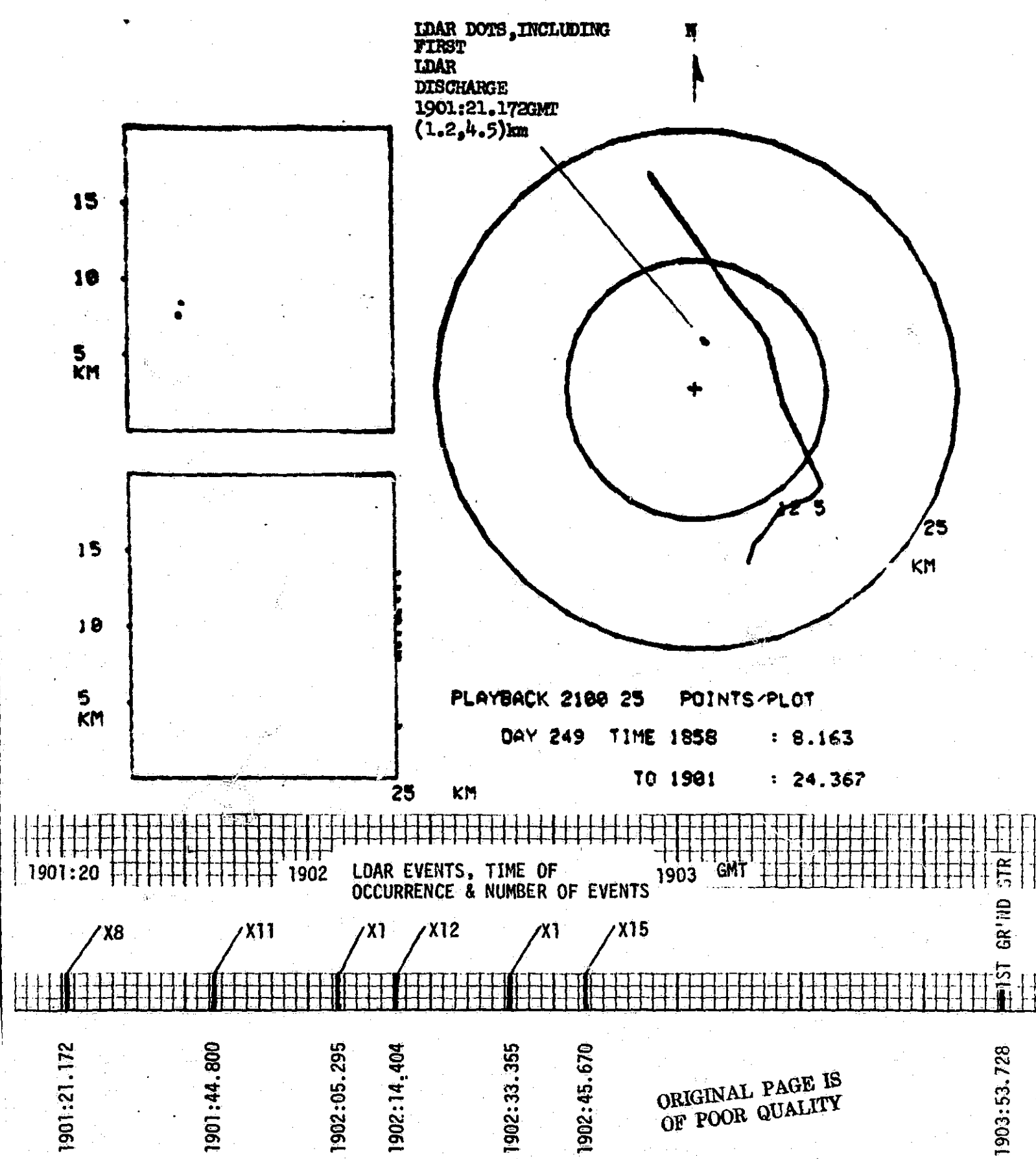

FIG. 9 FIRST LDAR RESPONSE, 1901:21.172 GMT, LDAR PLOT OF 1858:08-1901:24 GMT

Data compiled by James Nicholson, Assistant Staff Meterorologist KSC, is of interest. His correlation[3] of the maximum radar tops of the day with cloud discharges and ground discharges within the field-mill network, and with the maximum ground-base field mill reading (potential gradient in kV/m) is presented in Figure 10. With but a few exceptions, cloud discharges are associated with radar tops above 30,000 feet, and all the ground strikes occur when radar tops are above 30,000 feet.

The appearance of the first LDAR discharge on the LDAR plot is shown at the position (1.2, 4.5) km in Figure 9, which covers the time period 1858:08.163 to 1901:24.367. In this plot the center of the LDAR System is denoted by a "+" sign. The coastline is shown to the right. The scale in Figure 9 is indicated by the 12.5 and 25 km rings. Other scales will appear in the report, the 7.5 and 15 km rings being the most common. The boxes at the left show the height of the discharges detected by LDAR, as a function of range. Two boxes are shown. The upper box contains the height data for all the LDAR discharges north of the LDAR site, that is in the azimuth range 270 to 90 degrees. The lower box contains the height data for all the data points that occur south of the LDAR site, that is at azimuths 90 to 270 degrees. For each data point in the PPI plot, a corresponding point will appear on the height-range plot. Positive identification is best made in real time, since the two dots occur simultaneously. However, the range scale will in many cases identify the corresponding points. It should be noted however that each LDAR dot on the LDAR plot is often many (as many as 15) separate data points that occur so close together that they appear as one in the plot. The data points at the right of the 25 km line in the height plots represent data points beyond the outer range ring, in this case beyond 25 km. These

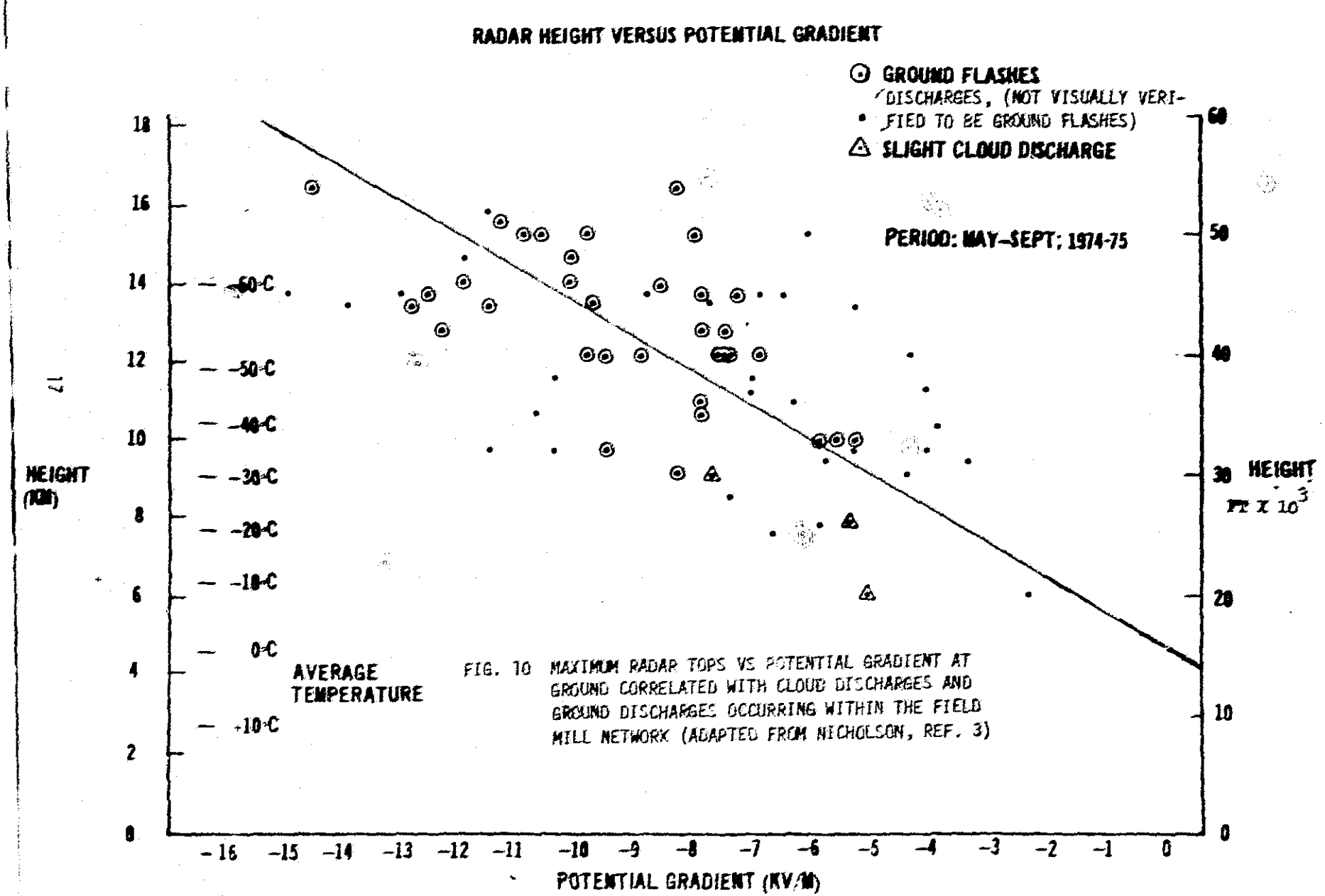

FIG. 10 MAXIMUM RADAR TOPS VS POTENTIAL GRADIENT AT GROUND CORRELATED WITH CLOUD DISCHARGES AND GROUND DISCHARGES OCCURRING WITHIN THE FIELD MILL NETWORK (ADAPTED FROM NICHOLSON, REF. 3)

data points are not shown in the PPI presentation, but are shown just to the right of the height plot. Clearly there were many distant discharges occurring during the time covered by the LDAR plot shown in Figure 9.

The first ground strike occurred at 1903:52.728 GMT. This ground strike was rapidly followed by twelve additional ground strikes, all within 41 minutes.

The question arises, how much and what type of warning did the LDAR and the Field Mill Systems provide of the impending ground strike?

The very first (but very faint) warning of the impending ground strike was a negative-going field mill reading of -0.17 kV/m at site #12 at 1853:52 GMT, Figure 11, some 10 minutes prior to the first ground strike, which was to occur some 4 km away from site #12. However, this field mill reading was no warning at all since a much higher value of 1 to 4 kV/m is considered* the warning level for a triggered strike to a missile of the Apollo-Soyuz type. Firstly, -0.17 kV/m is very small compared to 1 kV/m, and secondly a ground strike would require a much stronger field strength for its initiation than a triggered strike for a missile of the Apollo-Soyuz type. Realistically speaking, therefore, the negative field mill reading of -0.17 kV/m was too small, and really was no warning at all.

The airborne field mill detected a high F_z field reading of -1.86 kV/m at 1855:17 GMT some 9 minutes prior to the first ground strike. While such a reading might be interpreted as a warning, a ground strike warning system based on airplanes traversing the clouds is not practical. In Figure 12 the flight path has been superimposed on the nearest available field mill contour plot of 1855:55 GMT and the location of the airplane at 1855:17 GMT

---

* Kasemir[4], "All measurements of fields aloft so far confirm that the 1 kV/m field line at the ground is a good indicator for a safe launch condition outside the line and a no launch condition inside the line. There is a transition zone between the 1 and 4 kV/m field line where a launch still may be possible. However, in this zone field measurements aloft should be carried out before a launch is executed".

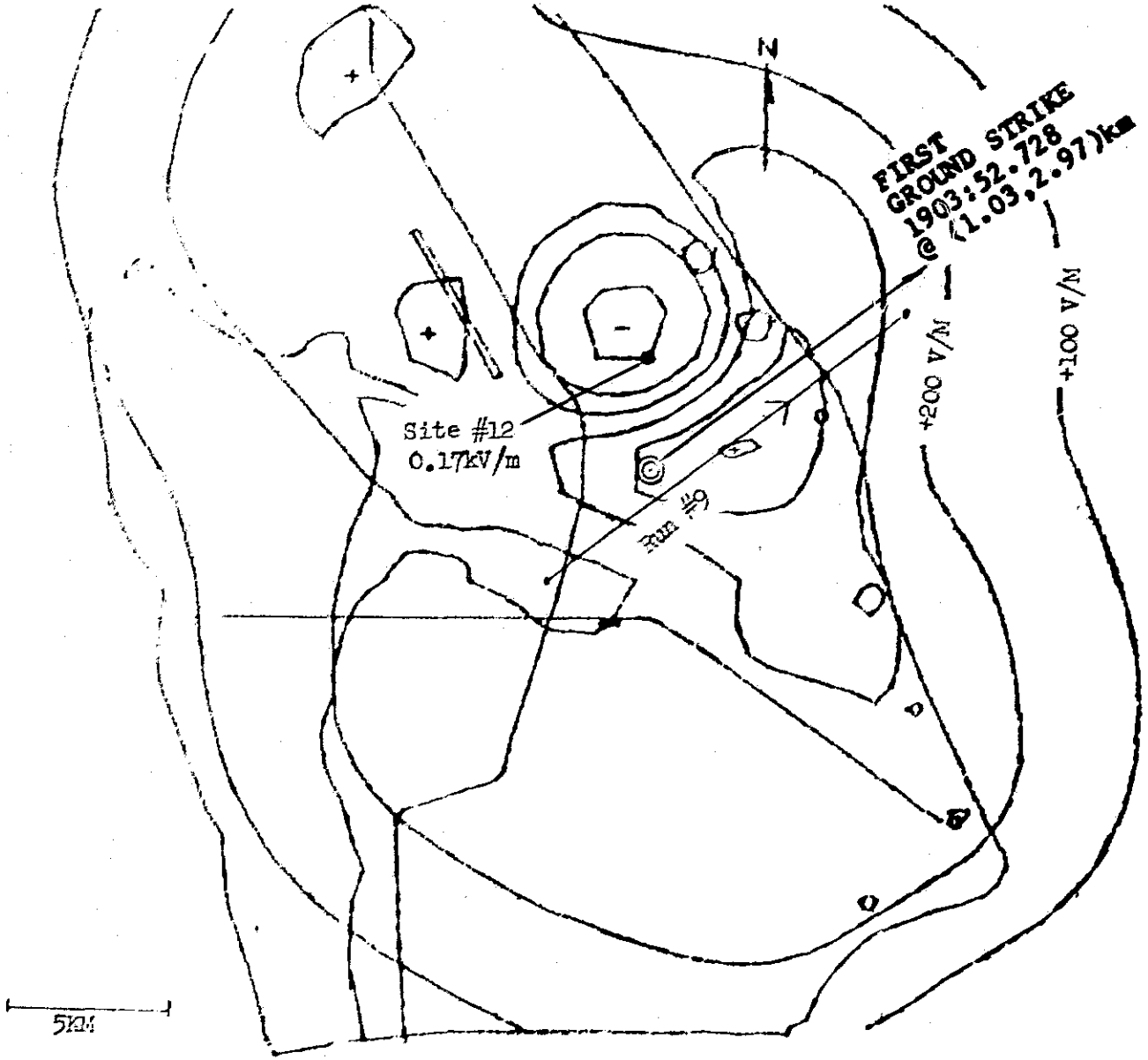

KSC EQUIPOTENTIAL
GRADIENT CONTOURS

09/06/77 1853:52.080 GMT

Line Scale - 100 V/M

Site #	Volts/M
1	323
2	323
3	261
4	292
5	230
6	261
7	292
8	261
9	292
10	292
11	169
12	-170
13	415
14	507
15	353
16	323
17	261
18	190
19	323
20	199
21	261
22	292
23	261
24	230

FIG. 11 FIELD MILL CONTOUR PLOT OF 1853:52.080 GMT

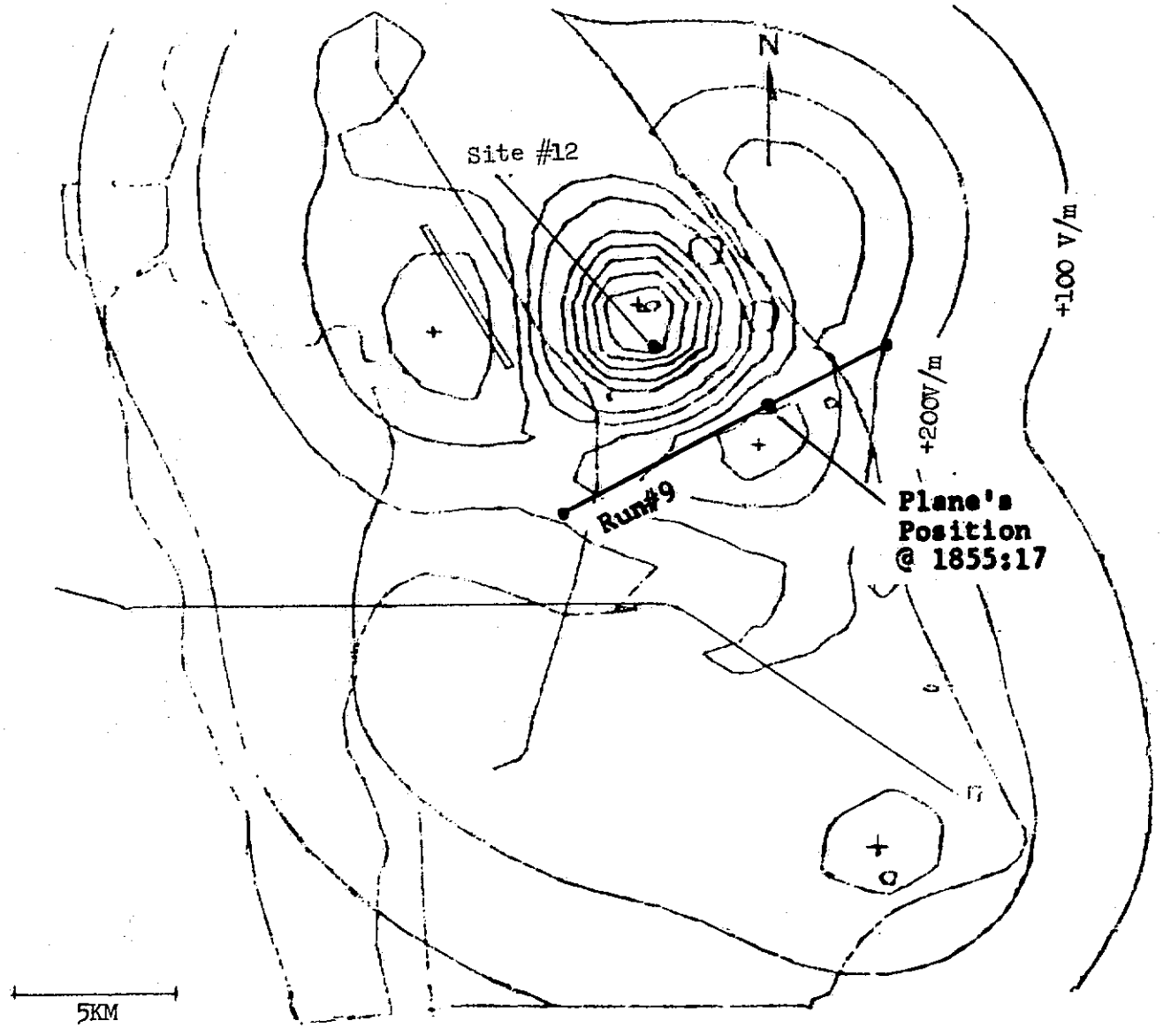

KSC EQUIPOTENTIAL
GRADIENT CONTOURS

09/06/77 1855:54.894 GMT

Line Scale - 100 V/M

Site #	Volts/M
1	292
2	323
3	261
4	292
5	261
6	199
7	292
8	261
9	261
10	292
11	169
12	-631
13	415
14	538
15	261
16	323
17	261
18	199
19	323
20	199
21	261
22	292
23	261
24	323

FIG. 12 FIELD MILL CONTOUR PLOT OF 1855:55 GMT

has been marked. Note that the airborne field strength is 4 times the corresponding (and highest) ground based field mill reading, pointing to a charge center aloft, since in the absence of a charge center the field decreases as one goes up.

The first LDAR response occurred at 1901:21.172, some 2.5 minutes prior to the first ground strike. An LDAR response represents a field gradient in the cloud sufficient to break down the dielectric strength of the air, and form an electrical discharge in the cloud. Therefore, it should reasonably be considered as a warning of a possible strike to the ground. Generally speaking the presence of LDAR responses in an area should be considered as a warning of an impending ground strike. Here the warning was 2.5 minutes.

Prior to the first ground strike at 1903:52.728 GMT there were some 48 LDAR discharges, as shown on the bottom of Figure 9. This pattern of discharges has been noted on other occasions, in particular prior to the ground strike discussed in some detail by Uman et al[5], and is worthy of discussion. For reference the time sequence of the LDAR discharges is shown at the bottom of Figure 9, and the (x,y,z,t) coordinates of the data points are given in Table I.

The LDAR discharges clearly appear in groups. In this instance, the groups have an intergroup spacing of 24, 30, and 31 milliseconds (mean 28 ms) and consist, on the average, of 12 LDAR discharges. The LDAR discharges within a group have a very close time spacing (median 4.5 ms), Table I. Further the LDAR discharges in a group are closely spaced in the cloud. Typically the mean spacing in X is 0.2 km, in Y is 0.3 km, and in Z is 0.5 km. The mean jump in Z is almost twice the mean jump in X or Y. It appears that the LDAR discharges in a group originate approximately at the same location, but at different levels of the cloud.

TABLE I LOCATION OF LDAR DISCHARGES OCCURRING JUST PRIOR TO THE FIRST GROUND STRIKE AT 1903:52.728 GMT

		Location In LDAR Coordinates		
Time, GMT	ΔT ms	X (East) Meters	Y (North) Meters	Z Meters
1901:21.172		1227	4520	7647
1901:21.184	12	563	4672	8793
1901:21.188	4	757	4888	8651
1901:21.191	3	864	4899	8709
1901:21.195	4	893	4869	8460
1901:21.213	18	650	3993	8772
1901:21.218	5	1029	4610	7491
1901:21.223	5	1261	4501	7769
Mean	7.2	906.5	4619	8287
Std. Dev.	5.5	254	300	553
Median	4.5			
1901:44.8		1490	4054	8062
1901:44.803	3	1421	3885	8332
1901:44.808	5	1202	3834	8539
1901:44.821	13	883	4774	8827
1901:44.833	12	1429	3701	8271
1901:44.838	5	1653	3518	8006
1901:44.862	24	525	5226	8278
1901:44.869	7	857	5350	8380
1901:44.872	3	927	5400	8530
1901:44.882	10	942	3914	8273
1901:44.886	4	492	3894	8477
Mean	8.5	1075	4323	8361
Std. Dev.	6.5	391	716	230
Median	4			
1902:05.295		1982	4830	7884
1902:14.404		807	4792	8038
1902:14.408	4	873	4744	7899
1902:14.416	8	1093	4718	9092
1902:14.418	2	1050	4876	9074
1902:14.421	3	1222	4786	8789
1902:14.432	11	1364	4389	8731
1902:14.442	10	1178	3669	8661
1902:14.448	6	956	3563	8626
1902:14.455	7	1832	4351	8757
1902:14.46	5	1869	4048	8125
1902:14.477	17	2538	3821	8350
1902:14.486	9	1217	4806	7210
Mean	7.4	1333	4380	8445
Std. Dev.	4.3	505	486	547
Median	7			

TABLE I (CONTINUED)

Time, GMT	ΔT ms	Location In LDAR Coordinates X (East) Meters	Y (North) Meters	Z Meters
1902:33.355		2180	5329	7504
1902:45.67		2287	4168	8013
1902:45.672	2	2180	4584	8203
1902:45.674	2	2411	4734	8236
1902:45.679	5	2776	4783	8046
1902:45.686	7	2179	5400	8040
1902:45.688	2	2014	5270	8042
1902:45.706	18	1489	3910	8744
1902:45.714	8	4394	4394	9179
1902:45.718	4	1191	4711	8836
1902:45.727	9	1490	4523	6958
1902:45.73	3	1533	4525	6934
1902:45.753	25	1790	4359	7343
1902:45.76	7	1931	5835	7851
1902:45.763	3	2131	5834	7594
1902:45.767	4	2050	5972	8107
Mean	6.9	2123	4867	8008
Std. Dev.	6.3	750	643	632
Median	4			
1903:16.926		763	4979	6465

Phase 3, Peak of the Storm, 1903-1947 GMT

Phase 3 represents the peak of the storm, starting with the first ground strike at 1903:52.73 GMT and continuing past the last ground strike (at 1944) to 1947 GMT. During that period there were 13 ground strikes.

Since 1840 GMT (Figure 4) the storm had grown somewhat in extent but considerably in elevation, as the PPI precipitation echo of 1904 GMT (Figure 13), superimposed on the LDAR plot, and the RHI plot of 1903 GMT (Figure 14) show.

NASA-6 flew around the storm as indicated in Figures 15-24. NASA-6 did not fly through the storm because of the level of thunderstorm activity. The corner positions of the flight path are automatically marked by the radiation from the lightning simulator, which was activated on the corners. The corner markings provided by the lightning simulator gave a very accurate location of the airplane relative to the electrical discharges in the clouds detected by LDAR. The use of the LDAR lightning simulator on the plane proved to be very fortuitous - since an operational failure left us without the scheduled S-Band radar track.

Plotting of the VHF Omni Range (VOR) data taken by the plane showed a considerable inconsistency in the plotted position, and emphasized the value of having the more-accurate lightning simulator on board.

Actually, a VORTAC System is not intended as a precision aircraft position locating system, especially at 50 nautical miles from a VOR/DME station, but rather is intended as a guidance system to guide the aircraft to the VORTAC station.

Errors in range, at best, are 0.1 n. mile or 182 meters according

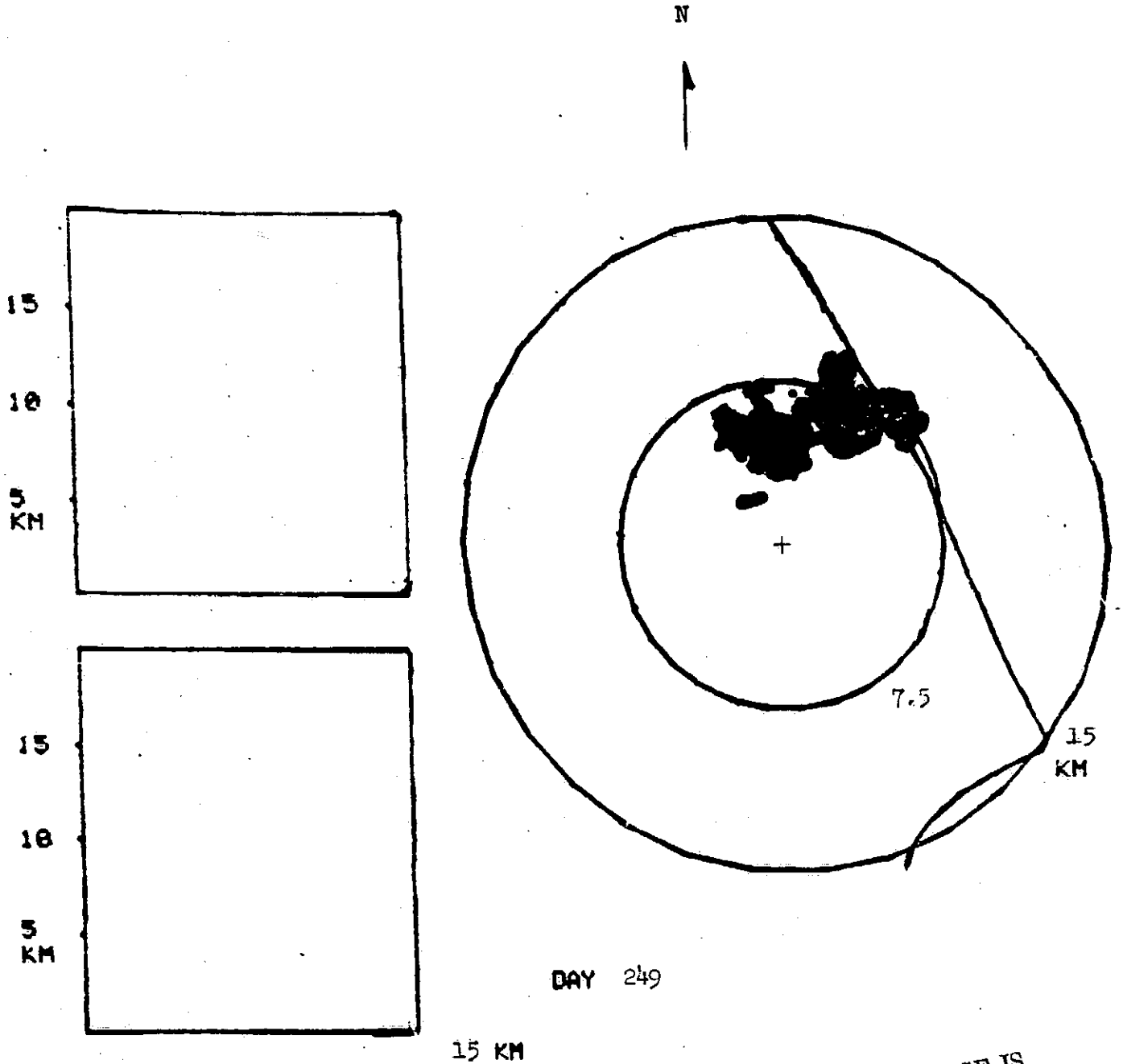

FIG. 13 RADAR PRECIPITATION ECHO OF 1904 GMT
SUPERIMPOSED ON LDAR MAP.
NO LDAR DOTS ARE SHOWN

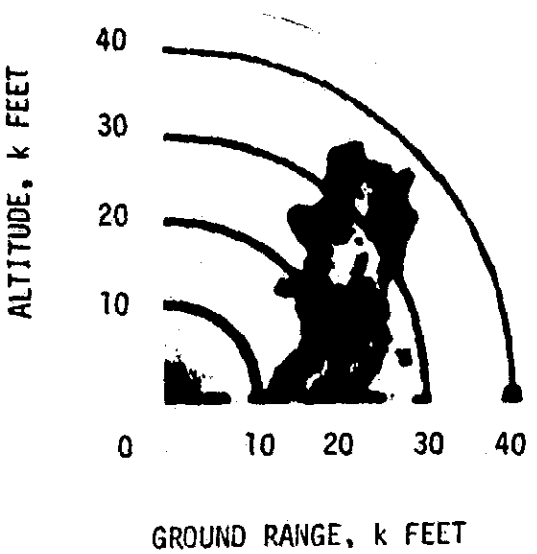

FIG. 14 RADAR RHI PLOT OF 1903 GMT
AZIMUTH 134°

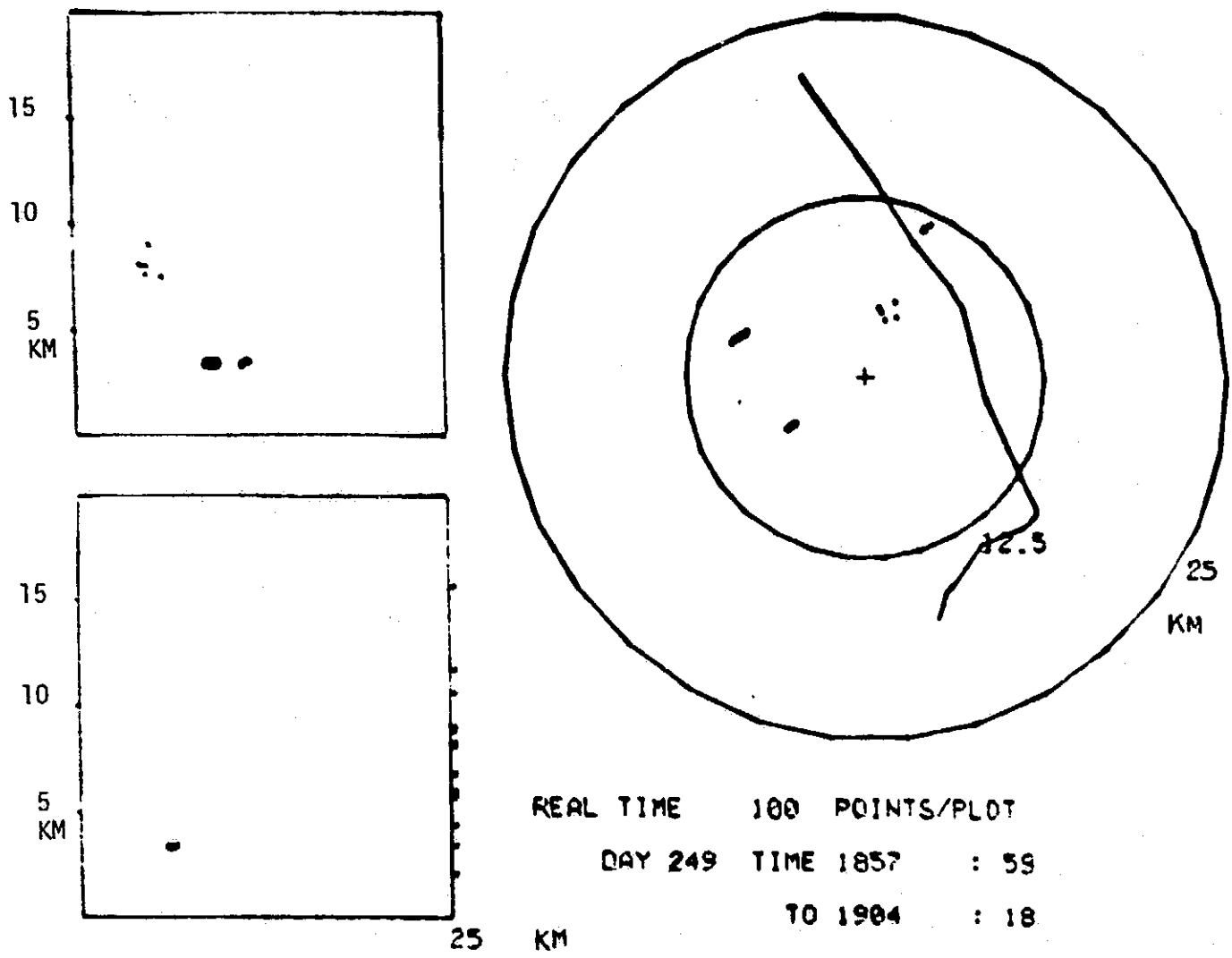

FIG. 15 LDAR PLOT, 1857-1904 GMT,
SHOWING NASA-6 FLIGHT PATH

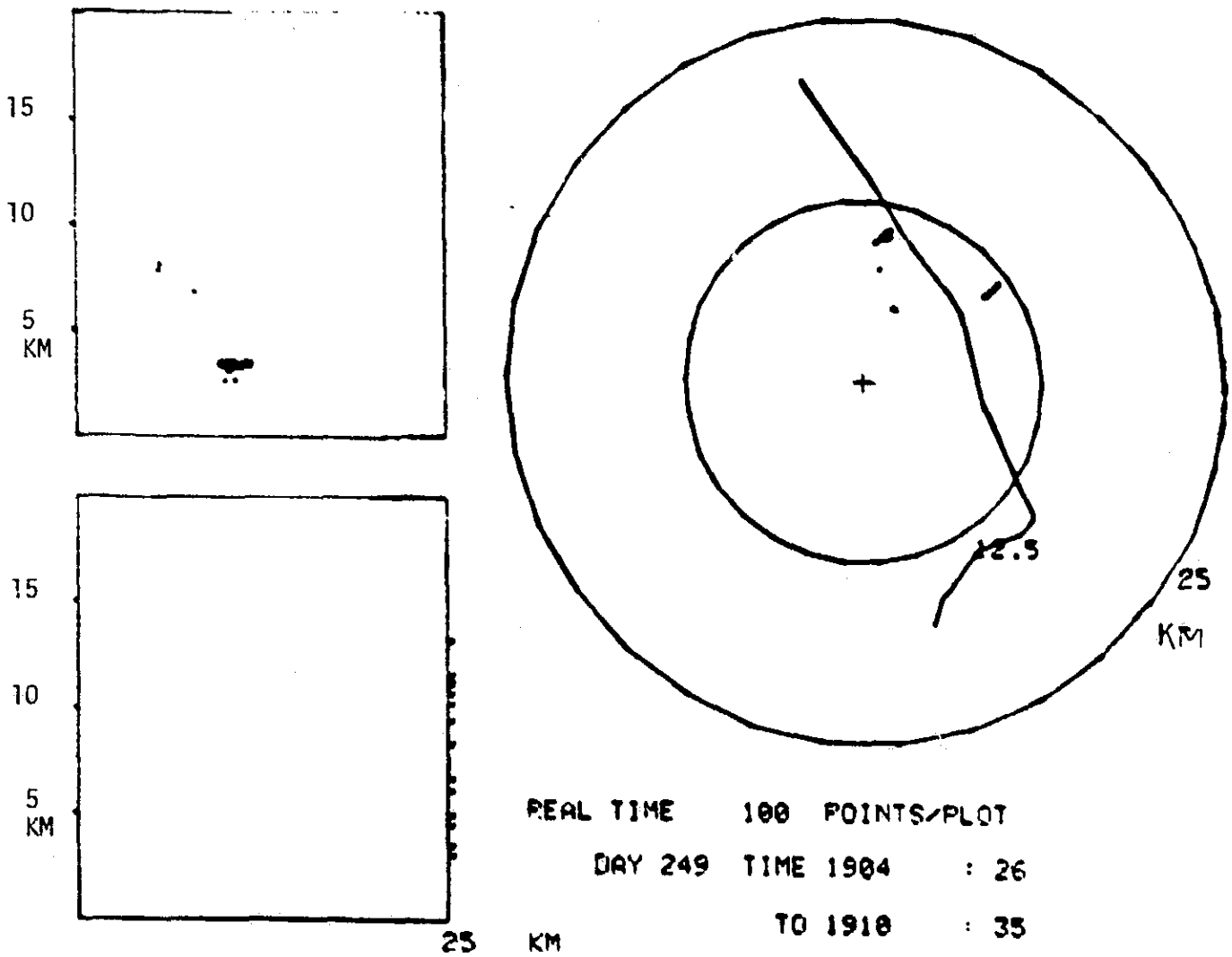

FIG. 16 LDAR PLOT, 1904-1910 GMT,
SHOWING NASA-6 FLIGHT PATH

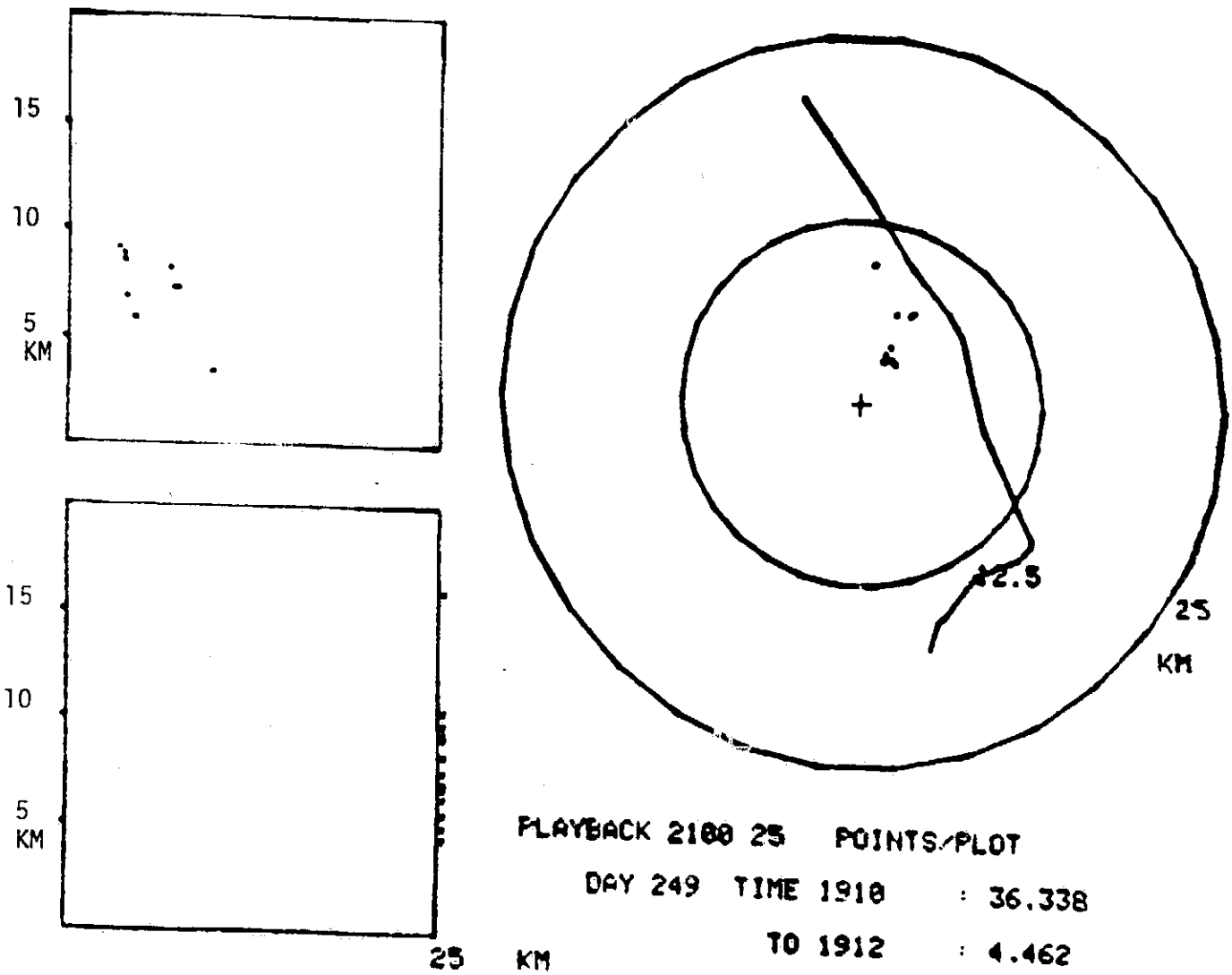

FIG. 17 LDAR PLOT, 1910-1912 GMT,
SHOWING NASA-6 FLIGHT PATH

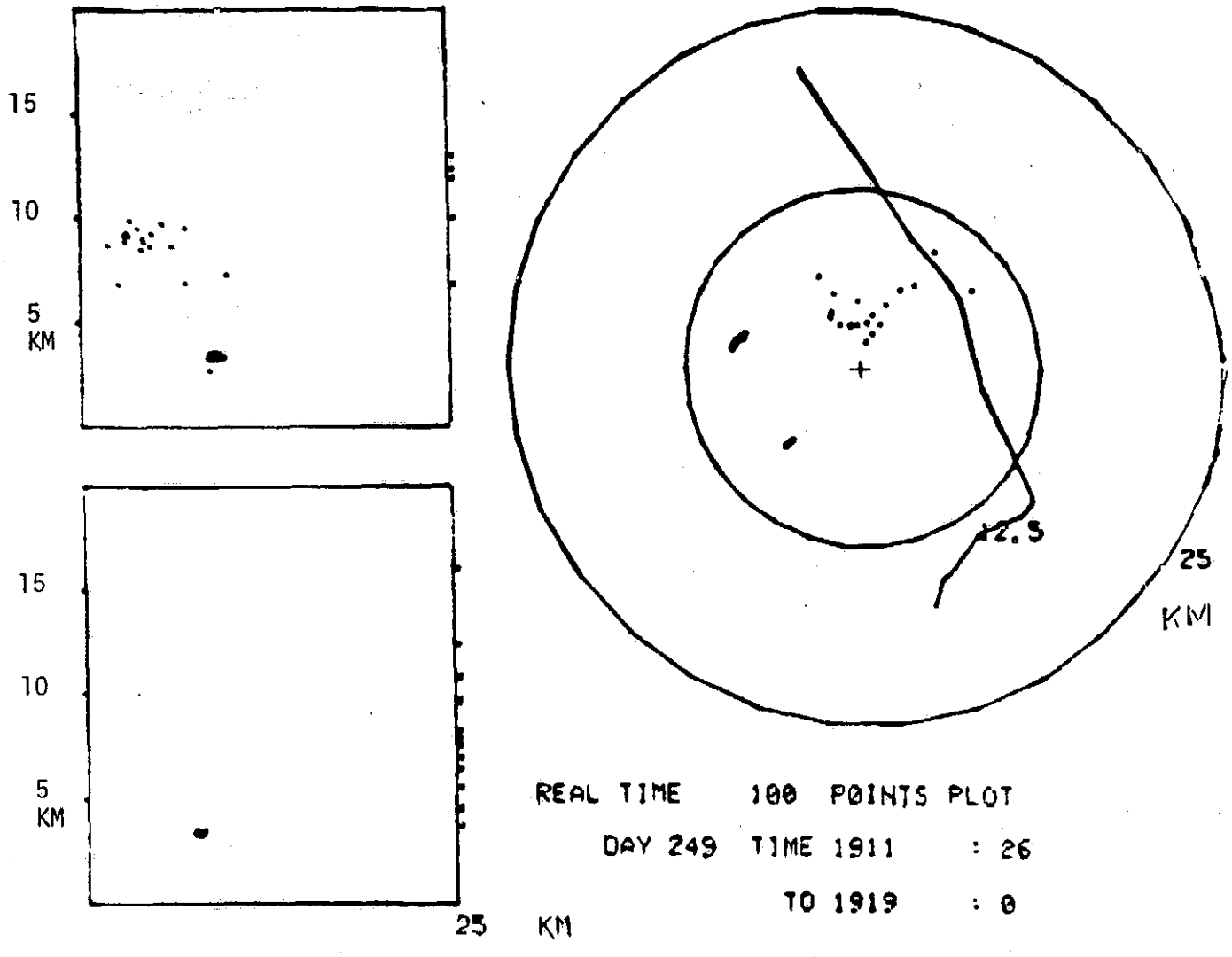

FIG. 18 LDAR PLOT, 1911-1919 GMT,
SHOWING NASA-6 FLIGHT PATH

ORIGINAL PAGE IS
OF POOR QUALITY

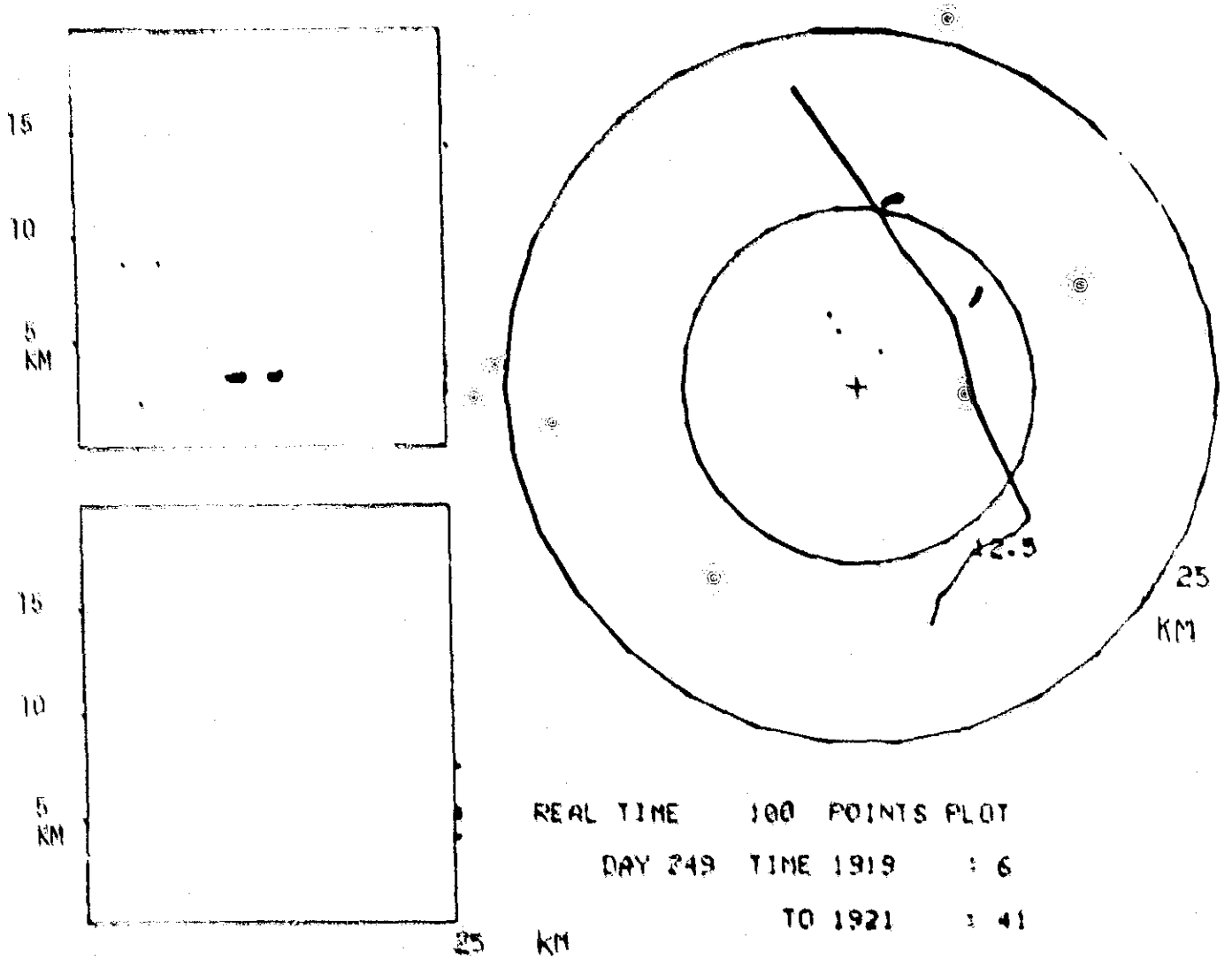

FIG. 19 LDAR PLOT, 1919-1621 GMT,
SHOWING NASA-6 FLIGHT PATH

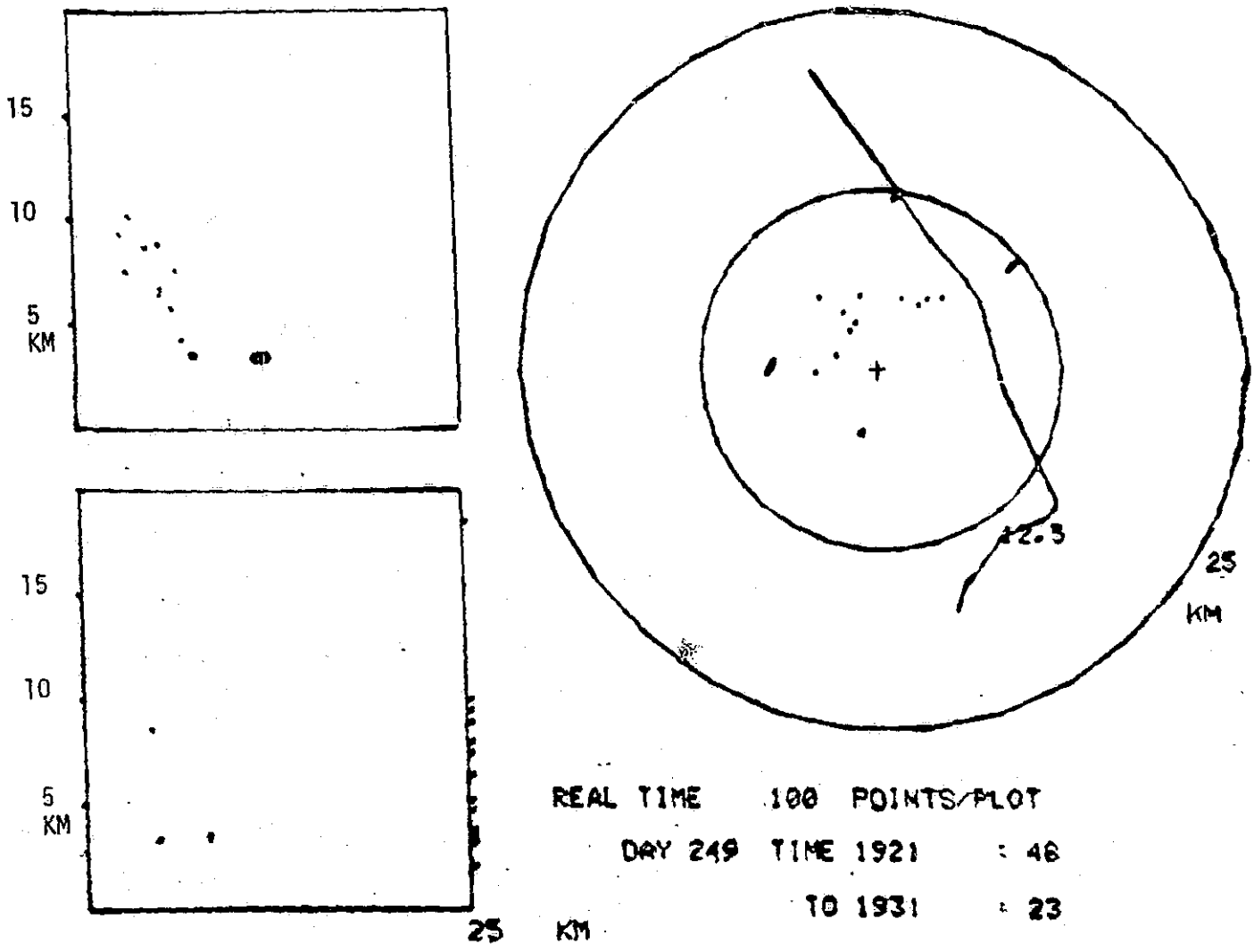

FIG. 20 LDAR PLOT, 1921-1931 GMT,
SHOWING NASA-6 FLIGHT PATH

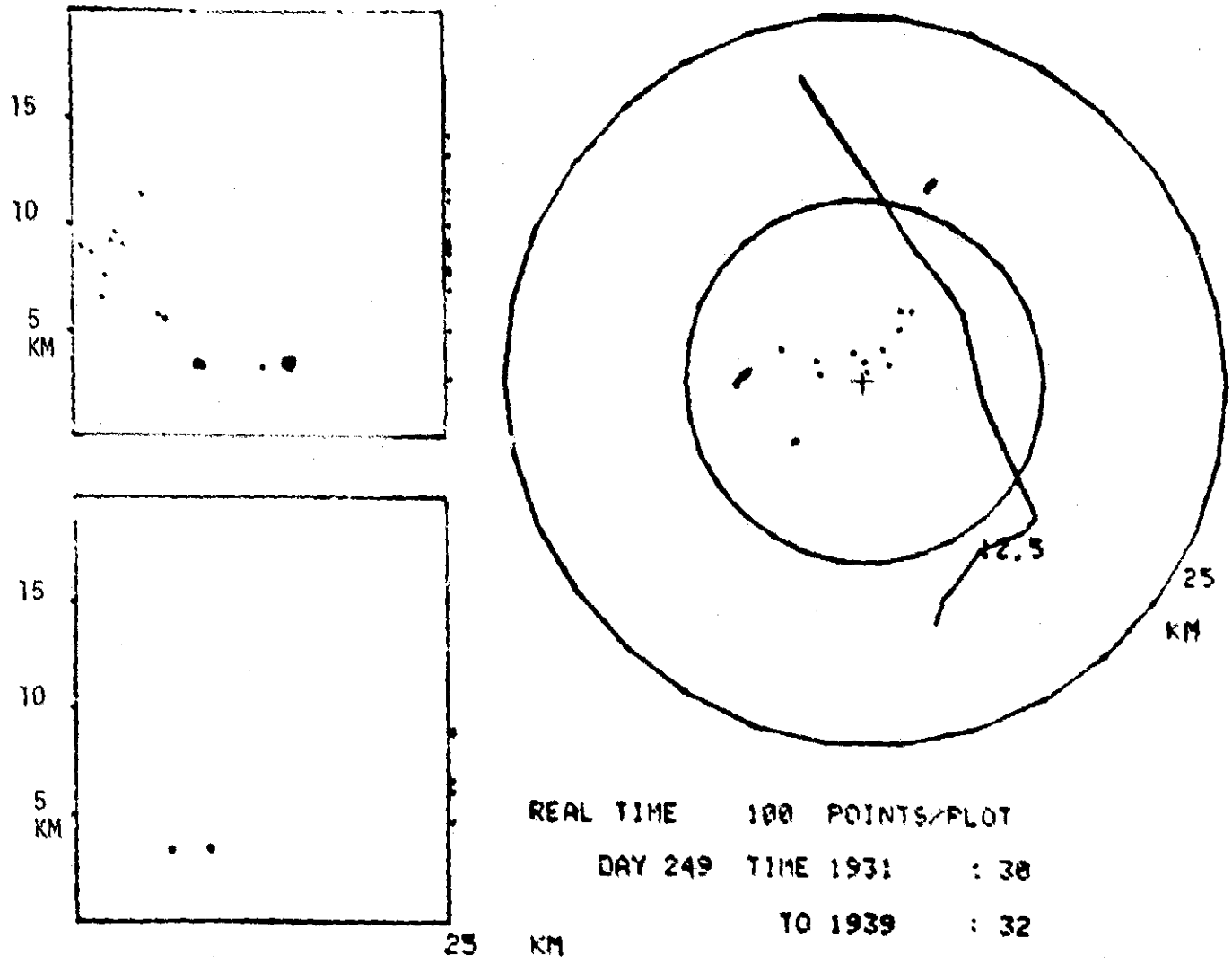

FIG. 21 LDAR PLOT, 1931-1939 GMT, SHOWING NASA-6 FLIGHT PATH

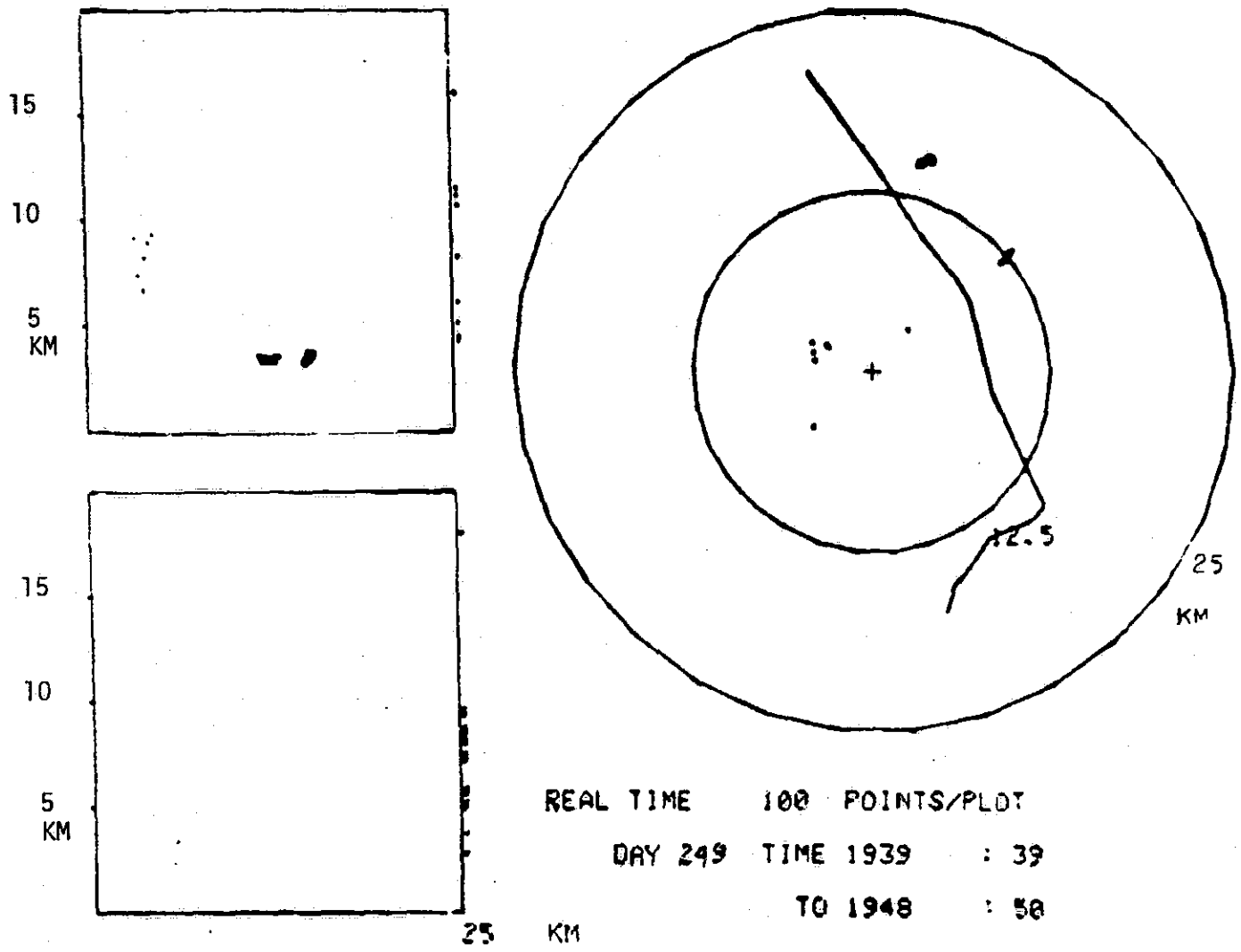

FIG. 22 LDAR PLOT, 1939-1948 GMT,
SHOWING NASA-6 FLIGHT PATH

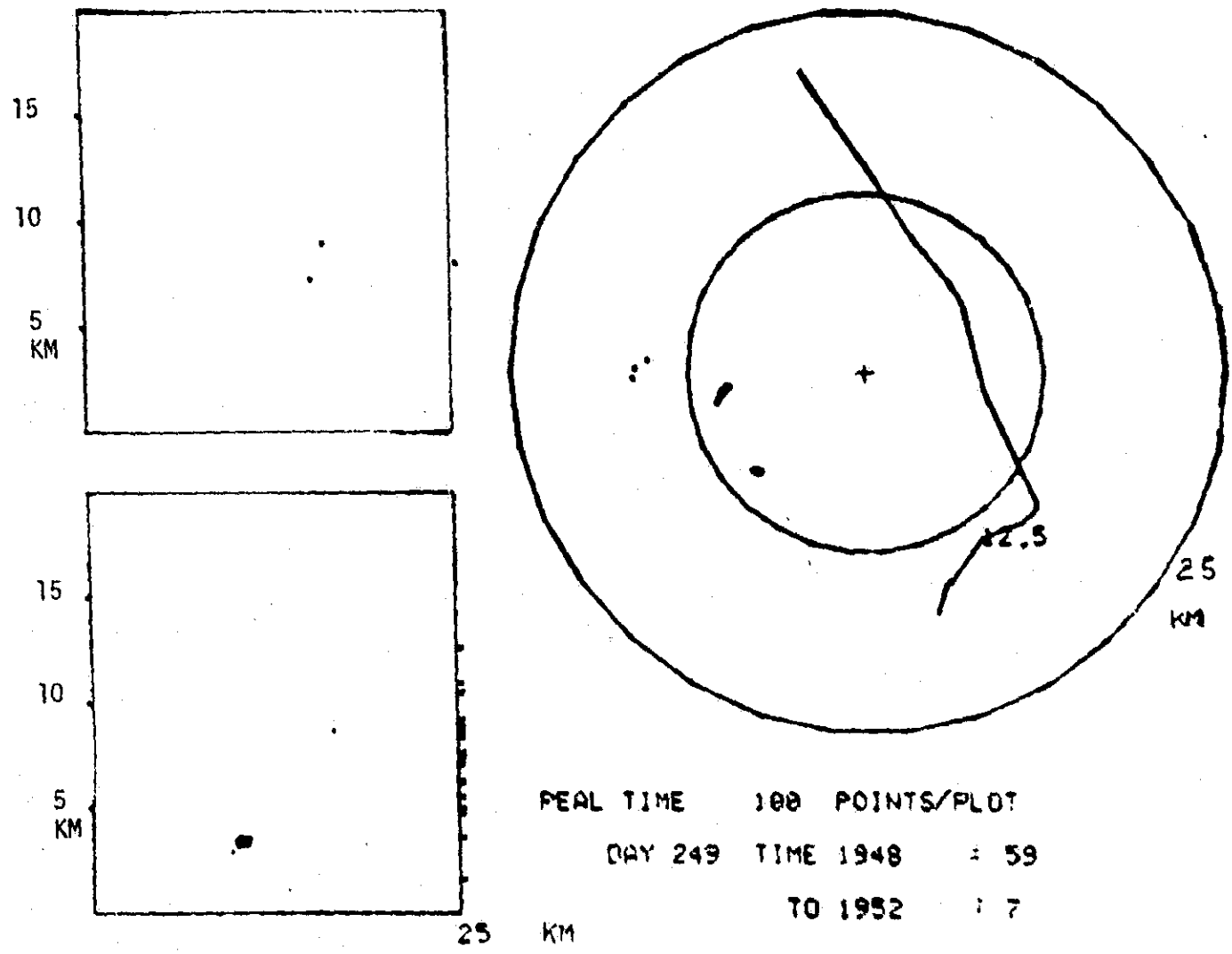

FIG. 23 LDAR PLOT, 1948-1952 GMT,
SHOWING NASA-6 FLIGHT PATH

ORIGINAL PAGE IS
OF POOR QUALITY

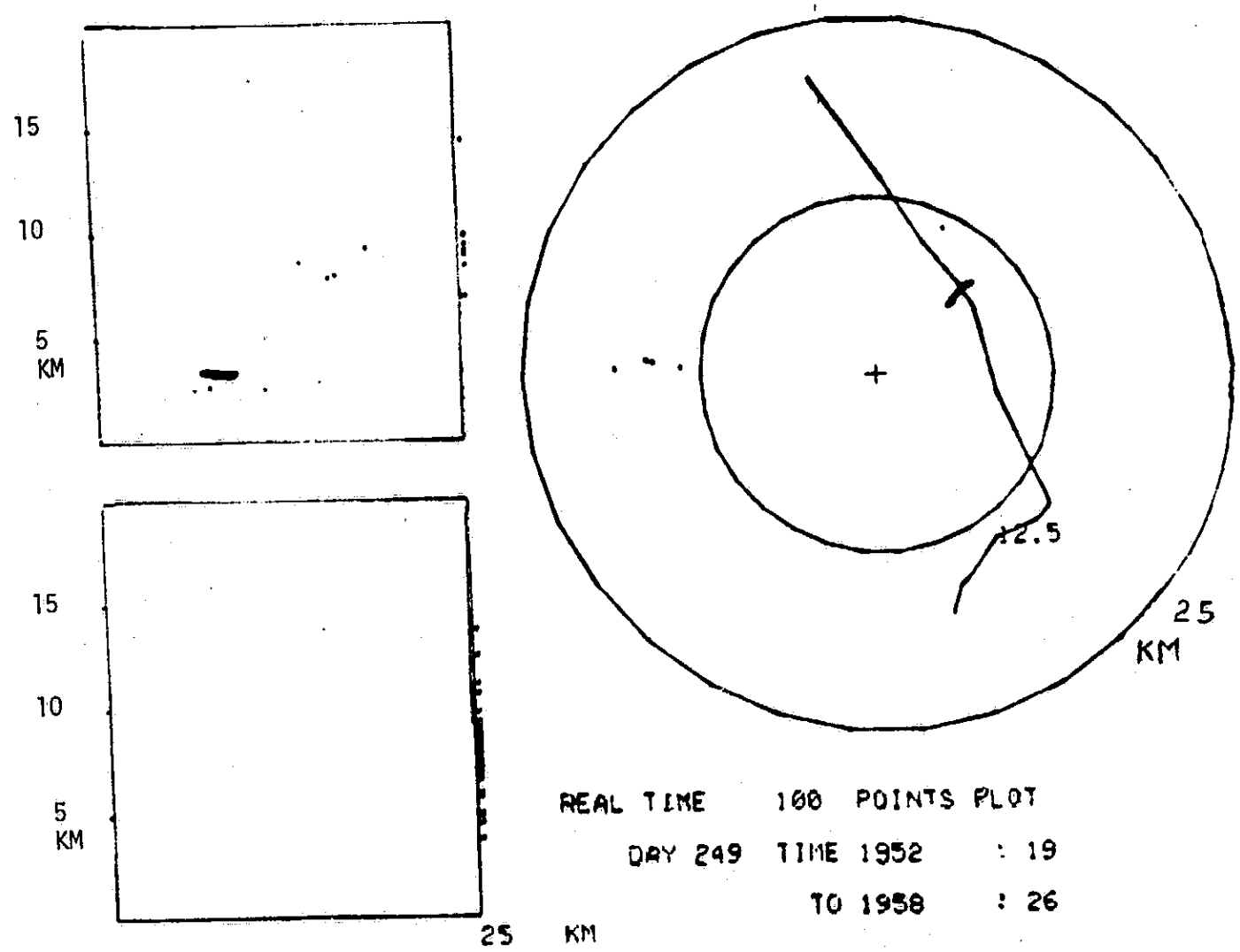

FIG. 24 LDAR PLOT, 1952-1958 GMT,
SHOWING NASA-6 FLIGHT PATH

to Latham[6]. Errors in azimuth, according to the NASA-6 pilot, Marvin Heckendorf, arise from reading of the dials, which are marked in 2 degree increments and can only be read to the nearest degree, and to an allowable 2 degree error in the mandatory 10-hour calibration checks.

Taking just the random one-degree reading error at 50 n. miles gives us a position error of 5236 feet, or 1596 meters. Clearly VOR/DME is not suited for measuring the aircraft position relative to the LDAR system at some 50 n. miles from the nearest VOR/DME station. On the other hand, LDAR is well suited for measuring aircraft position relative to the LDAR station. For example, for ranges up to 10 km the LDAR position error is of the order of 1%, or 100 meters at 10 km. (Poehler, References 2 and 7)

In Figure 15, the plane's flight path between the LDAR positions at the corners has been sketched in. In the other figures, only the corner positions are shown. By design the lightning simulator was only activated at the corners of the flight, so as to avoid competition between the simulator and actual lightning for LDAR system response. Necessary system processing limits the LDAR System response for consecutive signals to 2 milliseconds.

In Figures 25, 27 and 29, we present radar PPI precipitation echo plots superimposed on LDAR maps, at 1909, 1927, and 1945 GMT, respectively, illustrating the growth, and the change in position of the storm, during the peak storm period. In the plots, no LDAR dots are shown, even though there were LDAR discharges at the time.

In Figures 26, 28, and 30, we present the radar RHI precipitation echo plots at 1910, 1925, and 1944 GMT, respectively, illustrating the growth of the height of the cloud.

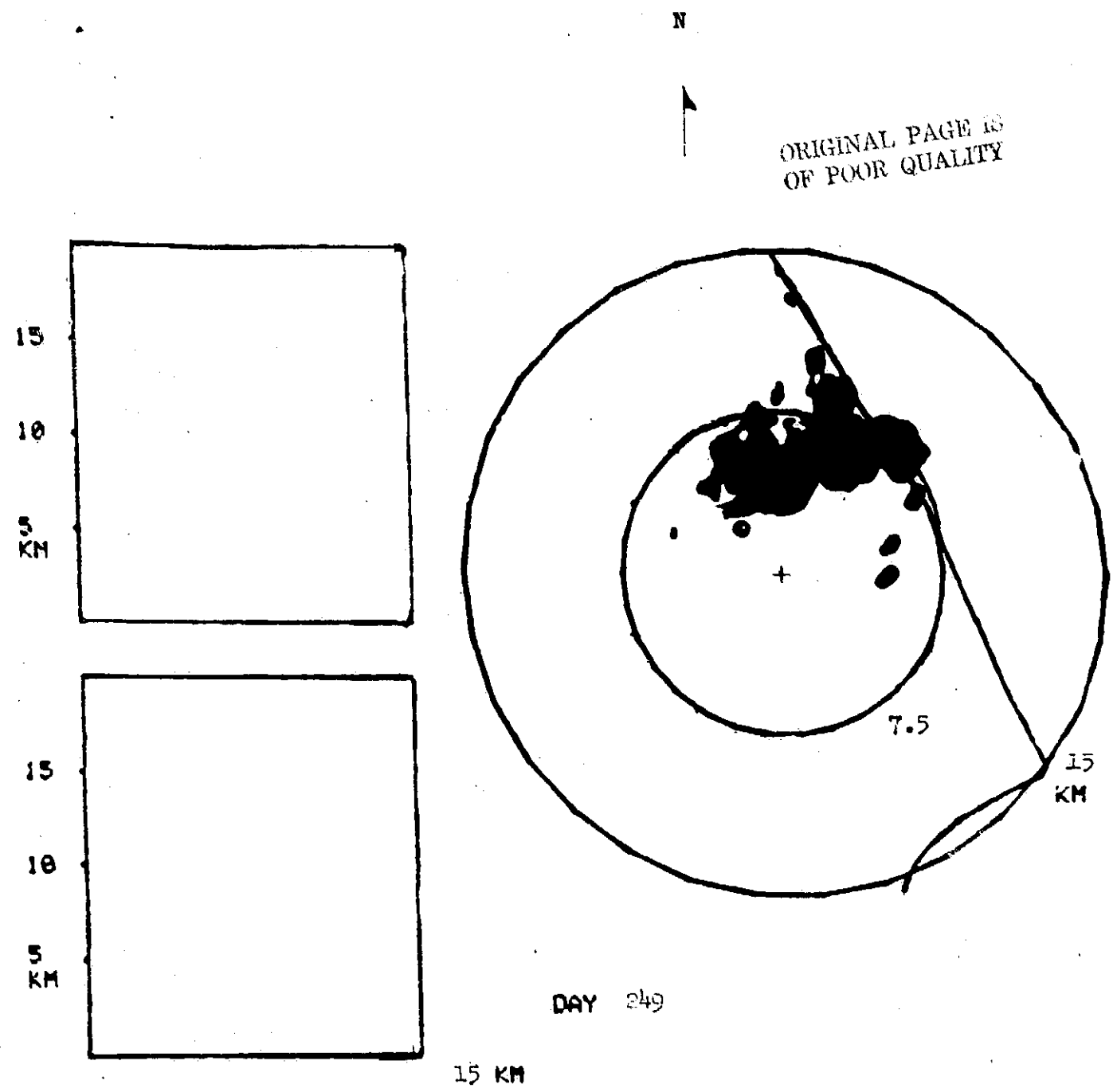

FIG. 25 RADAR PRECIPITATION ECHO OF 1925 GMT SUPERIMPOSED ON LDAR MAP OF 1909 GMT. NO LDAR DOTS ARE SHOWN

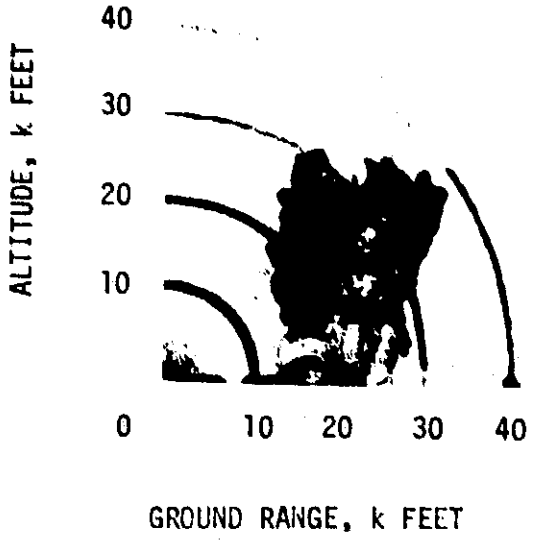

FIG. 26 RADAR PRECIPITATION ECHO,
RHI PLOT 1910 GMT
AZIMUTH 137°

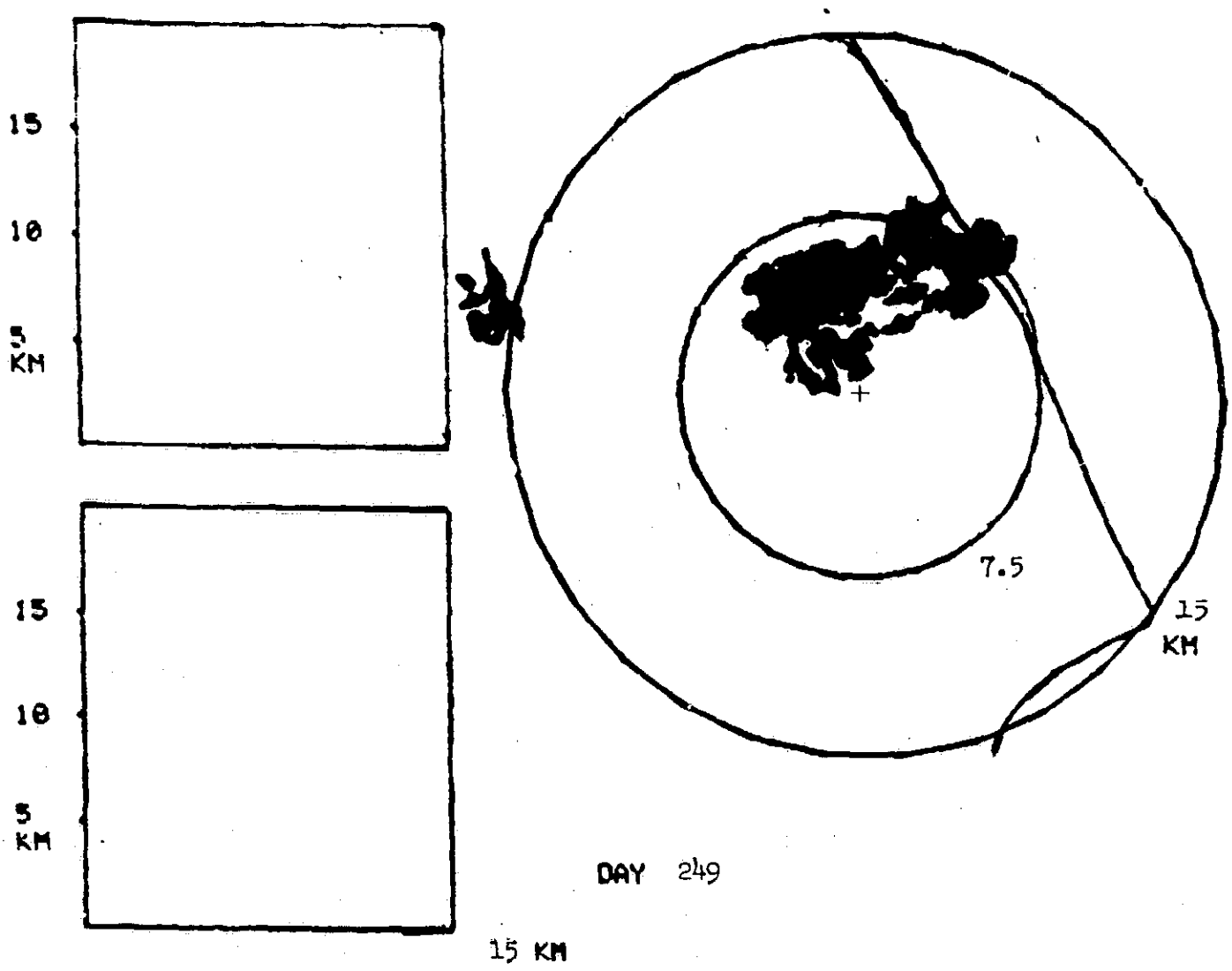

FIG. 27 RADAR PRECIPITATION ECHO OF 1927 GMT SUPERIMPOSED ON LDAR MAP OF 1927 GMT. NO LDAR DOTS ARE SHOWN

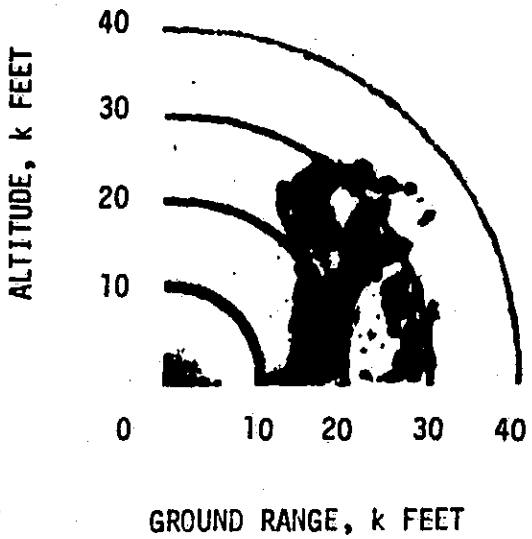

FIG. 28 RADAR PRECIPITATION ECHO,
RHI PLOT 1925 GMT
AZIMUTH 174°

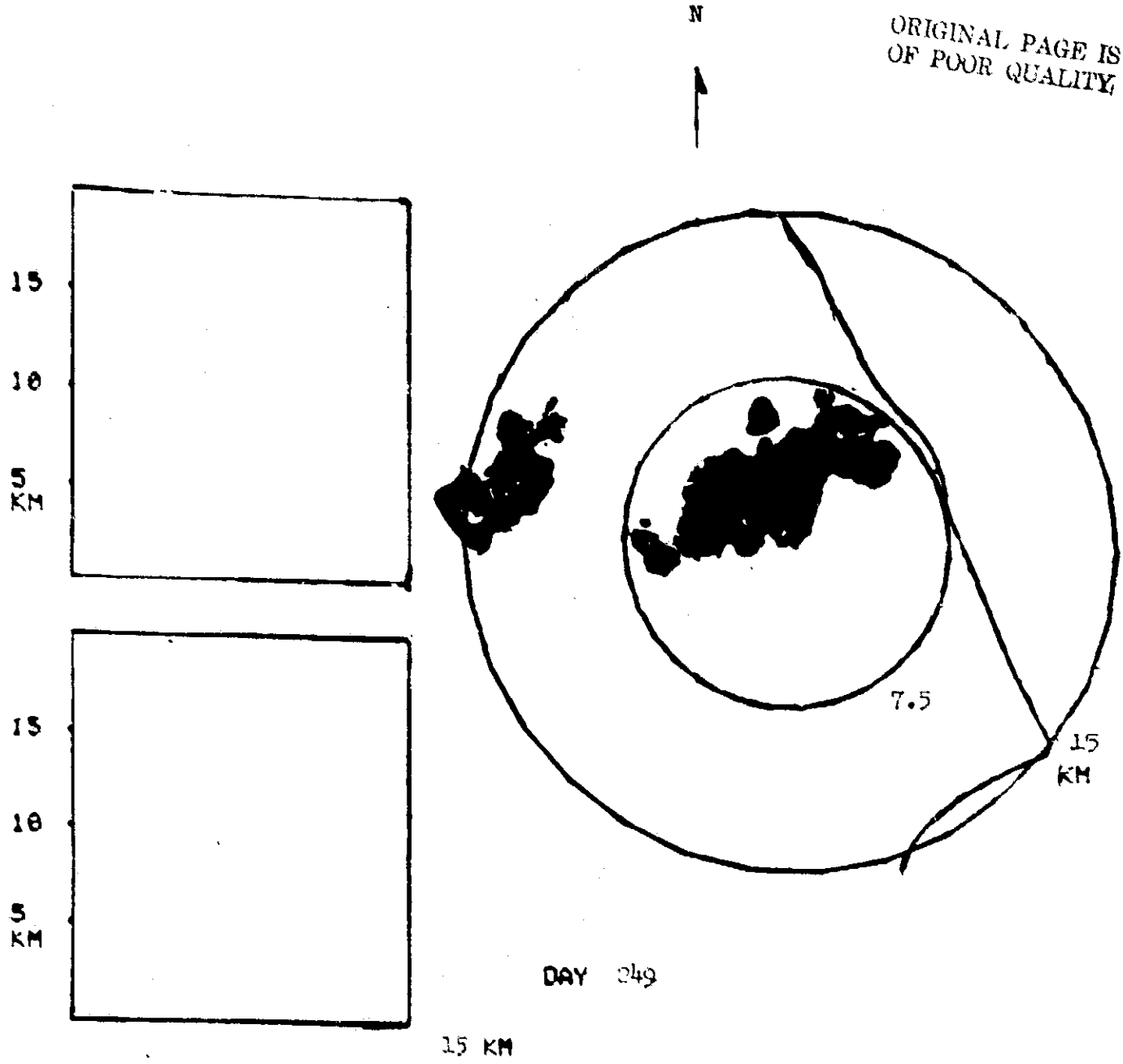

FIG. 29 RADAR PRECIPITATION ECHO OF 1945 GMT
SUPERIMPOSED ON LDAR MAP OF 1945 GMT.
NO LDAR DOTS ARE SHOWN

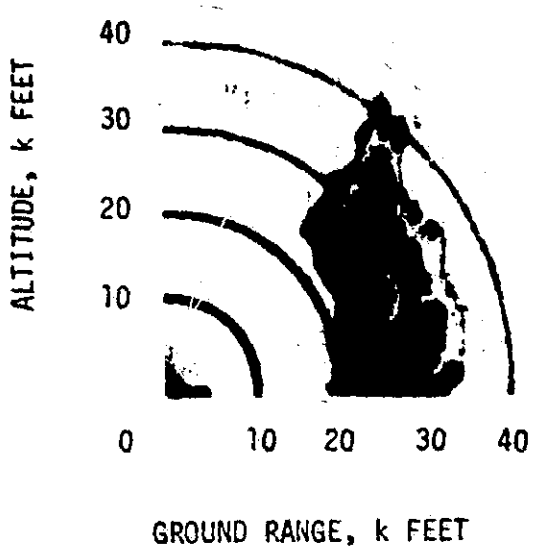

FIG. 30 RADAR PRECIPITATION ECHO,
RHI PLOT 1944 GMT
AZIMUTH 177°

During Phase 3, the Peak of The Storm:

The radar tops ranged from 32,000 to 43,000 feet, as Figure 3 shows.

The ground field mills registered values of as high as -4.39 kV/m at 1928 GMT.

The airborne field mills registered values of as high as -30 kV/m at 1939 GMT.

LDAR data points generally appeared in groups, and had a mean time spacing within the group of 10 milliseconds and a mean $\sqrt{x^2 + y^2}$ spacing of 1.5 km.

A detailed discussion of the "Peak of the Thunderstorm" 1903 to 1947 GMT will be given under the following headings:

III C. Correlation of LDAR, Radar, and Ground-Strike Data

III D. Correlation of LDAR with Field Mill Data

III E. Correlation of Ground Strike Location with Dynamic Field Mill Data

III F. LDAR Discharge Point Distribution Just Before and Just After Ground Strikes

III G. Airborne Field Mill Readings Along Flight Path, and Correlation of Distance to LDAR Discharge with Observed Airborne Field Strength

III H. Ground-Based Field Mills vs Airborne Field Mills

after we finish our discussion of Phase 4.

Phase 4, Decay, 1947-2002 GMT

Reference to Figure 3 indicate the period 1947-2002 GMT to be the decay phase. At 1947 GMT radar tops drop abruptly from 43,000 feet to 29,000 feet. After a ten minute period at 32,000 feet, the radar tops drop abruptly to 14,000 feet, marking the end of the thunderstorm.

No LDAR discharges were recorded after 1947:48.301 GMT.

At 1958 GMT the weather office reported an anvil overhead (at KSC) stretching towards the coast.

During the decay period the ground field mill and airborne field mill readings were surprisingly high, in the face of the absence of any LDAR responses and the absence of any ground strikes. The high readings are attributed to debris from the thundercloud.

Airborne field mills indicated negative F_Z fields from -1 to -4 kV/m, reaching a peak value of -21.7 kV/m on Pass #8 at 1955. Ground field mills generally read negative values above 1 kV/m, reaching a peak of -4.6 kV/m at Site #19 at 2000 GMT. A field mill contour plot for 1956:18 GMT, with the NASA-6 flight path of Run #19 (1952:08 to 1955:56) superimposed, is shown in Figure 31.

Figure 32 shows a 1948-1951 GMT LDAR plot, onto which a radar precipitation PPI plot of 1948 GMT has been superimposed. No LDAR dots are to be seen on this plot, since there were no LDAR discharges during this period. The storm was rapidly decaying. The last LDAR discharge occurred at 1947:48.301 GMT at the (x,y) LDAR coordinates, (-2950, 2317) meters.

The radar RHI precipitation echo of 1949 GMT, Figure 33, shows that there is not much left of the storm.

Phase 4, Decay, 1947-2002 GMT

Reference to Figure 3 indicate the period 1947-2002 GMT to be the decay phase. At 1947 GMT radar tops drop abruptly from 43,000 feet to 29,000 feet. After a ten minute period at 32,000 feet, the radar tops drop abruptly to 14,000 feet, marking the end of the thunderstorm.

No LDAR discharges were recorded after 1947:48.301 GMT.

At 1958 GMT the weather office reported an anvil overhead (at KSC) stretching towards the coast.

During the decay period the ground field mill and airborne field mill readings were surprisingly high, in the face of the absence of any LDAR responses and the absence of any ground strikes. The high readings are attributed to debris from the thundercloud.

Airborne field mills indicated negative F_Z fields from -1 to -4 kV/m, reaching a peak value of -21.7 kV/m on Pass #8 at 1955. Ground field mills generally read negative values above 1 kV/m, reaching a peak of -4.6 kV/m at Site #19 at 2000 GMT. A field mill contour plot for 1956:18 GMT, with the NASA-6 flight path of Run #19 (1952:08 to 1955:56) superimposed, is shown in Figure 31.

Figure 32 shows a 1948-1951 GMT LDAR plot, onto which a radar precipitation PPI plot of 1948 GMT has been superimposed. No LDAR dots are to be seen on this plot, since there were no LDAR discharges during this period. The storm was rapidly decaying. The last LDAR discharge occurred at 1947:48.301 GMT at the (x,y) LDAR coordinates, (-2950, 2317) meters.

The radar RHI precipitation echo of 1949 GMT, Figure 33, shows that there is not much left of the storm.

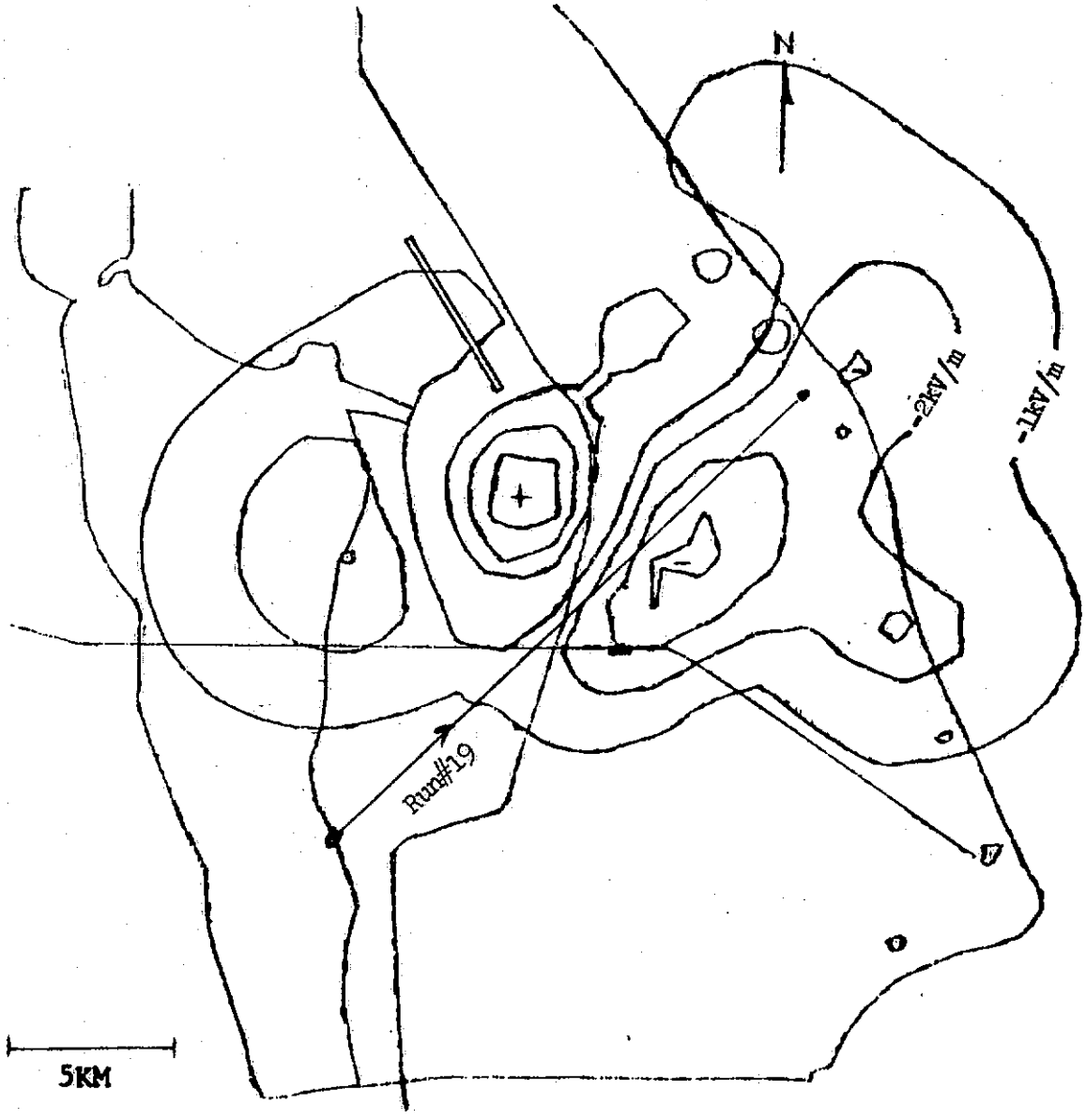

KSC EQUIPOTENTIAL
GRADIENT CONTOURS

09/06/77 1956:18.209 GMT

Line Scale - 1000 V/M

Site #	Volts/M
1	-2385
2	569
3	-447
4	-324
5	261
6	232
7	15
8	-847
9	-477
10	-290
11	-416
12	1215
13	-2908
14	-3000
15	-754
16	-1985
17	3799
18	-903
19	-4139
20	-3554
21	-2324
22	-847
23	-321
24	-139

FIG. 31 FIELD MILL CONTOUR PLOT, 1956 GMT

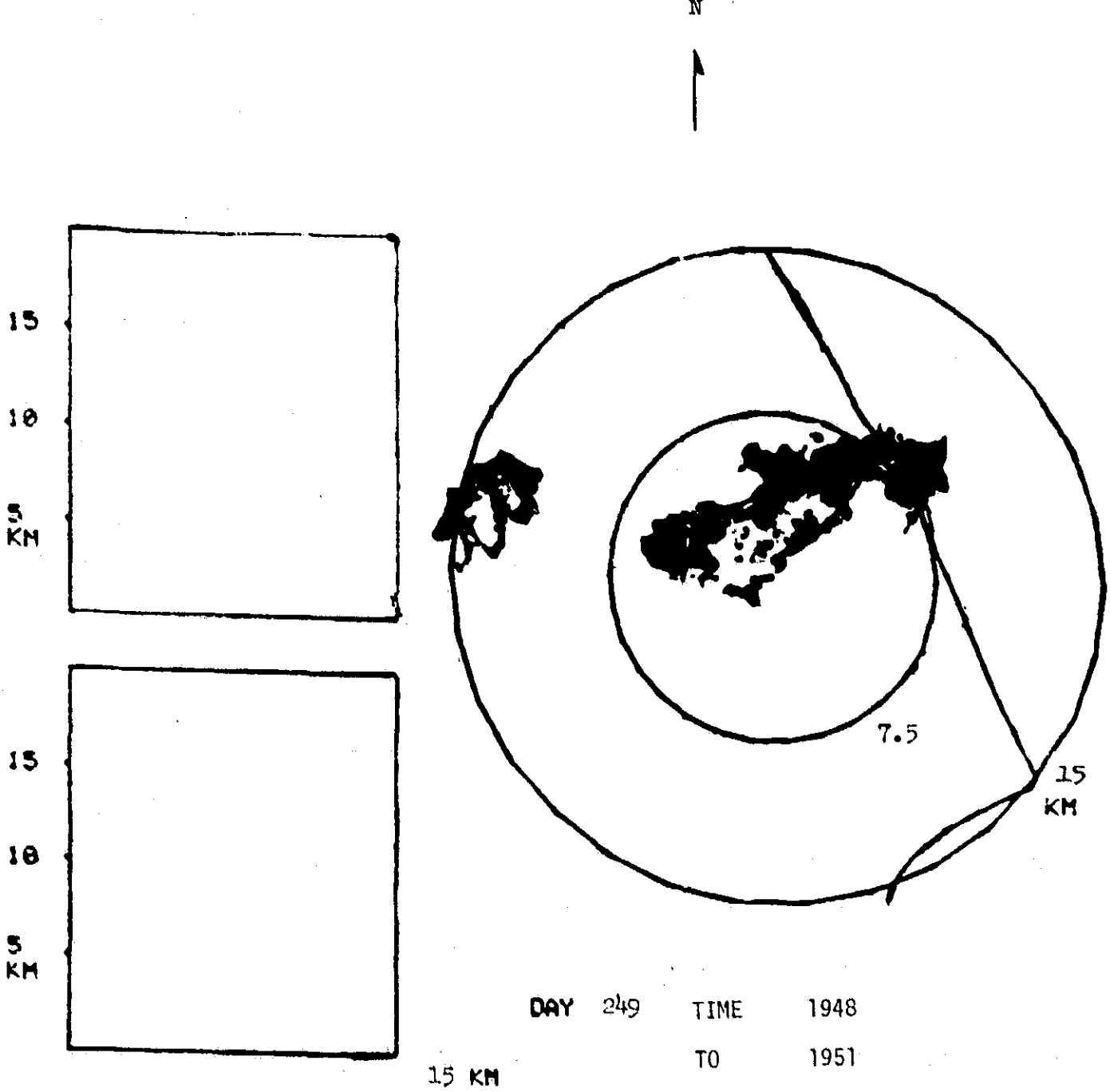

FIG. 32 RADAR PRECIPITATION ECHO,
PPI PLOT 1948 GMT
SUPERIMPOSED ON LDAR PLOT
1948-1951 GMT

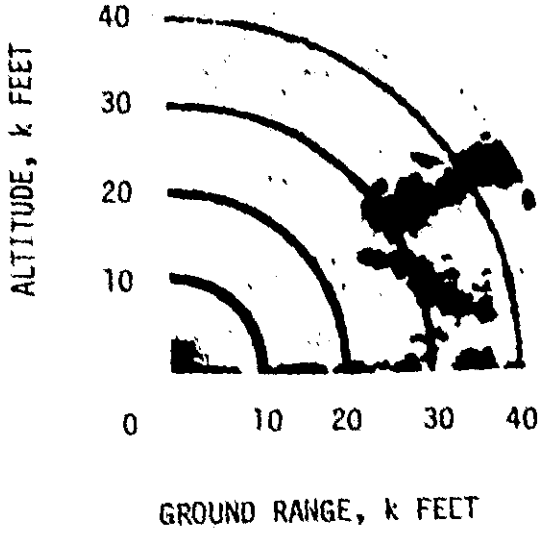

FIG. 33 RADAR PRECIPITATION ECHO,
RHI PLOT 1949
AZIMUTH 129°

III C. CORRELATION OF LDAR, RADAR, AND GROUND STRIKE DATA

Data for the thirteen ground strikes occurring during the peak (1903 to 1947 GMT) thunderstorm period are presented. Radar precipitation echoes and ground strike locations (as determined by the Ground Strike Location System) have been added to the LDAR plots covering the period of approximately two minutes before the ground strike.

The composite LDAR plots for ground strikes that occurred at

1903:52.728 GMT	1920:06.001 GMT	1926:09.005 GMT
1908:04.285 GMT	1920:06.059 GMT	1929:43.902 GMT
1916:11.625 GMT	1922:38.290 GMT	1933:01.796 GMT
1918:52.212 GMT	1926:09.002 GMT	1944:20.670 GMT

and 1944:55.384 are given in Figures 34 to 43. In these plots the position of the ground strike is indicated by two small concentric circles ◎. The plots were selected to show all the LDAR discharges that occurred approximately two minutes before the ground strike. The exact time of coverage is shown on each plot.

In Figure 34 the path of the airplane between the two corner positions is sketched in. In the other plots the position of the airplane may or may not appear on one of the corners, depending on the position of the airplane during the interval of the plot.

The mean X, Y, and R, and the standard deviation σ_X, σ_Y, σ_R of the ground strike location, as determined by the Ground Strike Location System, are given in Table II.

The standard deviation was derived from the various independent solutions for ground strike location made possible by the redundant data provided by the seven electric field ground stations (see Appendix D). An estimate of the precentage error in range is provided by taking the standard

TABLE II

GROUND STRIKE LOCATION AS DETERMINED BY THE GROUND STRIKE LOCATION SYSTEM

TIME GMT	POSITION, IN LDAR COORDINATES						
	X, meters		Y, meters		R, meters	σ_R meters	Estimated Accuracy, in Range $\frac{\sigma_R \times 100}{R}$ %
	$\bar{X}$	σ_X	$\bar{Y}$	σ_Y			
1903:52.728	1033	201	2969	68	3143	212	6.7
1908:04.285	1945	73	5058	50	5419	88	1.6
1916:11.625	7462	118	-744	22	7499	120	1.6
1918:52.212	1836	44	3137	96	3634	105	2.9
1920:06.001	35	15	3880	80	3880	81	2.0
1920:06.059	-1231	10	3748	10	3944	14	0.4
1922:38.290	-501	11	4771	45	4797	46	0.96
1926:09.002	-4462	19	7590	33	8808	38	0.4
1926:09.005	-861	153	4106	205	4195	255	6.1
1929:43.902	-5224	154	7893	108	9455	188	2.0
1933:01.796	-2067	17	1297	61	2440	63	2.6
1944:20.670	-6485	44	1557	15	6669	46	0.7
1944:55.384	-6742	32	2441	56	7170	64	0.9
						Mean	2.2
						Std. Dev.	1.9
						Median	1.6

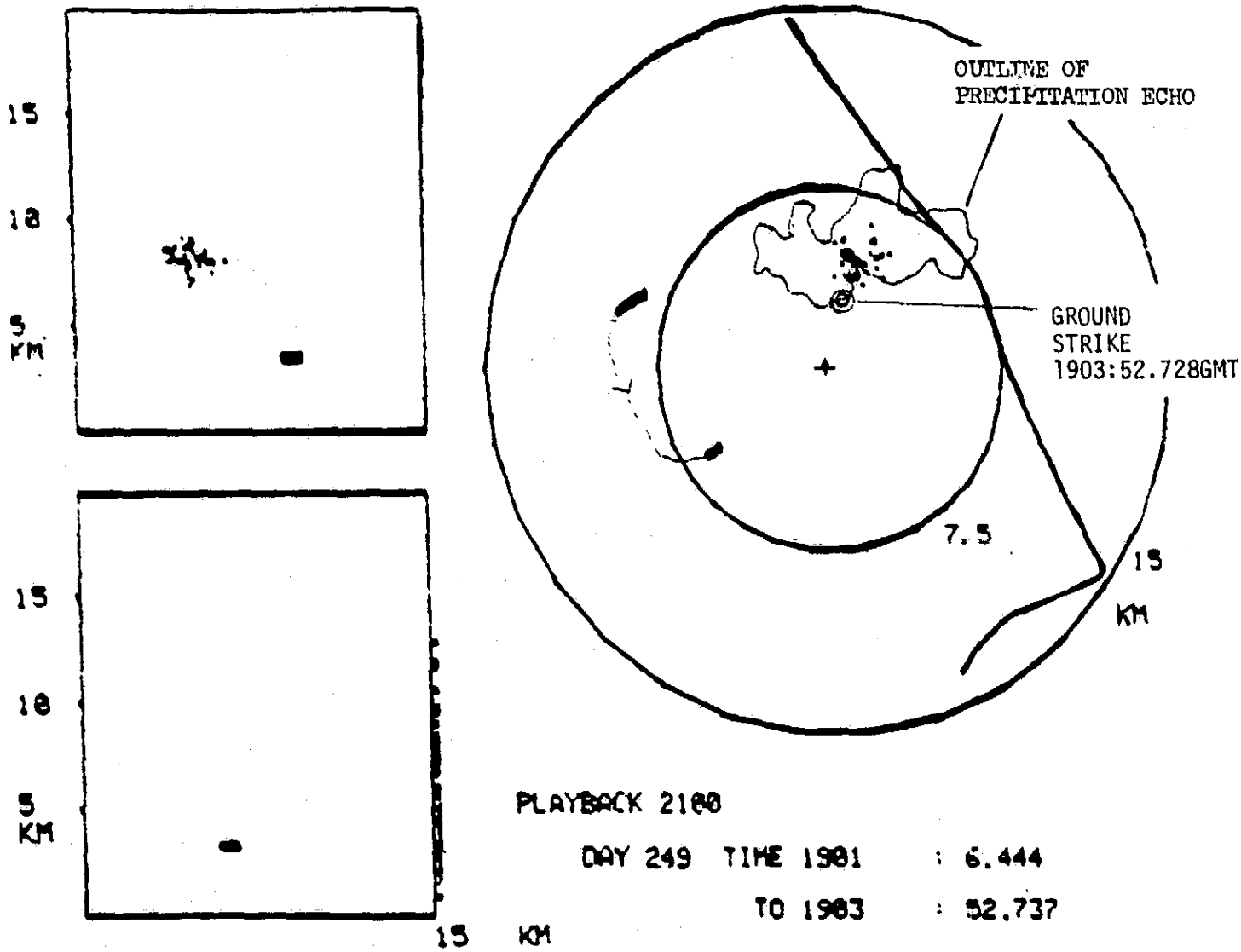

FIG. 34 COMPOSITE LDAR PLOT WITH RADAR PRECIPITATION ECHO OF 1904 GMT, AND GROUND STRIKE LOCATION © AT 1903:52.728 GMT @ (1.03, 2.97) km

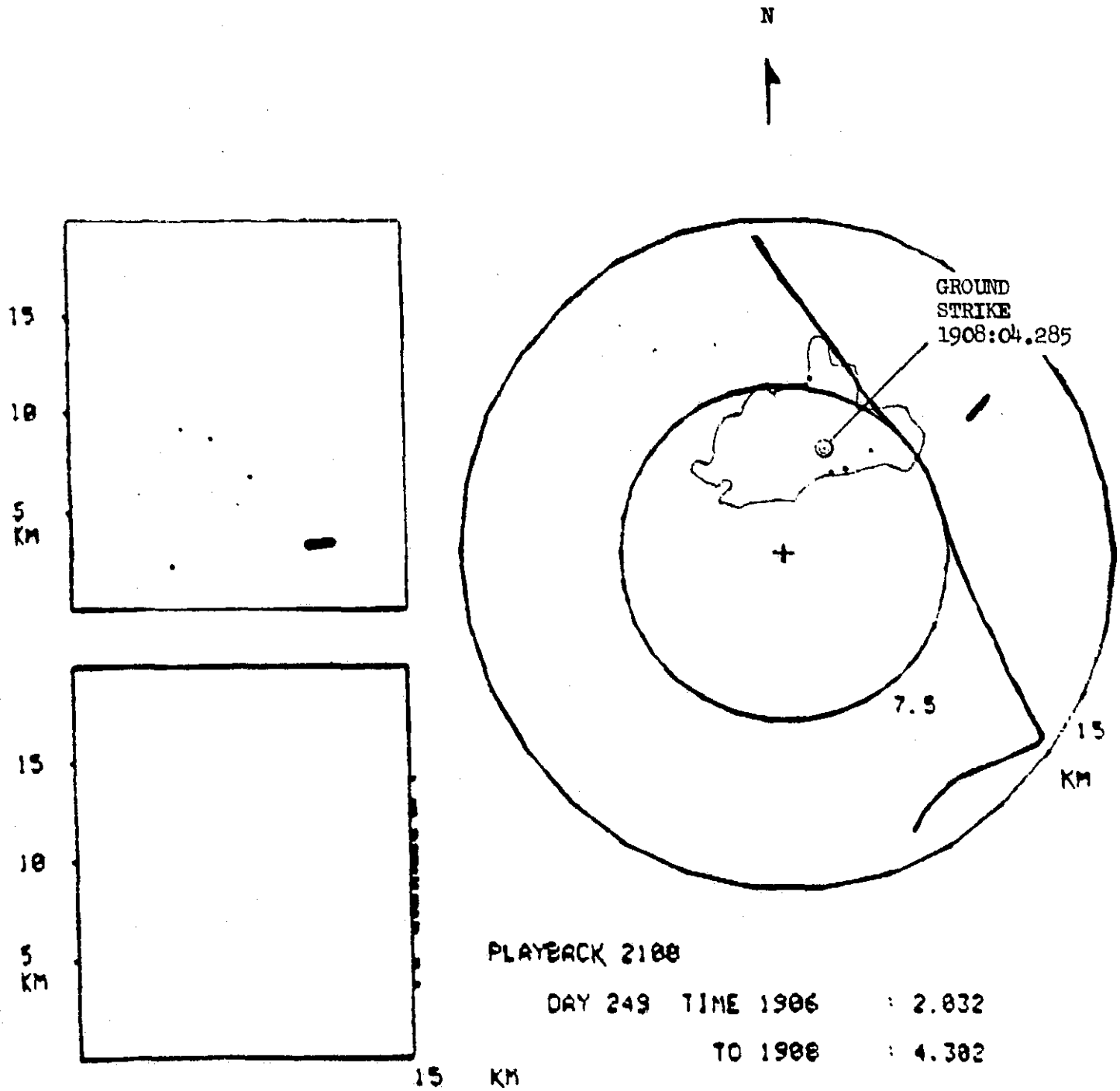

FIG. 35 COMPOSITE LDAR PLOT WITH RADAR PRECIPITATION ECHO OF 1905 GMT, AND GROUND STRIKE LOCATION @ AT 1908:04.285 GMT @ (1.95, 5.06) km

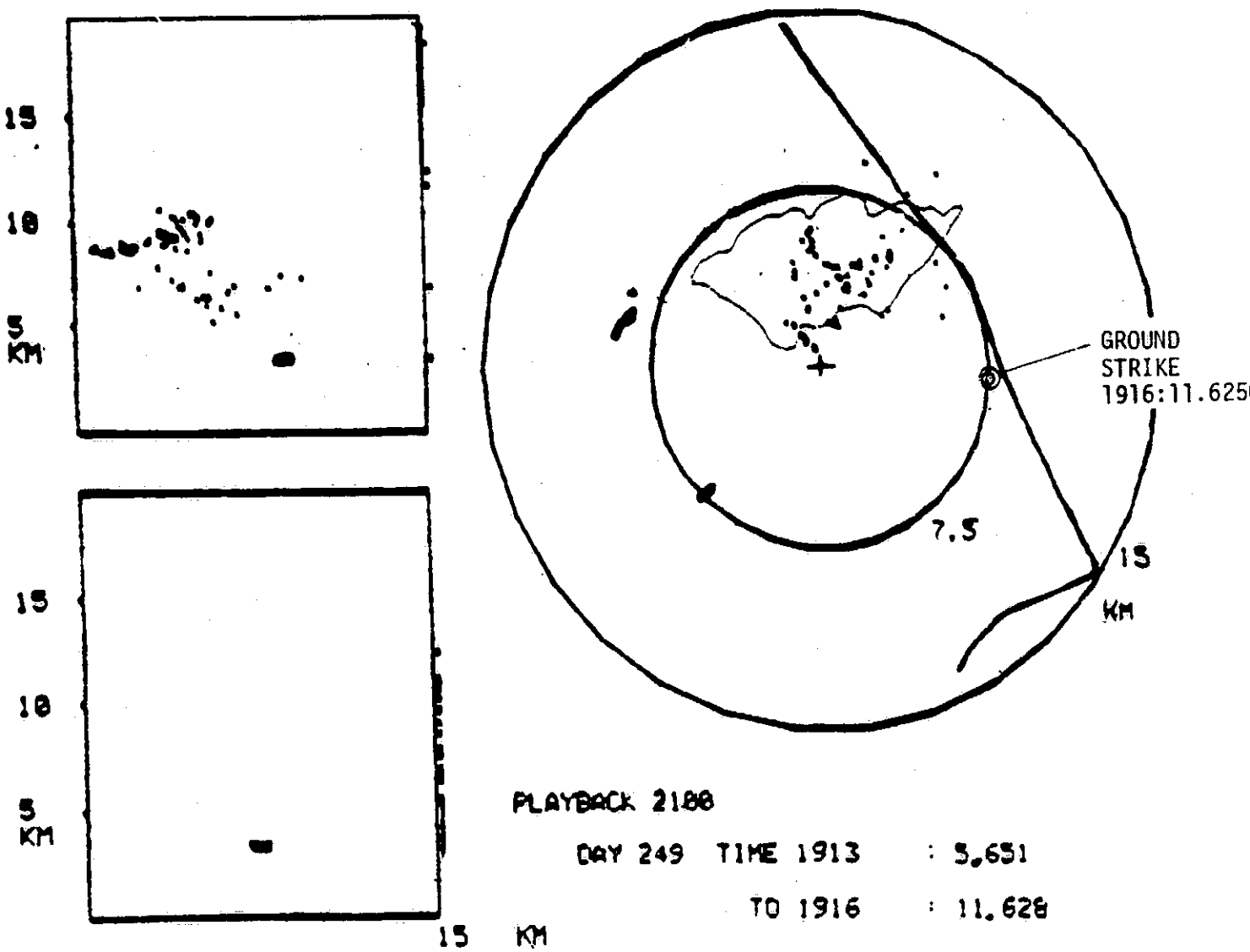

FIG. 36 COMPOSITE LDAR PLOT, WITH RADAR PRECIPITATION ECHO OF 1918 GMT, AND GROUND STRIKE LOCATION © AT 1916:11.625 GMT @ (7.46, -0.74) km

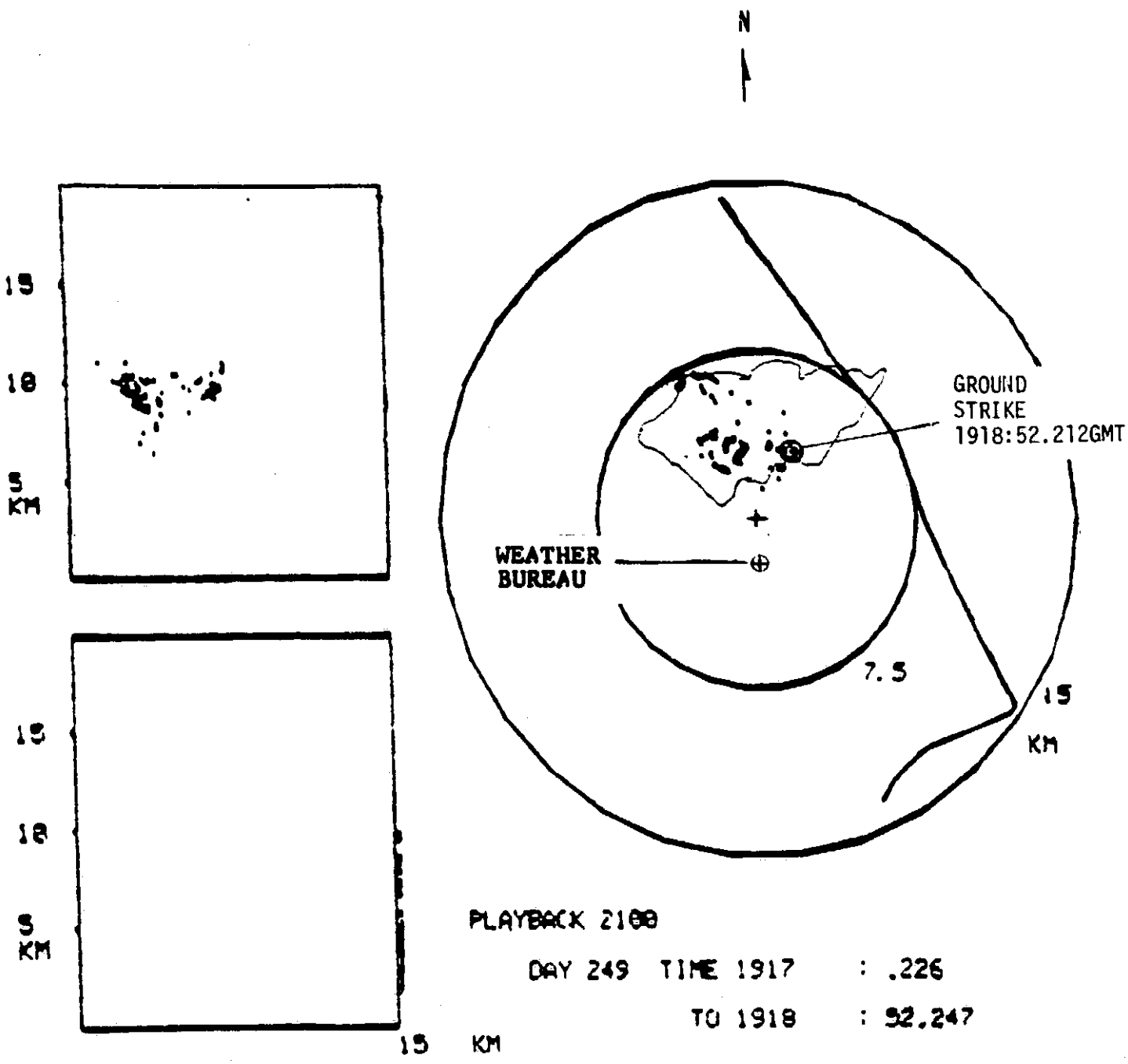

FIG. 37 COMPOSITE LDAR PLOT, WITH RADAR PRECIPITATION ECHO OF 1918 GMT, AND GROUND STRIKE LOCATION◎ AT 1918:52.212 GMT @ (1.84, 3.14) km

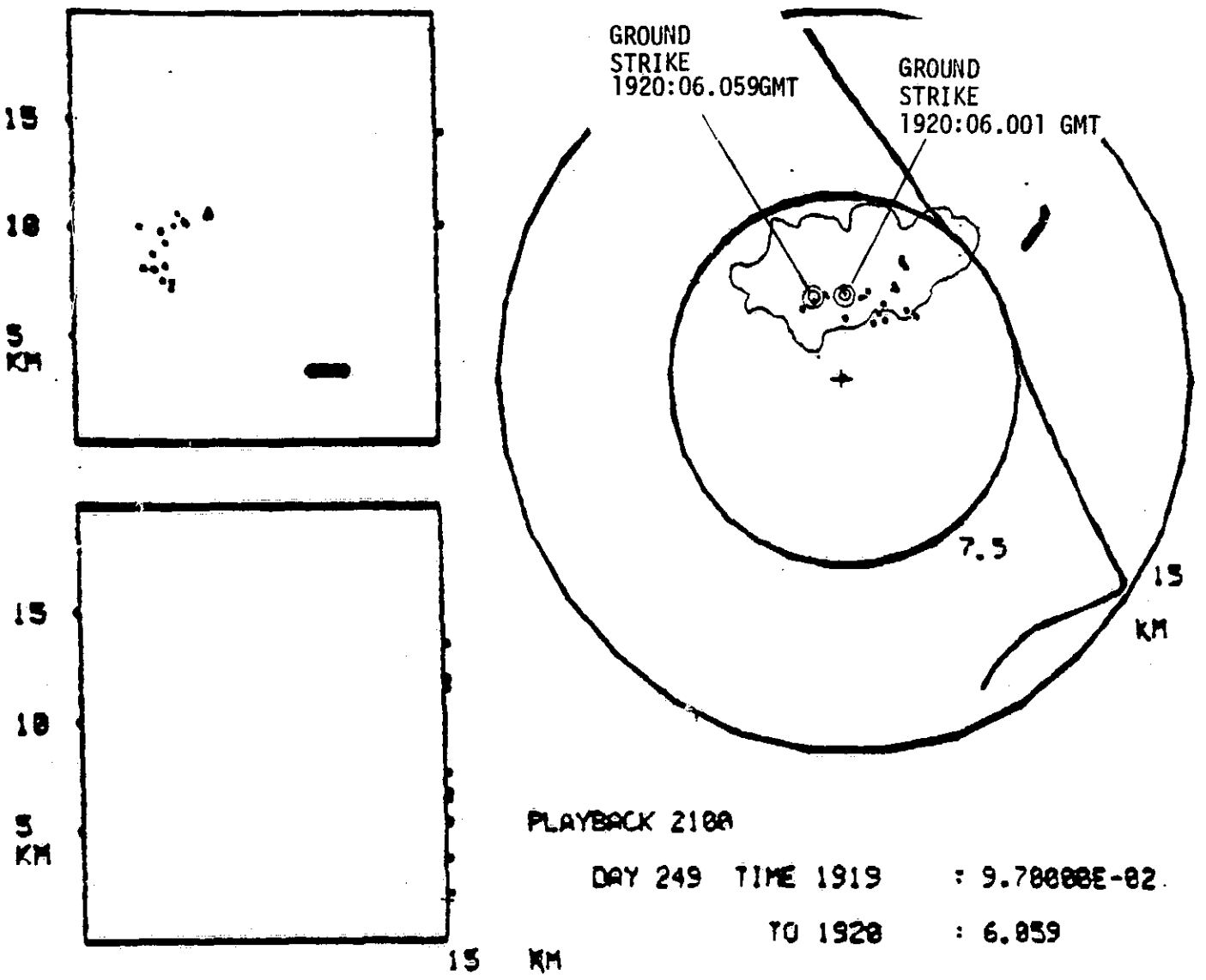

FIG. 38 COMPOSITE LDAR PLOT, WITH RADAR PRECIPITATION ECHO OF 1919 GMT, AND GROUND STRIKE LOCATIONS AT 1920:06.001 AND 1920:06.059 GMT @ (0.04, 3.88) and (-1.23, 3.75) km

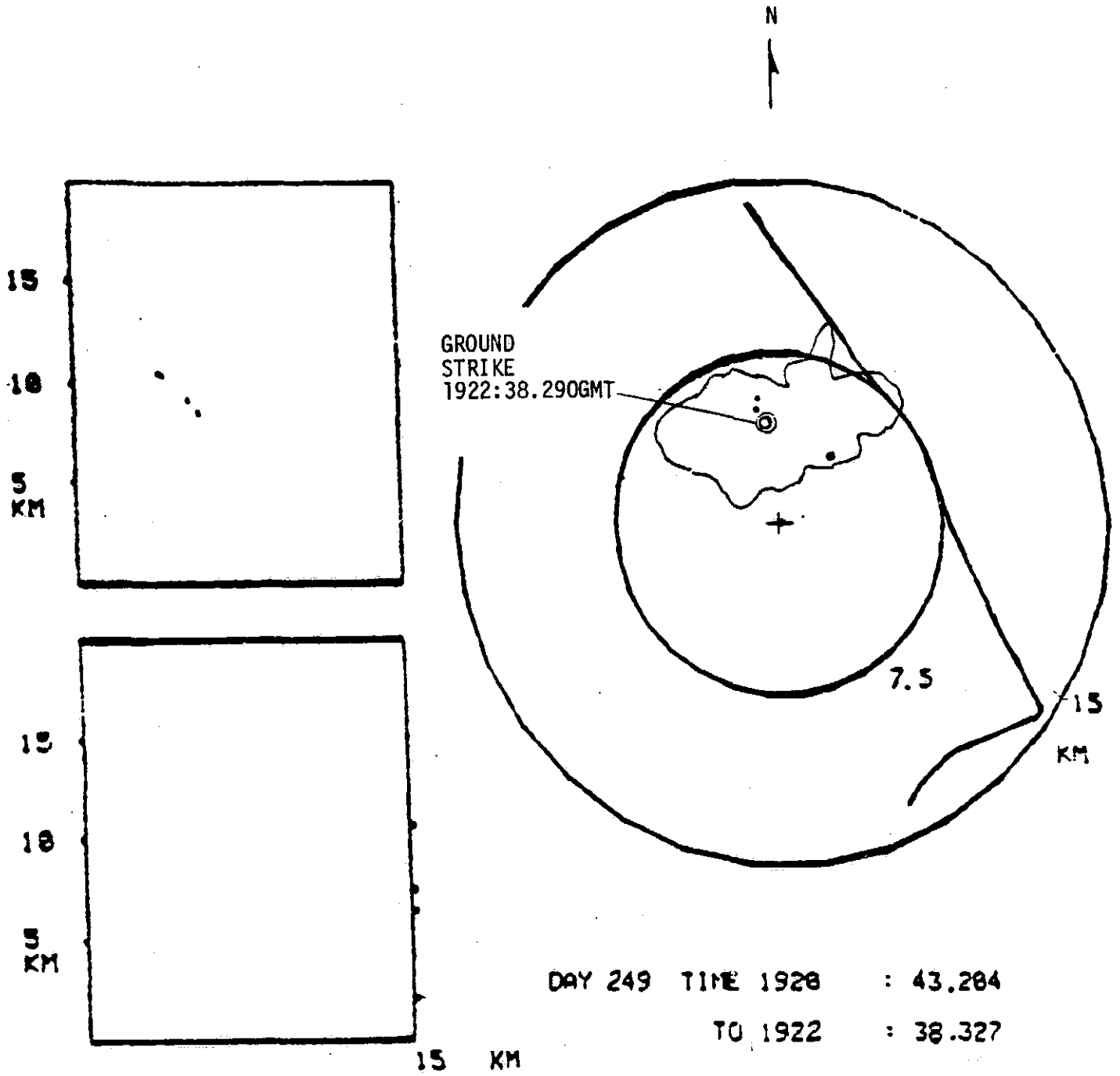

FIG. 39 COMPOSITE LDAR PLOT, WITH RADAR PRECIPITATION ECHO OF 1920 GMT, AND GROUND STRIKE LOCATIONS AT 1922:38.290 GMT @ (-0.50, 4.77) km

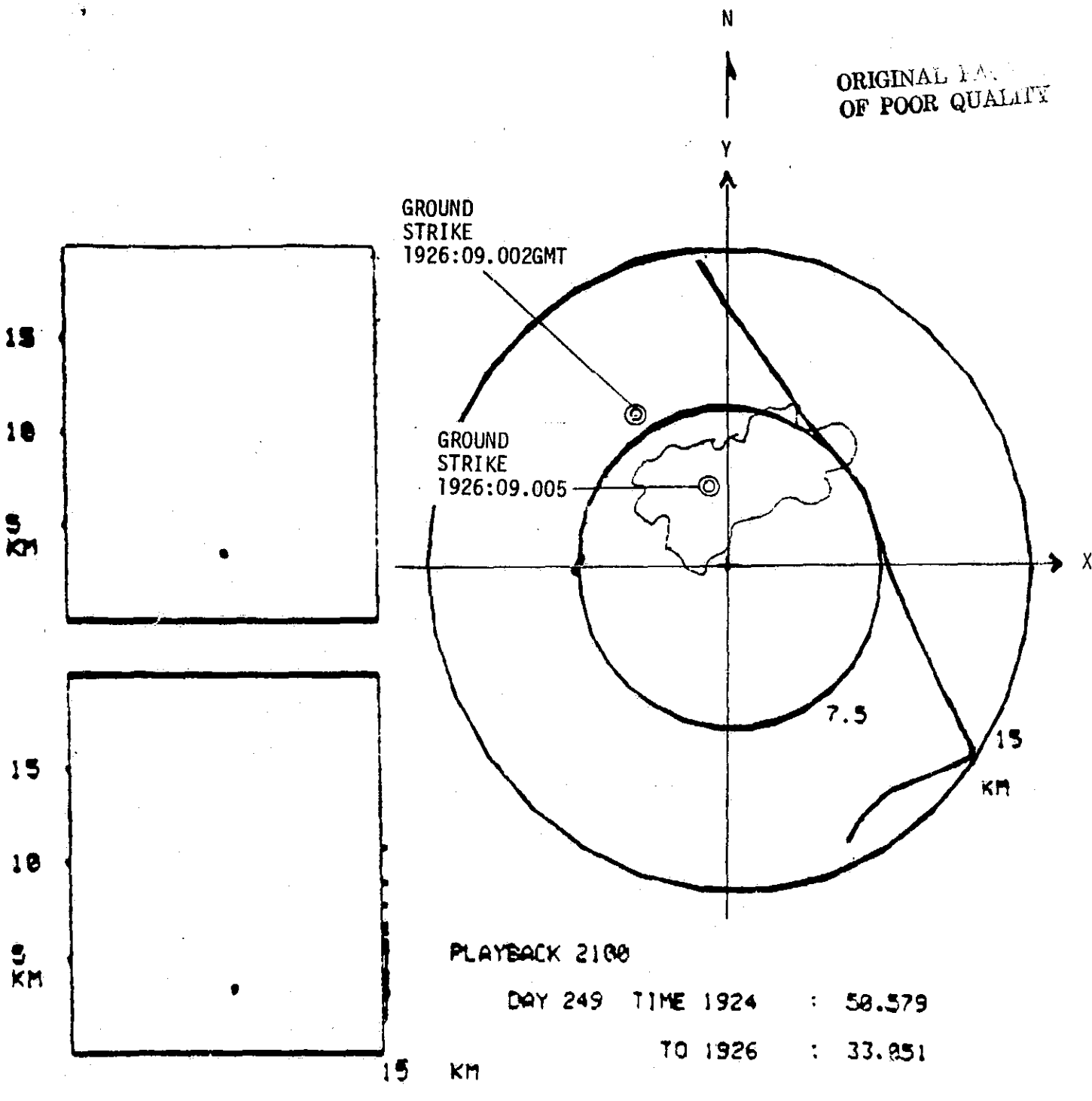

FIG. 40 COMPOSITE LDAR PLOT, WITH RADAR PRECIPITATION ECHO OF 1927 GMT, AND GROUND STRIKE LOCATIONS AT 1926:09.002 AND 1926:09.005 GMT @ (-4.46, 7.59) and (0.86, 4.11) km

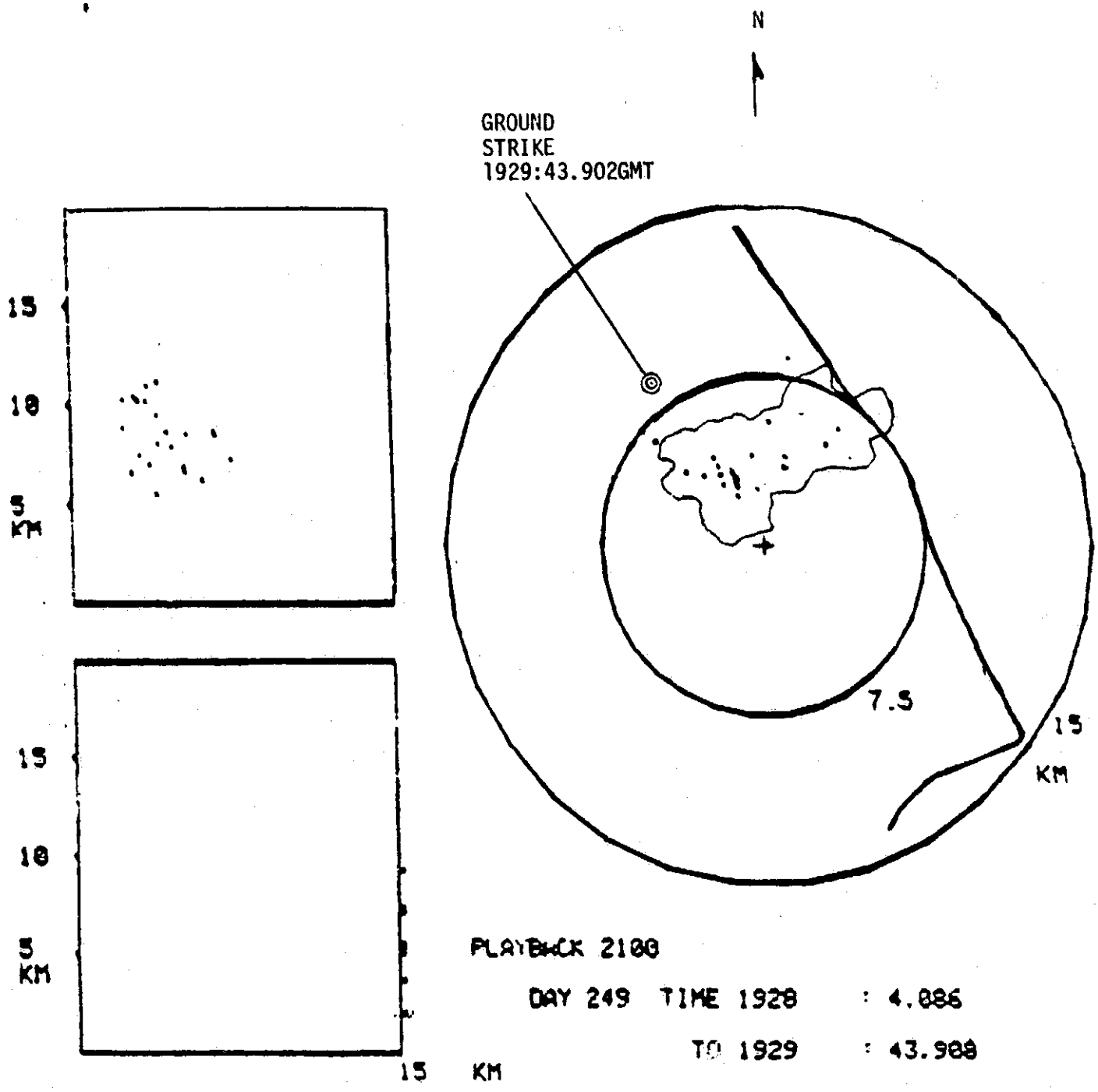

FIG. 41 COMPOSITE LDAR PLOT, WITH RADAR PRECIPITATION ECHO OF 1928 GMT, AND GROUND STRIKE LOCATION AT 1929:43.902 GMT @ (-5.22, 7.89) km

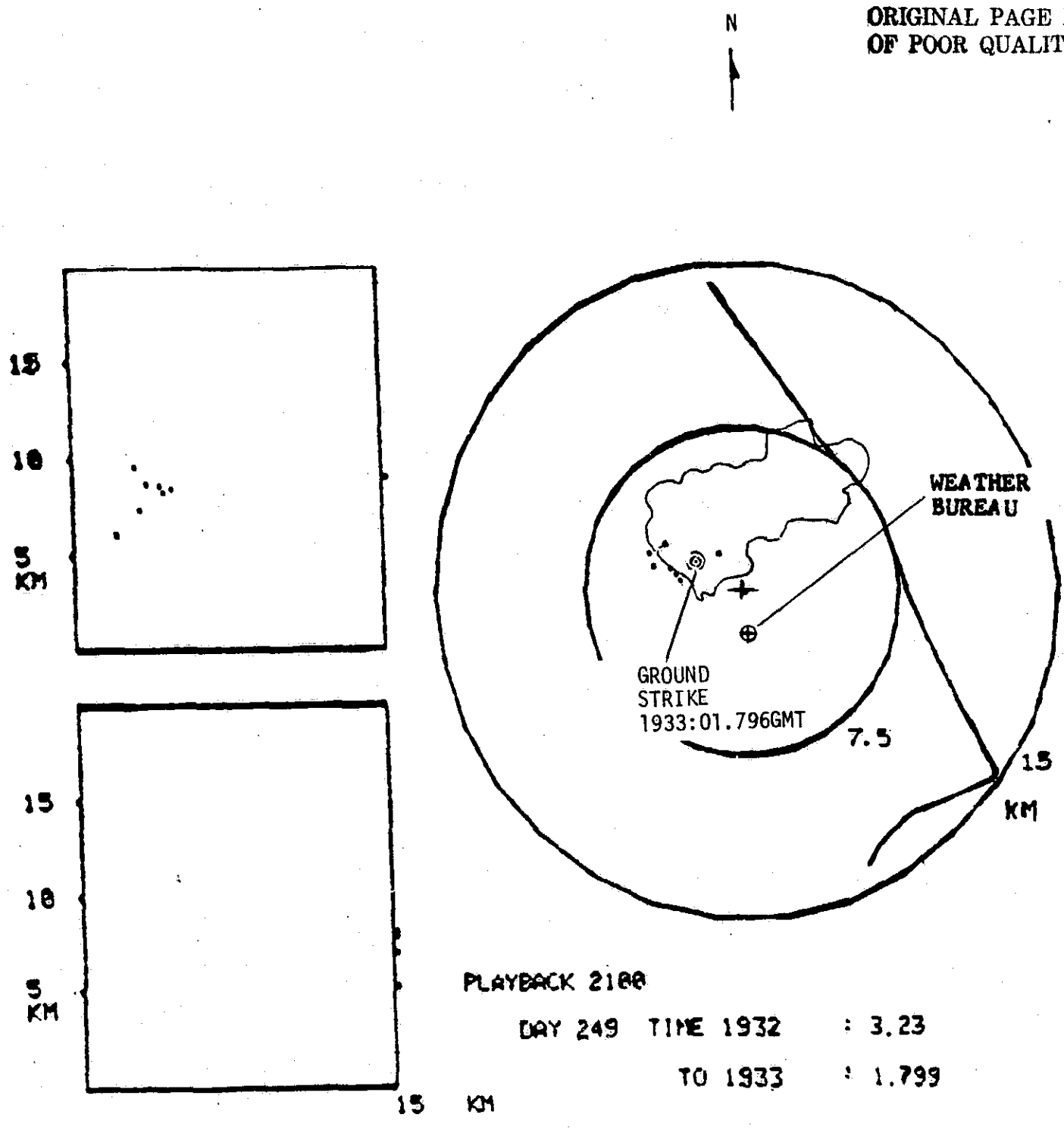

FIG. 42 COMPOSITE LDAR PLOT, WITH RADAR PRECIPITATION ECHO OF 1928 GMT, AND GROUND STRIKE LOCATION AT 1933:01.796 GMT @ (-2.07, 1.30) km

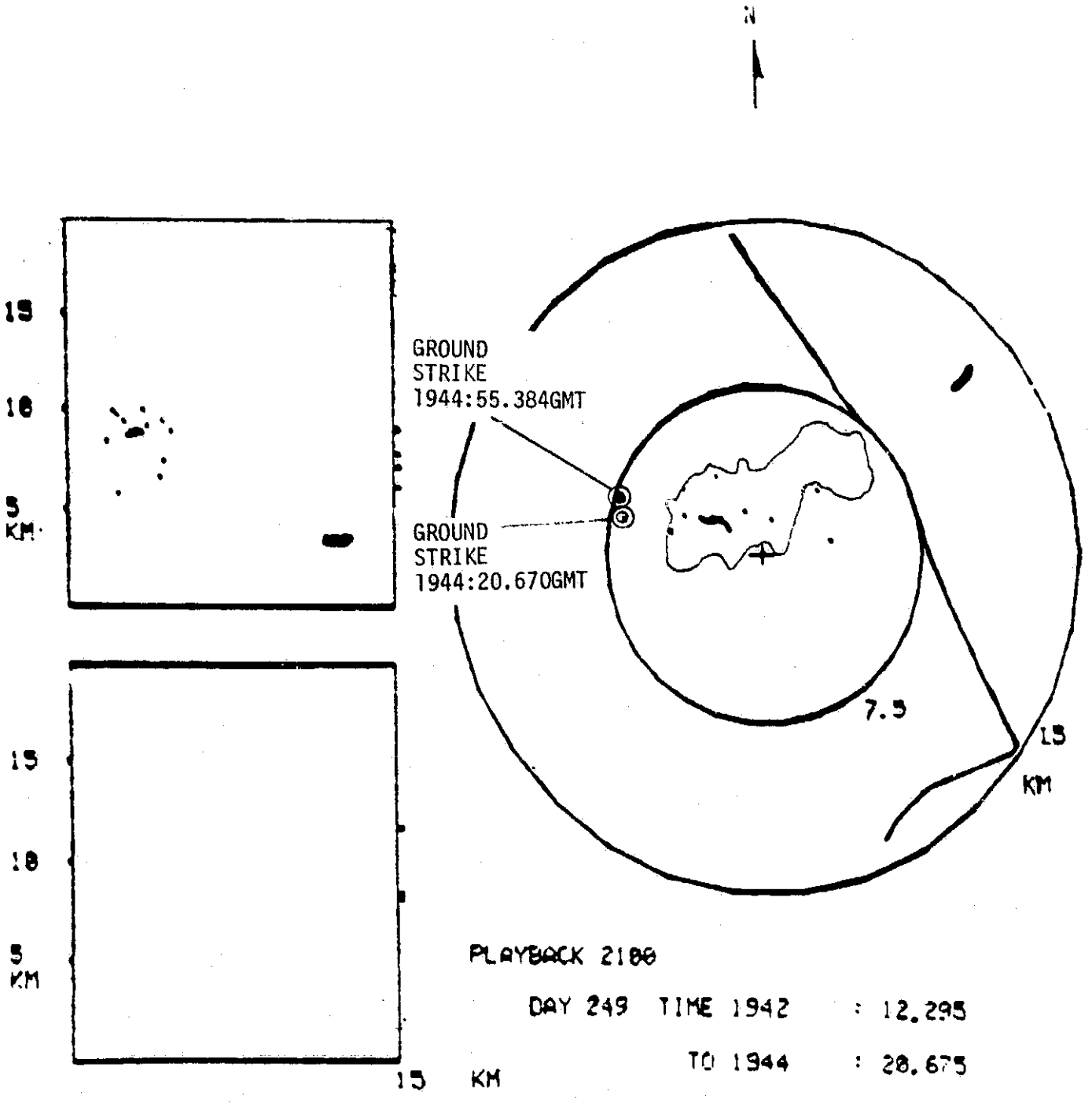

FIG. 43 COMPOSITE LDAR PLOT, WITH RADAR PRECIPITATION ECHO AT 1945 GMT, AND GROUND STRIKE LOCATIONS AT 1944:20.670 GMT AND 1944:55.384 GMT @ (-6.49, 1.56) and (-6.74, 2.44) km

deviation σ_R as a percentage of the range, R. The calculations give a mean of 2.2%, and a median of 1.6%.

Physical verification of the location of the ground strikes was not readily available because they took place in the undeveloped areas of the Kennedy Space Center. However, two of the ground strikes that were detected with the GSLS System were confirmed* by the KSC Weather Bureau, with the following notations of visual sightings in their logs: "1918 GMT cloud-to-ground strike at 30 degrees, 10-15 seconds delay" and "1933 GMT cloud-to-ground strike, 330 degrees azimuth, 7 second delay". The location of the KSC weather station has been marked on Figure 37 (1918:51.212 strike), and on Figure 42 (1933:01.796) strike. From Figures 37 and 42 we determine the azimuth and delay time to be 15 degrees, 15 seconds, and 325 degrees, 12 seconds, respectively. For ready comparison, the Weather Bureau observations, together with the GSLS observations are listed in Table III.

TABLE III

COMPARISON OF VISUALLY-OBSERVED GROUND-STRIKE LOCATIONS WITH GROUND-STRIKE LOCATIONS DETERMINED BY GSLS SYSTEM

	VISUAL OBSERVATION BY THE WEATHER BUREAU		GSLS LOCATION, (FROM FIGS. 37 & 42)	
TIME	AZIMUTH	DELAY	AZIMUTH	DELAY
1918:51.212	30°	10-15 sec.	15°	15 sec.
1933:01.796	330°	7 sec.	325°	12 sec.

---

* Note added in printing. Excellent confirmation of GSLS ground strike data was obtained on a recent strike to the catenary wire at Pad 39A. The catenary wire was instrumented to measure its current and waveform. Confirming photographic data was available. The GSLS System determined the ground strike to be at (4059,7596) which differs by only 23 m.,(0.3%) in range from the known position of the catenary wire (4048,7616)m.

Considering that the Weather Bureau observations of azimuth were made visually, and that the delay time was determined by looking at a wall clock, the agreement is remarkably good.

More than two of the thirteen ground strikes recorded by the GSLS System might have been confirmed by the Weather Bureau except that:1) at least four (Figures 40, 41, and 43) of the ground strikes occurred on the other side of the cloud, and possibly could not be observed through the cloud, 2) one (Figure 36) would not have been visible from the Weather Bureau because of lack of visibility in this direction, and 3) the observations of ground strikes is secondary to other functions of the Weather Bureau.

Correlation of Ground Strike Location with the Position of LDAR Cloud Discharges

Figures 34-43 not only correlate the position of the radar precipitation echoes with the position of the LDAR cloud discharges, but also correlate the LDAR cloud discharges with the subsequent ground strikes. The latter is a first. This is the first time that a correlation of LDAR cloud discharge data with subsequent ground strikes has been presented. This type of data is important since it helps to predict the position that a ground strike is likely to take place, given the position of the LDAR discharges.

Figures 34 to 43 provide us with the ground strike/to the edge of the radar precipitation echo distances, and the "ground strike/to the LDAR data point center distances" shown in Table IV.

The data shows that 50% of the ground strikes fell within 2.1 km of the center of the LDAR discharge data points, 90% fell within 5.5 km, and 100% fell within 7.8 km.

TABLE IV

STATISTICS OF STRIKE DISTANCES FROM THE EDGE OF THE PRECIPITATION ECHO, AND FROM THE CENTER OF THE LDAR DISCHARGES

TIME	FROM THE EDGE OF THE PRECIPITATION ECHO	FROM THE CENTER OF THE LDAR DISCHARGES
GMT	km	km
1903:52.728	0	2
1908:04.285	1.5	1.6
1916:11.625	5.5	7.8
1918:52.212	0.5	2.1
1920:06.001	1.4	1.9
1920:06.059	1.4	2.9
1922:38.290	1.9	1
1926:09.002	2.0	---
1926:09.005	2.3	---
1929:43.902	2.7	5.5
1933:01.796	0.9	1.2
1944:20.67	2	4.3
1944:55.384	2.0	4.5
Mean	1.9	3.2
Std. Dev.	1.3	2.1
Median	1.7	2.1

LDAR Data Point Distribution Relative to the Radar Precipitation Echo

It is significant that the ground strikes generally fell very near the edge of the precipitation echo. In our series 50% fell within 1.7 km of the edge, and 100% fell within 2.7 km of the edge.

The fact that LDAR discharge data points occur only over a small portion of the radar precipitation echo has already been pointed out in an earlier report[1], and should not come as a surprise. Basically the radar and the LDAR Systems respond to different phenomena. Radar responds to precipitation, and the radar echo is therefore properly termed a precipitation echo. LDAR responds to electrical discharges in the sky that occur when the electric field rises to such a level as to break down the dielectric insulation of the air, and an electrical discharge occurs. The acceleration of the electrons in an electrical discharge produce the radiation that is detected by the LDAR System.

III D. CORRELATION OF LDAR WITH FIELD MILL DATA

Data for nine of the ground strikes occurring during the peak (1903 to 1947 GMT) thunderstorm period are presented. Radar precipitation echoes, LDAR cloud discharge locations, as well as ground strike locations (determined from the Ground Strike Location System) have been added to the field mill contour plots. The LDAR data points encompass a period approximately two minutes before the ground strike. The radar and field mill data shown are those closest to, yet prior, to the occurrance of the ground strikes.

Data for the following ground strikes

1903:52.728 GMT	1918:52.212 GMT	1926:09.005 GMT
1908:04.285 GMT	1922:38.290 GMT	1944:20.670 GMT
1916:11.625 GMT	1926:09.002 GMT	

and 1944:55.384 GMT are presented in Figures 44 to 50.

In each plot, the E-field readings for each site are shown. Reference to Figure 6 will permit one to locate the position of the individual field mill sites. The convention used in plotting the E-field contours is to start the outermost ring at 100 V/m, or 1 kV/m, and proceed inwards in steps of 100 V/m, or 1 kV/m, whichever applies. In some copies of this report the outline* of the precipitation echo will be shown in red.

For each of the strikes, the electrostatic field (as determined) by the field mill network) at the location of the ground strike, but just prior to the ground strike - was determined. This data, together with the maximum electrostatic field reading in the entire Field Mill Network has been tabulated in Table V. Also shown in Table V are the means, the standard deviations, and the medians of the absolute values of the electrostatic field readings.

* Where not shown in red, reference to the corresponding plot from the group Figures 34 to 43 will help to identify the precipitation echoes.

TABLE V

GROUND-BASED FIELD-MILL READINGS, JUST PRIOR TO GROUND STRIKES

TIME OF GROUND STRIKE GMT	ELECTROSTATIC FIELD AT THE LOCATION OF THE GROUND STRIKE, JUST PRIOR TO THE STRIKE	MAXIMUM ELECTROSTATIC FIELD READING IN THE FIELD-MILL NETWORK
	kV/m	kV/m
1903:52.727	+0.9	+0.9
1908:04.285	-1.2	-1.2
1916:11.625	-0.8	-1.9
1918:52.247	+3.3	-3.2
1922:38.327	+2.0	-4.4
1926:09.002	-1.0	-2.8
1926:09.005	-2.5	-2.8
1944:20.670	-1.5	-5.3
1944:55.384	-1.5	-5.3
Mean	1.6	3.0
Std. Dev.	0.8	1.6
Median	1.3	2.8

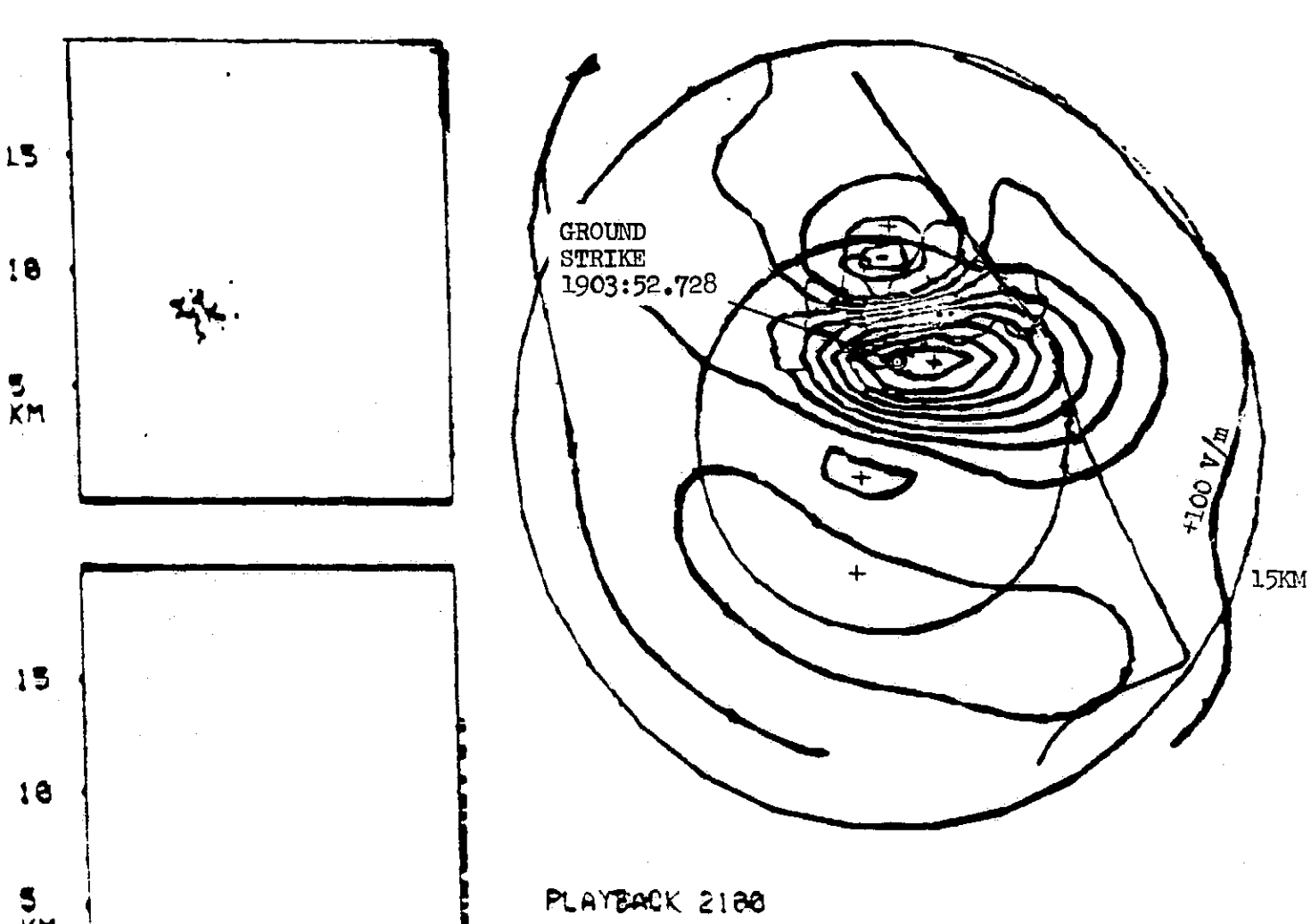

09/06/77 1903: 4.851 GMT
Line Scale - 100 V/M

Site #	Volts/Meter
1	230
2	292
3	199
4	199
5	169
6	138
7	292
8	76
9	138
10	261
11	138
12	-47
13	384
14	876
15	907
16	538
17	384
18	169
19	507
20	230
21	138
22	261
23	261
24	261

FIG. 44 OVERLAY OF THE FIELD MILL CONTOUR PLOT OF 1903:04.851 GMT ONTO THE COMPOSITE LDAR, RADAR PRECIPITATION PLOT OF 1903 GMT, (FIG. 34)

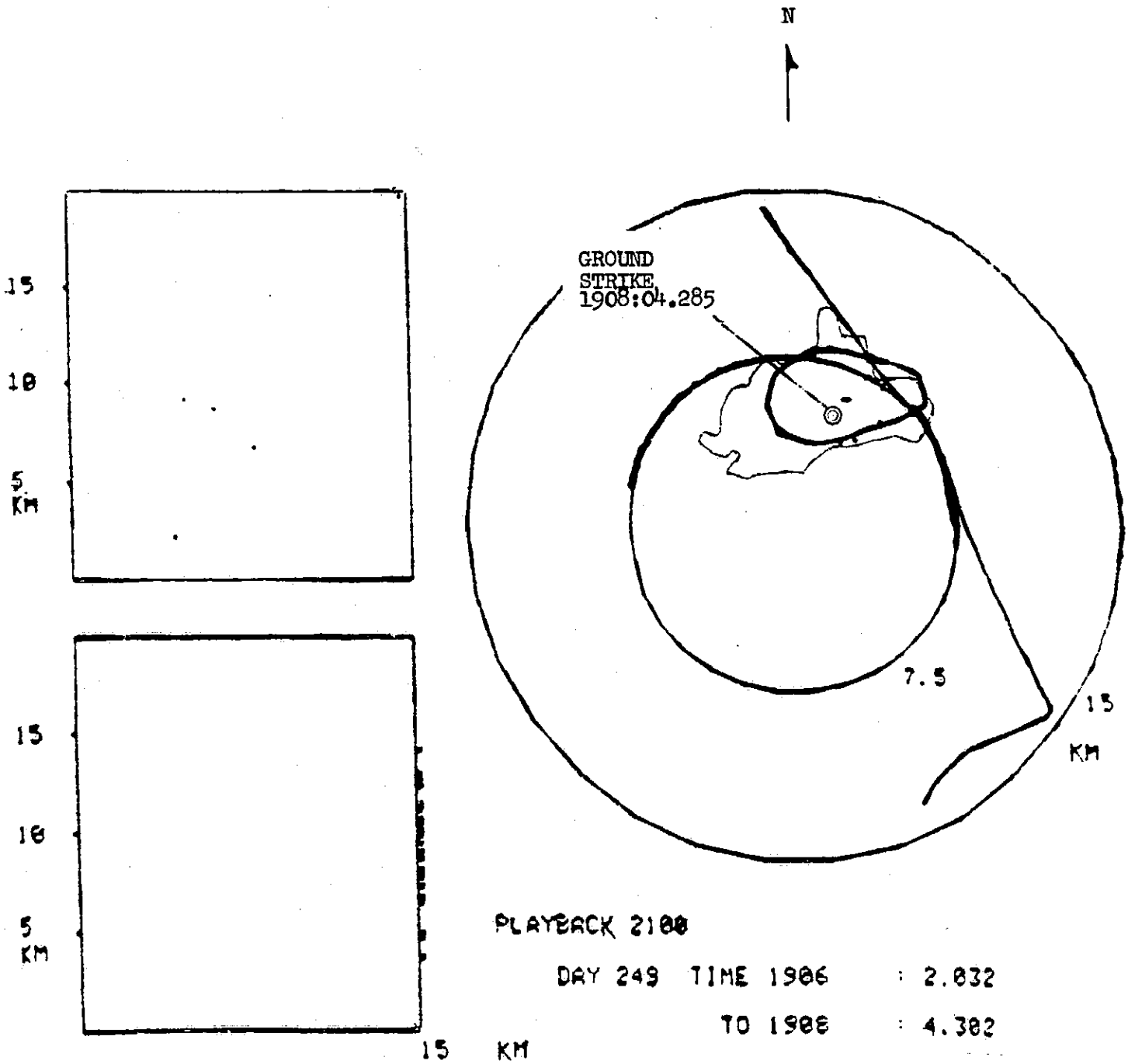

09/06/77 1907: 10.568 GMT
Line Scale - 1000 V/M

Site #	Volts/Meter
1	-20
2	230
3	138
4	169
5	76
6	-201
7	261
8	-693
9	-1000
10	230
11	-539
12	-1247
13	-1093
14	-908
15	-908
16	-662
17	-539
18	46
19	-908
20	-385
21	-324
22	199
23	230
24	199
25	199

FIG. 45 OVERLAY OF THE FIELD MILL CONTOUR PLOT OF 1907:10.568 GMT ONTO THE COMPOSITE LDAR, RADAR PRECIPITATION PLOT OF 1908 GMT, (FIG. 35)

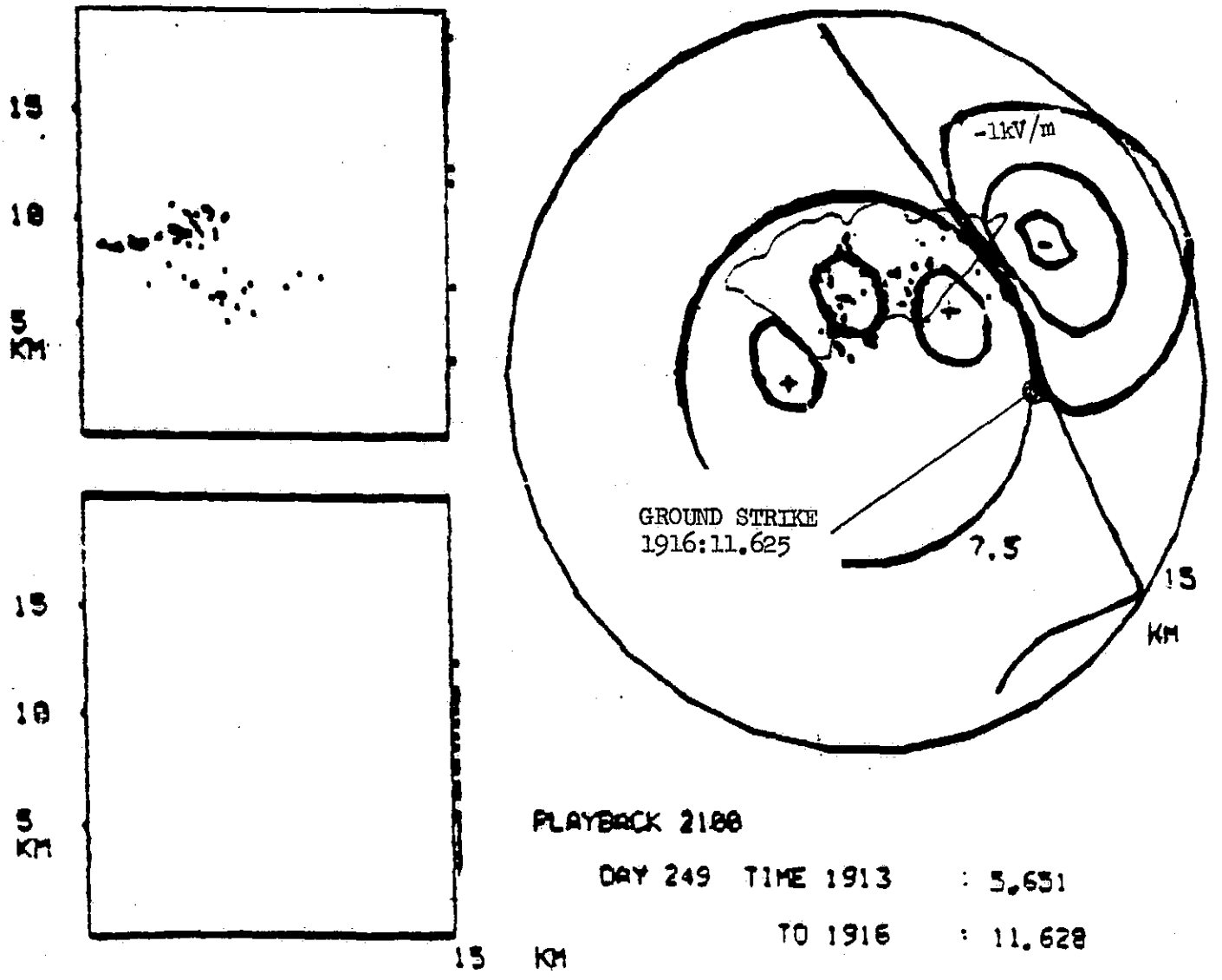

09/06/77 1915: 21.955 GMT
Line Scale - 1000 V/M

Site #	Volts/Meter
1	-816
2	138
3	-139
4	-16
5	-77
6	-324
7	138
8	-693
9	-816
10	-47

FIG. 46 OVERLAY OF THE FIELD MILL CONTOUR PLOT OF 1915:21.955 GMT ONTO THE COMPOSITE LDAR, RADAR PRECIPITATION PLOT OF 1916 GMT, (FIG. 36)

Site #	Volts/Meter
11	15
12	-601
13	-1708
14	2261
15	-1924
16	-1216
17	1215
18	15
19	199
20	107
21	-754
22	-139
23	-16
24	76

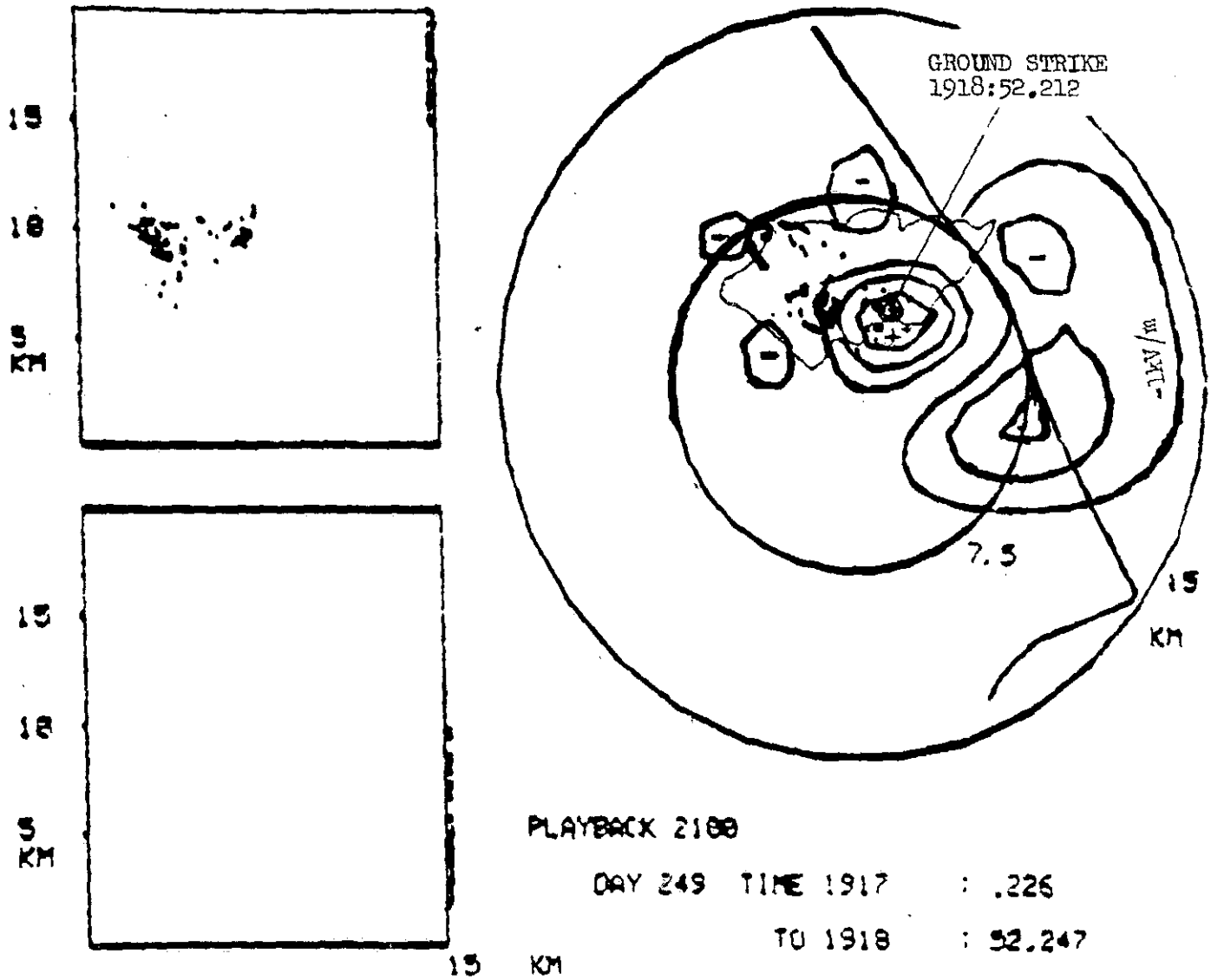

09/06/77 1918: 26.197 GMT
Line Scale - 1000 V/M

Site #	Volts/Meter
1	-3216
2	76
3	-324
4	-201
5	-262
6	-477
7	-16
8	-785
9	-570
10	-139
11	661
12	-385
13	-1370
14	2938
15	2846
16	-1216
17	-1216
18	-19
19	1399
20	969
21	-785
22	-262
23	-139
24	-47

FIG. 47 OVERLAY OF THE FIELD MILL CONTOUR PLOT OF 1918:26.197 GMT ONTO THE COMPOSITE LDAR, RADAR PRECIPITATION PLOT OF 1918 GMT, (FIG. 37)

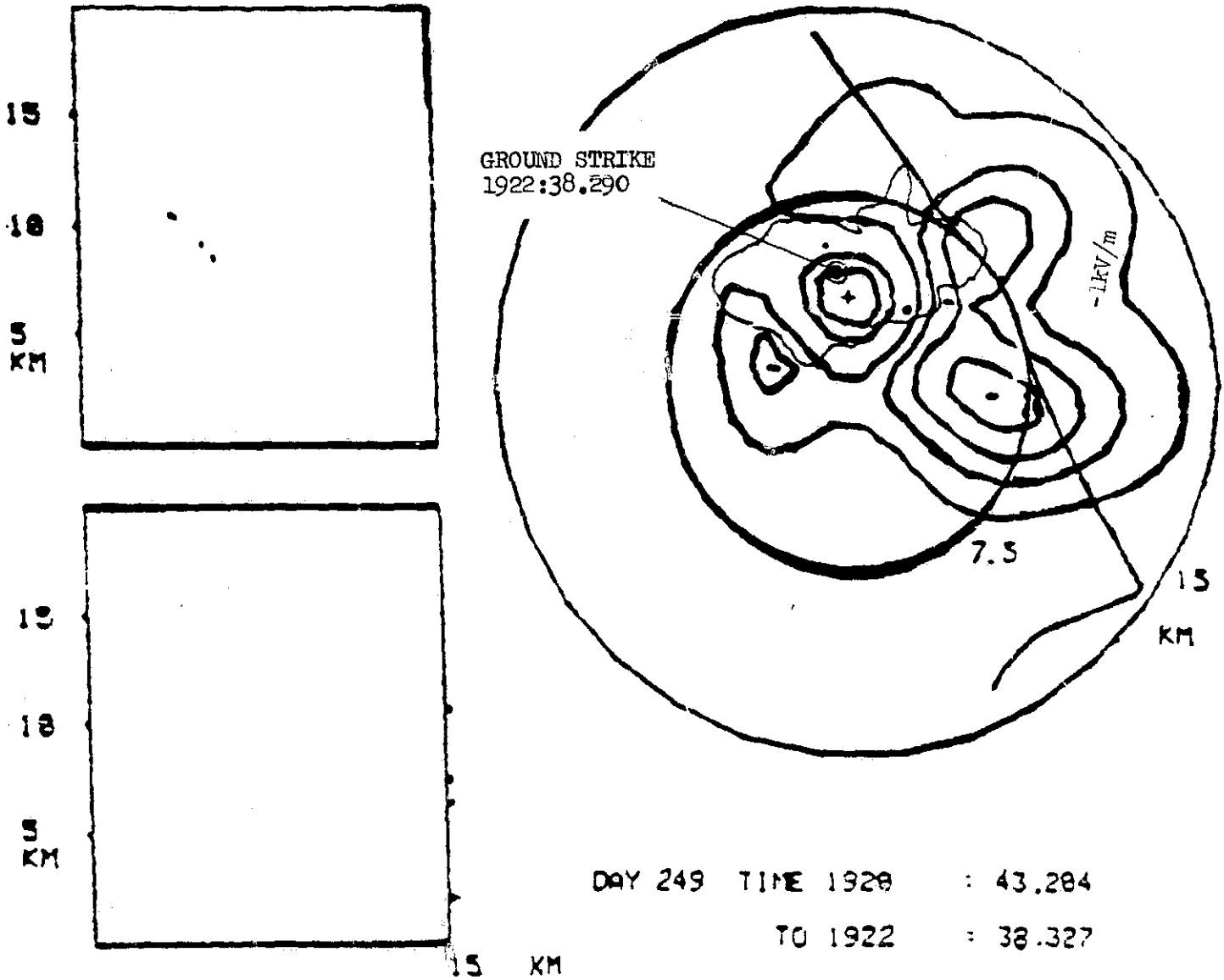

09/06/77 1922: 31.873 GMT
Line Scale - 1000 V/M

Site #	Volts/Meter
1	-4447
2	-16
3	-785
4	-539
5	-508
6	-877
7	-139
8	-1401
9	-1616
10	-447

FIG. 40 OVERLAY OF THE FIELD MILL CONTOUR PLOT OF 1922:31.873 GMT ONTO THE COMPOSITE LDAR, RADAR PRECIPITATION PLOT OF 1922 GMT, (FIG. 39)

Site #	Volts/Meter
11	-724
12	138
13	-3954
14	-1677
15	3338
16	-2508
17	-1616
18	-724
19	-2385
20	-1154
21	-1893
22	-785
23	-324
24	-231

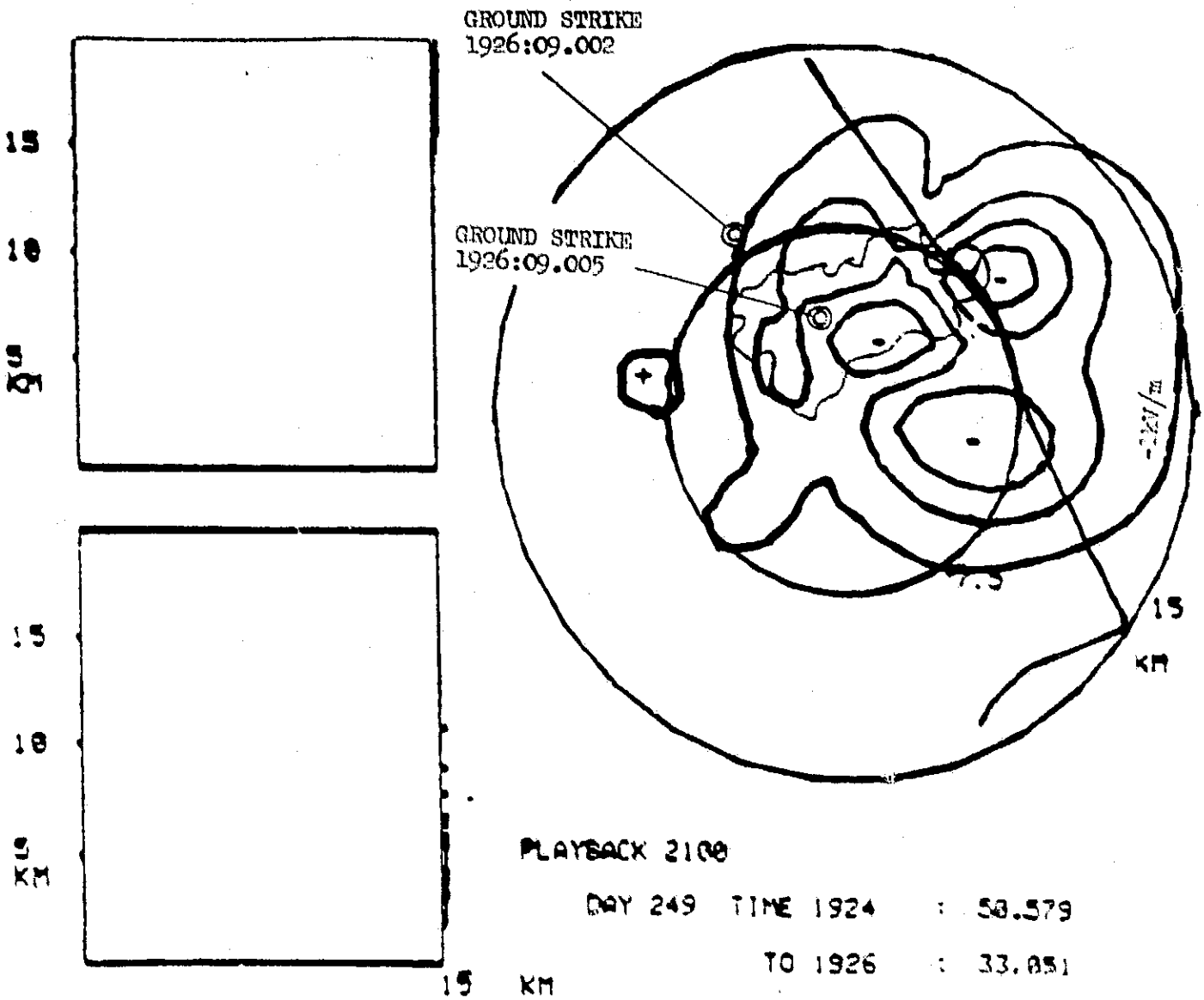

09/06/77 1925:36.115 GMT

Line Scale - 1000 V/M

Site #	Volts/Meter
1	-3739
2	-108
3	-1062
4	-785
5	-631
6	-1093
7	-324
8	-1339
9	-1554
10	-631
11	-1893
12	-2539
13	-4201
14	-754
15	-416
16	-2816
17	-2539
18	169
19	-2631
20	-1616
21	-2600
22	-1124
23	-508
24	-354

FIG. 49 OVERLAY OF THE FIELD MILL CONTOUR PLOT OF 1925:36.115 GMT ONTO THE COMPOSITE LDAR, RADAR PRECIPITATION PLOT OF 1926 GMT, (FIG. 40)

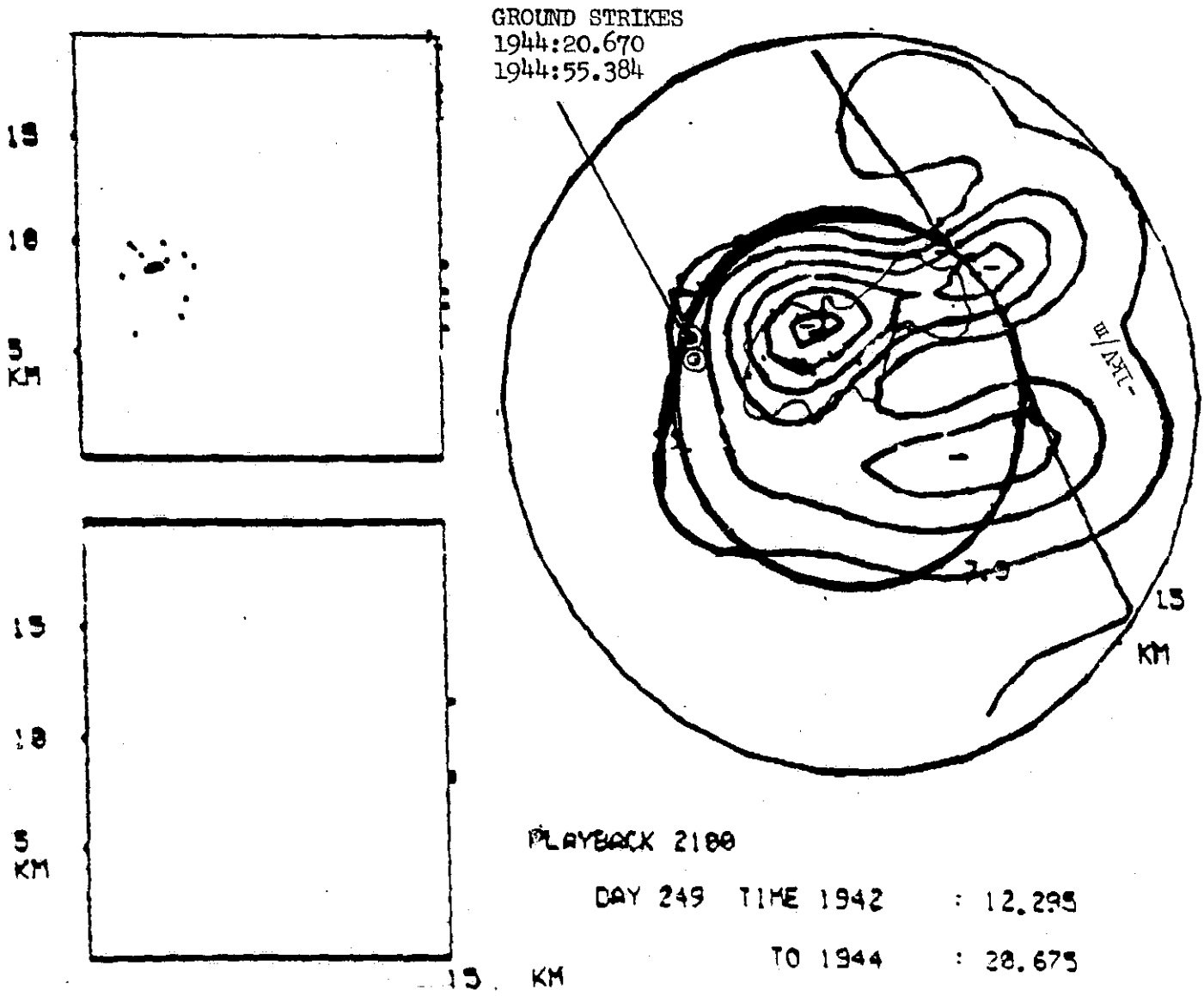

09/06/77 1944:02.501 GMT
Line Scale - 1000 V/M

Site #	Volts/Meter
1	-3401
2	446
3	-1524
4	-1062
5	507
6	507
7	415
8	-1062
9	-108
10	-847

FIG. 50 OVERLAY OF THE FIELD MILL CONTOUR PLOT OF 1944:02.501 GMT ONTO THE COMPOSITE LDAR, RADAR PRECIPITATION PLOT OF 1944 GMT, (FIG. 43)

Site #	Volts/Meter
11	-2108
12	-2539
13	-4385
14	-3524
15	-5262
16	-2231
17	-5708
18	-2385
19	-1185
20	-2662
21	-2754
22	-2016
23	-631
24	-508

It is worthy of note that the electrostatic fields at the point about to be struck is remarkably low : mean, 1.6, median 1.3 kilovolts/meter.

Generally, the maximum electrostatic field, in the network is used as an indicator of the probability of a ground strike. Referring to Figure 10, we should expect a ground strike when the field at the ground exceeds 6 kV/m. Two of the ground strikes (-5.5, -5.5 kV/m) in Table V come close to meeting this criteria, and a third (-4.4 kV/m) deserves consideration. The rest are below 3.2 kV/m, which is unusually low. In fact the first ground strike took place when the maximum field reading in the entire Field Mill Network was below 0.91 kV.m.

Clearly one cannot require the presence of a high (5 kV/m) field mill reading as a necessary criterion for an impending ground strike. As our data show, ground strikes can occur at much lower readings of the field.

The Value of Field Mills in Telling Where a Ground Strike Will Take Place

While the LDAR and ground strike data can be seen to lie in regions of disturbed field mills, it is apparent that it would be impossible to tell from the field mill contour plots where the ground strike will take place. Field mill contour plots are useful in telling that a disturbed condition exists, but are of limited value in telling where a ground strike is likely to take place.

III E. CORRELATION OF GROUND STRIKE LOCATION WITH DYNAMIC FIELD MILL PLOTS

Data for seven of the ground strikes that occurred during the peak (1903 to 1947 GMT) of the thunderstorm are presented. Ground strike locations determined from the Ground Strike Location System have been added to the dynamic or flash field mill plots. Dynamic field mill plots differ from the field mill contours presented so far in that they present contours of equal field strength changes, whereas field mill contours represent contours of equal field strength. In the dynamic field mill plots, the outer ring represents a change of 100 V/m, or 1 kV/m. As we proceed inward, each ring represents a change 100 V/m or 1 kVm, as indicated. The center of the contours represents the position of the charge that was neutralized in the ground strike.

Data for the following ground strikes at

1903:52.728 GMT	1916:11.625 GMT	1920:06.001 GMT
1908:04.285 GMT	1918:52.212 GMT	1920:06.059 GMT

and 1922:38.290 are presented in Figures 51 to 56.

As is apparent from the figures, there is excellent agreement between the ground strike locations determined from the Ground Strike Location System and those indicated by the centers of the dynamic field mill plots, that is by the centers of the charges that were removed by the ground strikes.

The 0.1 second discrepancy that exists between the time shown in the computer-generated dynamic field mill plots and the time given by LDAR for the ground strike, arises from the manner in which time is assigned to the computer-generated plot. The time assigned is approximately 0.1 second too late. The correct time for the ground flash, and for the dynamic change in the field mills, is that given by LDAR for the ground strike.

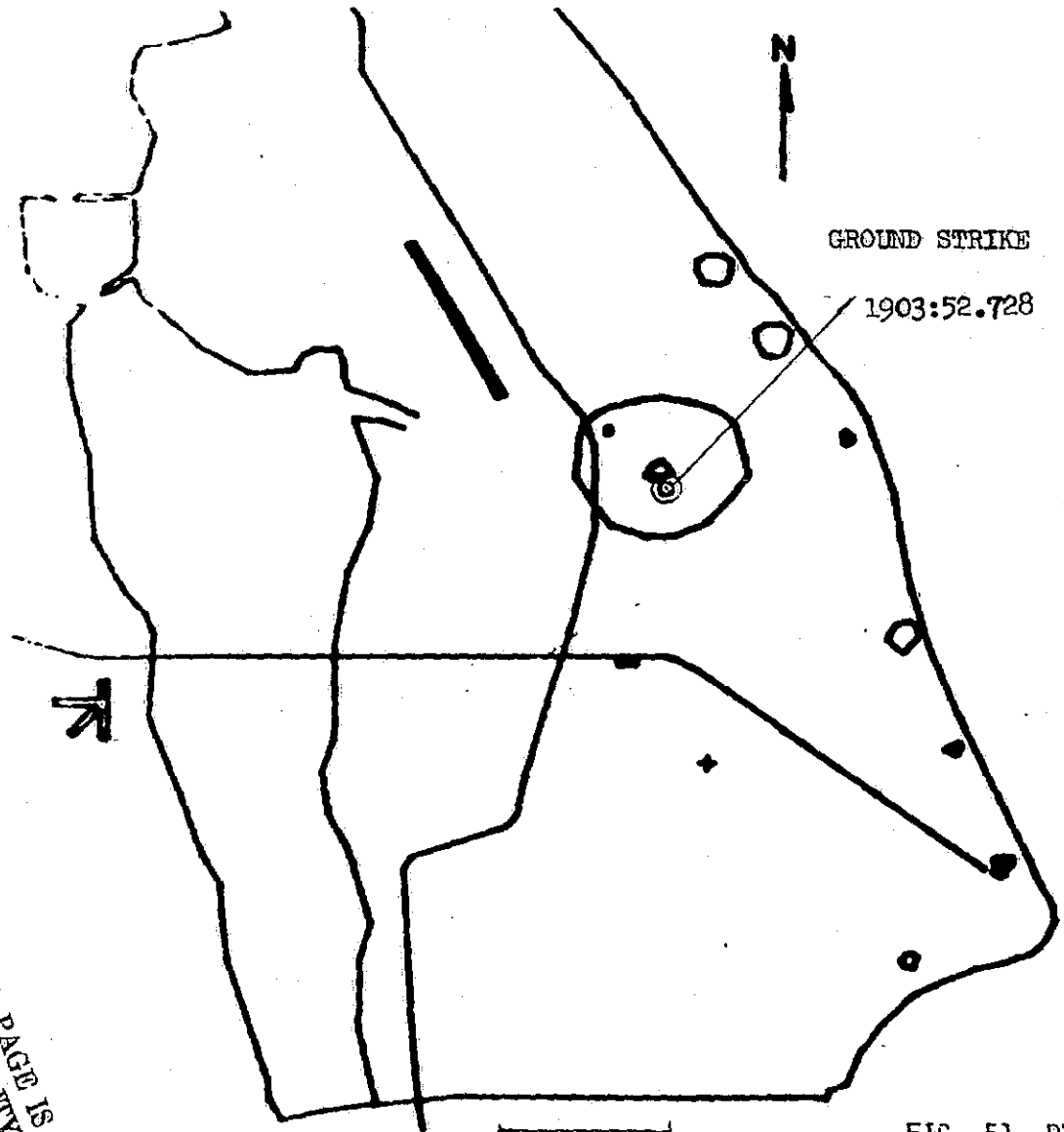

09/06/77 GMT 1903:52.801

LINE SCALE = 1000 V/M

SITE #	VOLTS/METER
1	292
2	76
3	107
4	76
5	169
6	261
7	107
8	415
9	415
10	76
11	230
12	-231
13	446
14	-847
15	-2077
16	415
17	169
18	169
19	-16
20	138
21	830
22	138
23	107
24	76
25	15

FIG. 51 DYNAMIC FIELD MILL PLOT, WITH ADDED GROUND STRIKE LOCATION, 1903:52.728 GMT

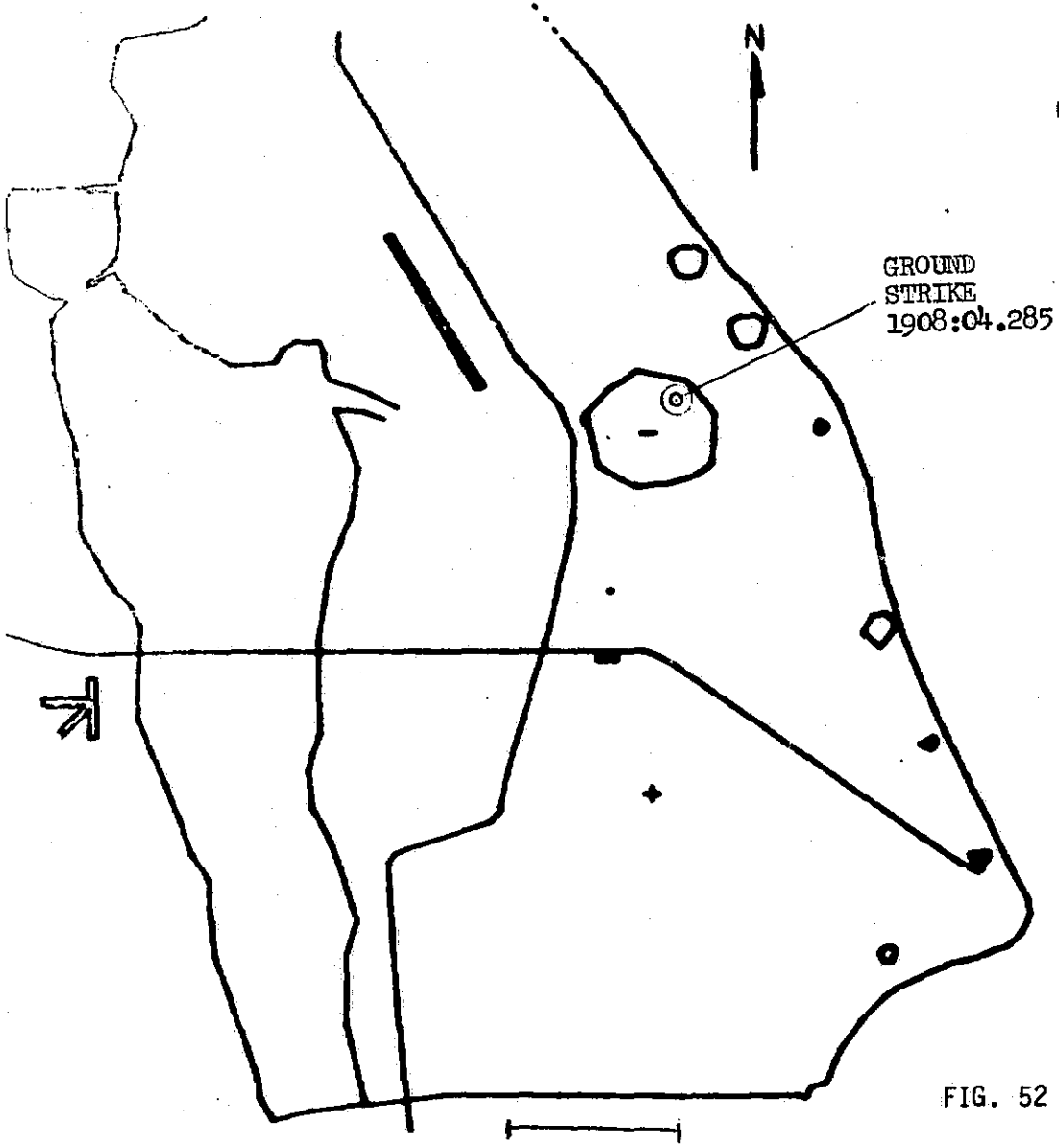

09/06/77 GMT 1908: 4.421

LINE SCALE = 1000 V/M

SITE #	VOLTS/METER
1	261
2	-47
3	46
4	76
5	-108
6	-262
7	-47
8	-324
9	-77
10	15
11	-201
12	-847
13	446
14	-877
15	-1216
16	661
17	76
18	76
19	76
20	107
21	230
22	46
23	15
24	15
25	-16

FIG. 52 DYNAMIC FIELD MILL PLOT, WITH ADDED GROUND STRIKE LOCATION, 1908:04.285 GMT

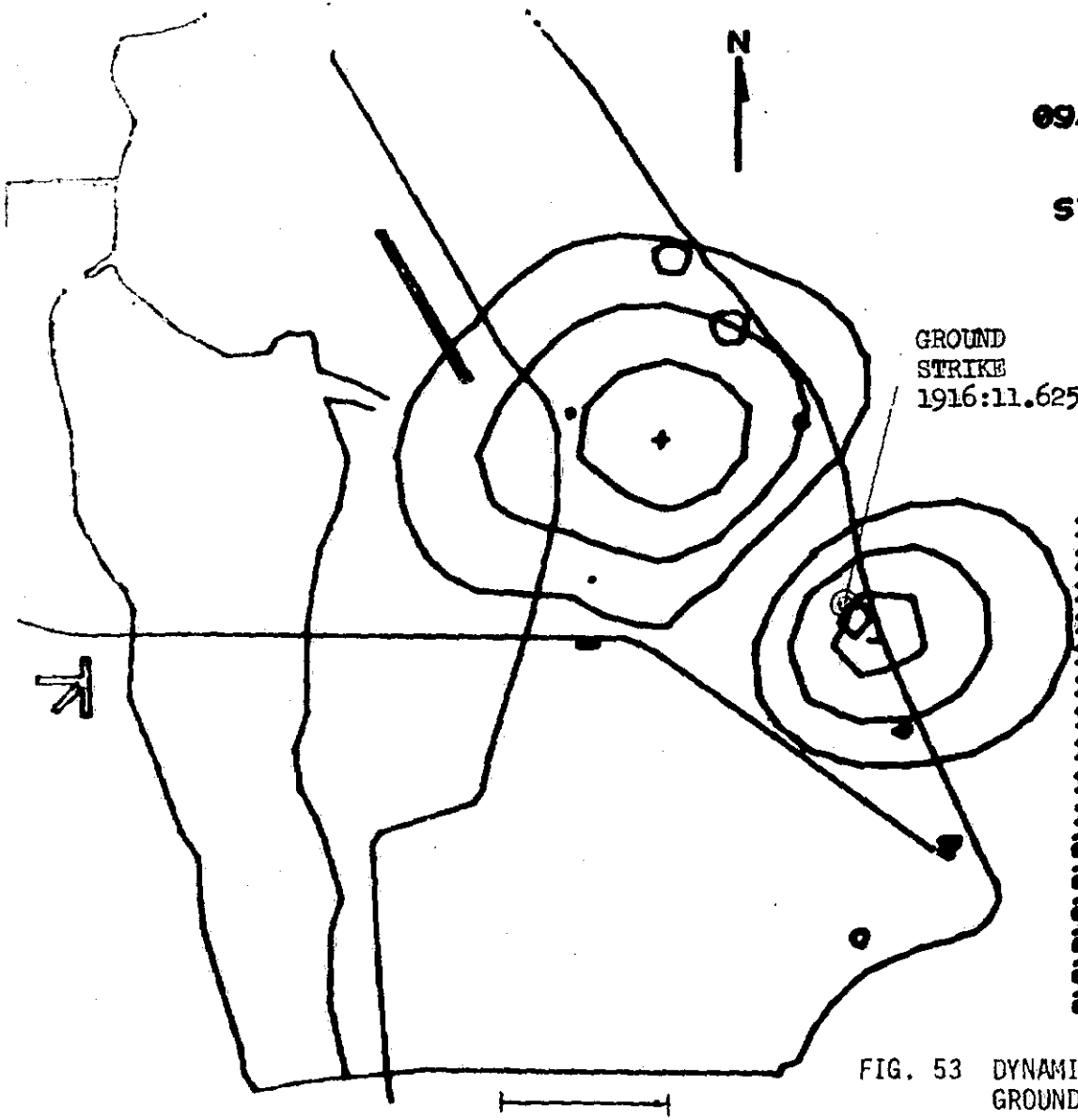

09/06/77 GMT 1916:11.695

LINE SCALE = 1000 V/M

SITE #	VOLTS/METER
1	-3308
2	107
3	46
4	-16
5	261
6	507
7	230
8	753
9	1369
10	76
11	1307
12	2630
13	1984
14	3553
15	3184
16	1123
17	2107
18	846
19	2200
20	1307
21	815
22	538
23	199
24	46
25	76

FIG. 53 DYNAMIC FIELD MILL PLOT, WITH ADDED GROUND STRIKE LOCATION, 1916:11.625 GMT

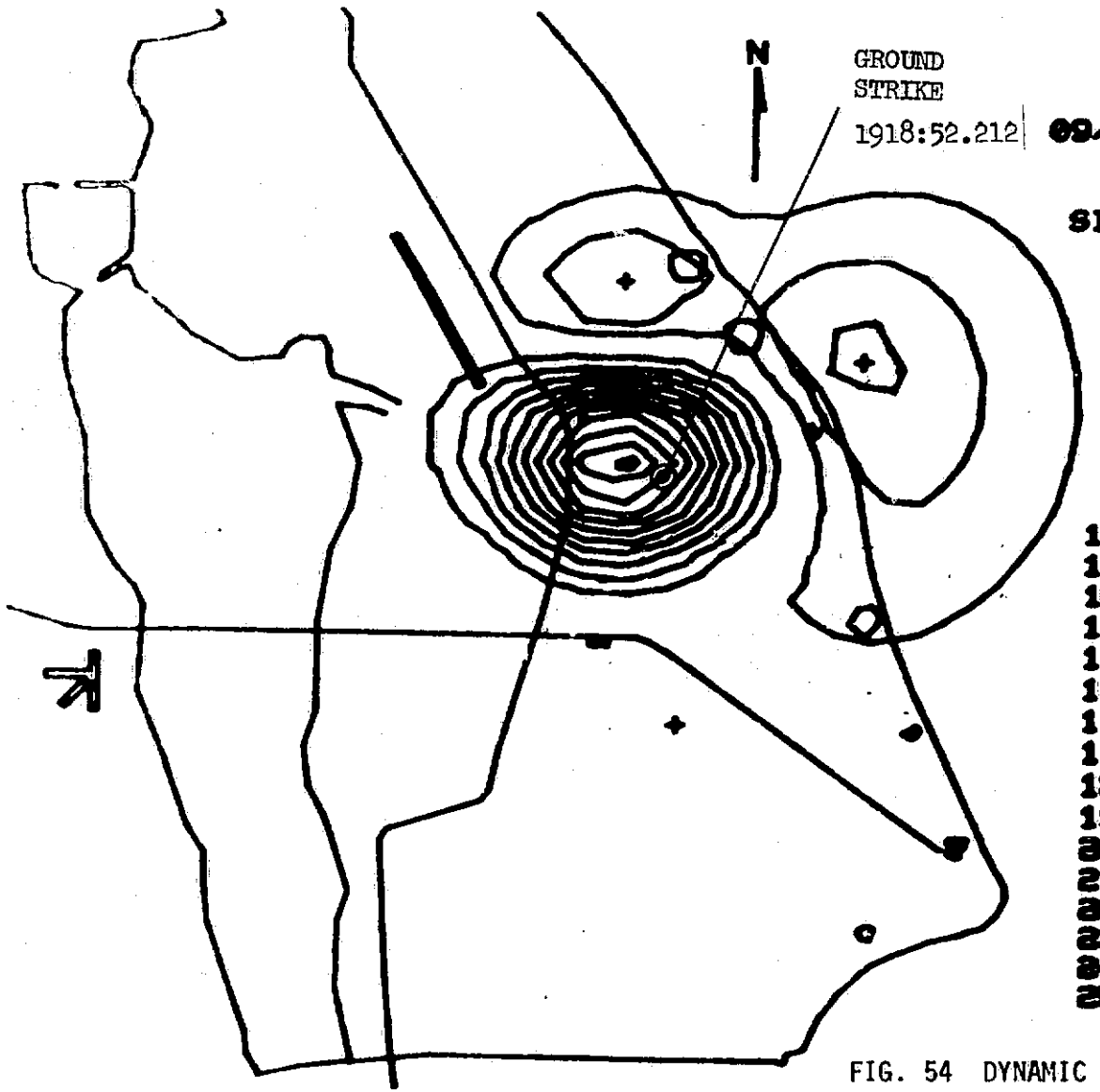

SITE #	VOLTS/METER
1	1092
2	261
3	384
4	353
5	415
6	753
7	323
8	1492
9	1830
10	323
11	-170
12	-970
13	2282
14	-4631
15	-11216
16	1984
17	-3770
18	-16
19	-2324
20	-1616
21	230
22	353
23	323
24	261
25	169

FIG. 54 DYNAMIC FIELD MILL PLOT, WITH ADDED GROUND STRIKE LOCATION, 1918:52.212 GMT

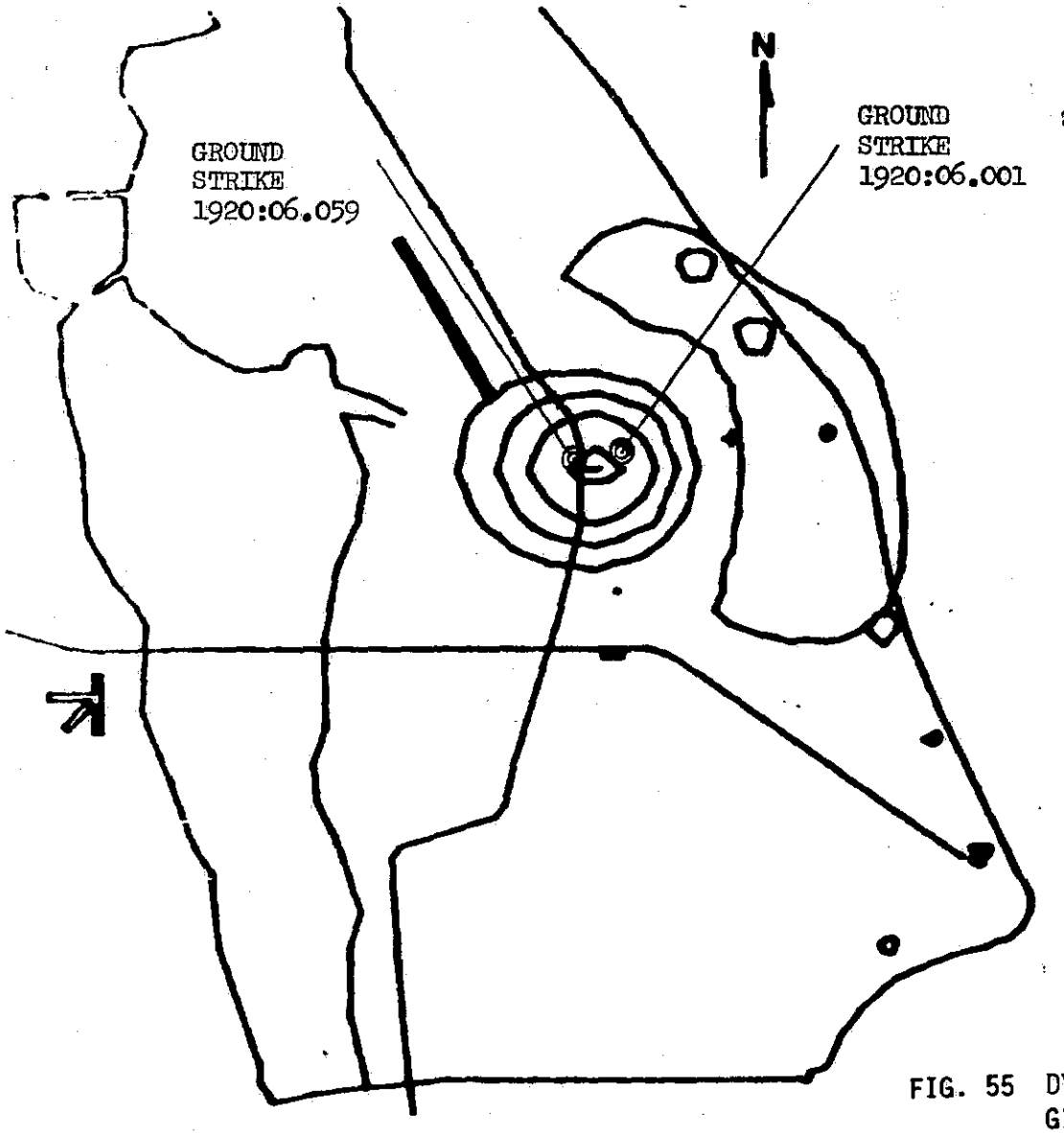

20/06/77 GMT 1920: 6.100	
LINE SCALE - 1000 V/M	
SITE #	VOLTS/METER
1	938
2	169
3	323
4	292
5	292
6	538
7	261
8	938
9	1153
10	261
11	-170
12	-293
13	1461
14	1000
15	-4262
16	1399
17	-2170
18	107
19	538
20	-16
21	753
22	446
23	292
24	199
25	169

FIG. 55 DYNAMIC FIELD MILL PLOT, WITH ADDED GROUND STRIKE LOCATIONS, 1920:06.001 and 1920:06.059 GMT

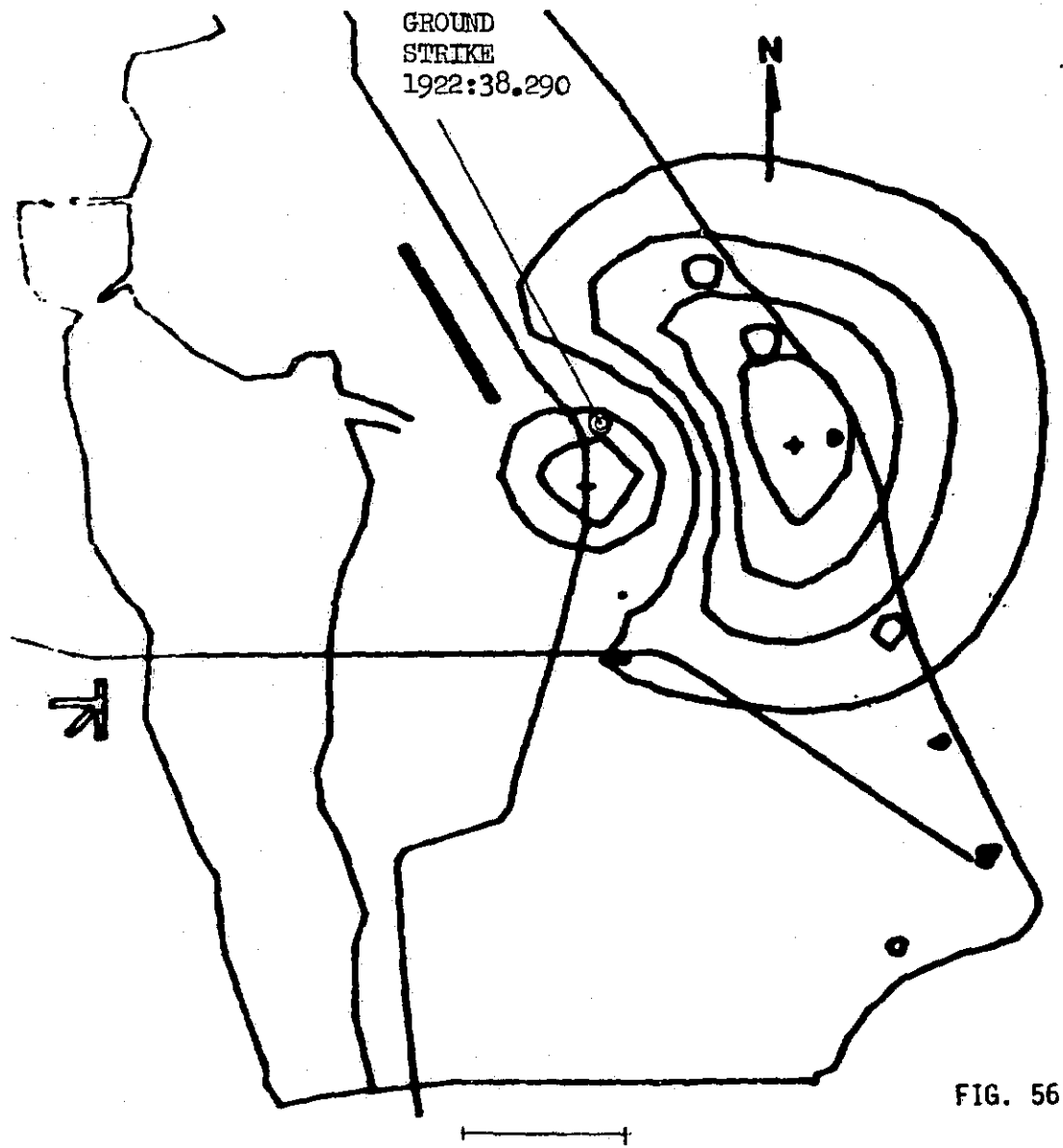

09/08/77 GMT 1922:38.470

LINE SCALE - 1000 V/M

SITE #	VOLTS/METER
1	1584
2	76
3	323
4	261
5	199
6	661
7	76
8	1923
9	2969
10	230
11	476
12	1676
13	4107
14	3799
15	-2506
16	3653
17	-1124
18	323
19	2046
20	600
21	1523
22	415
23	230
24	138
25	46

FIG. 56 DYNAMIC FIELD MILL PLOT, WITH ADDED GROUND STRIKE LOCATION, 1922:38.290 GMT

For the few cases where the ground strike position is several kilometers from the charge location indicated by the dynamic field mill plots, we suspect that the ground strike was not a vertical one. This point will have to be clarified by future observations.

III F. LDAR DATA DISPOSITION JUST BEFORE AND JUST AFTER A GROUND STRIKE

LDAR data for four of the ground strikes occuring during the peak (1903 to 1947 GMT) of the thunderstorm period are presented.

LDAR plots for strikes at

1916:51.625 GMT

1918:52.212 GMT

1920:06.059 GMT

and 1944:20.670 GMT are presented in Figures 57 to 64, two figures for each strike.

The data is presented in pairs, that is two LDAR plots for each ground strike. The first plot presents the location of all the LDAR data points for approximately two minutes prior to the ground strike. The second plot shows the position of the LDAR discharge points just after the ground strike.

The common feature of the plots presented is that the ground strike serves to clear the air of most of the electrical discharge centers, as well as to concentrate the remaining discharges centers to a narrow altitude level, as well as within a narrow ground area.

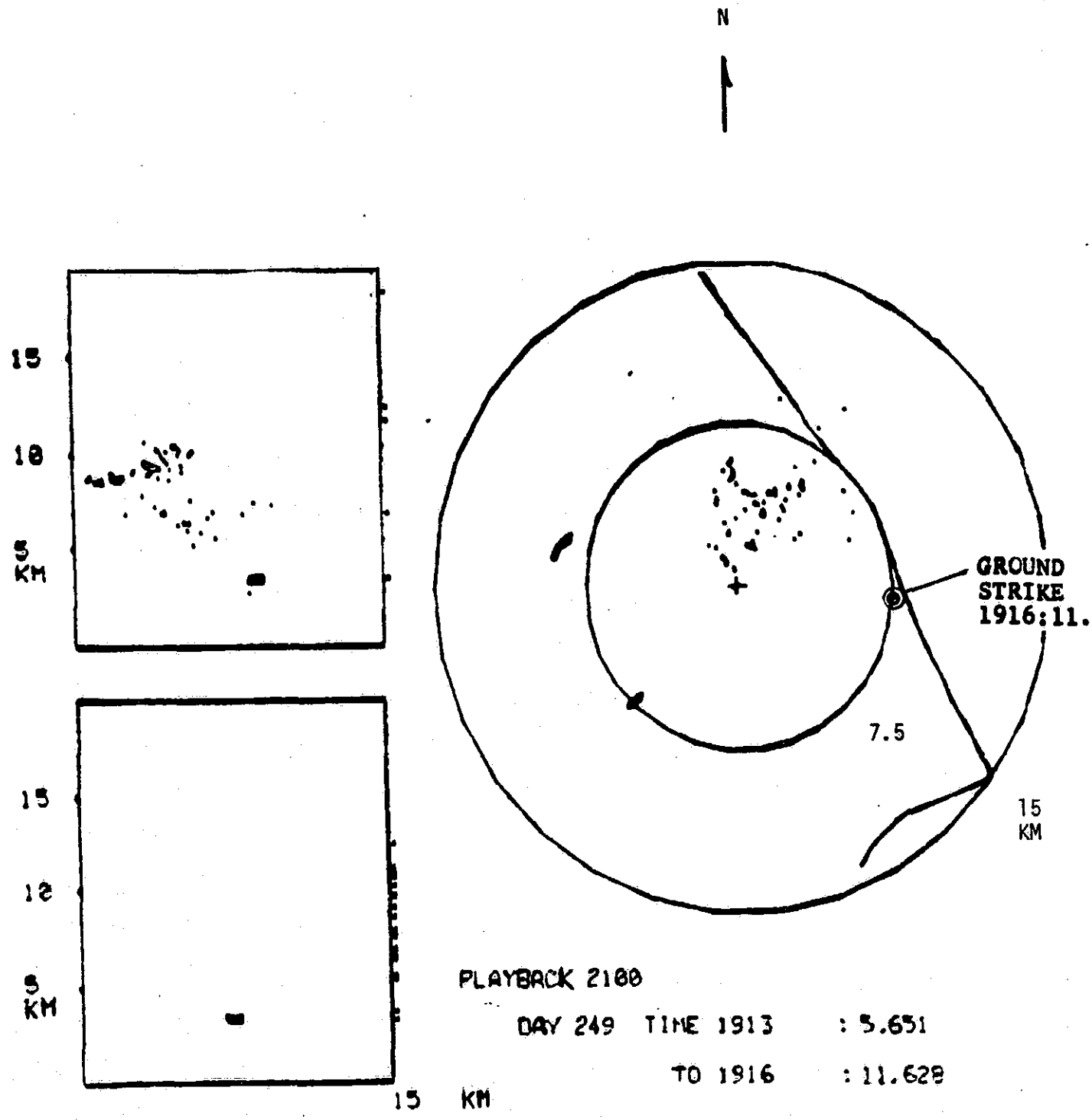

FIG. 57 LDAR PLOT, JUST BEFORE GROUND STRIKE
AT 1916:11.625 GMT

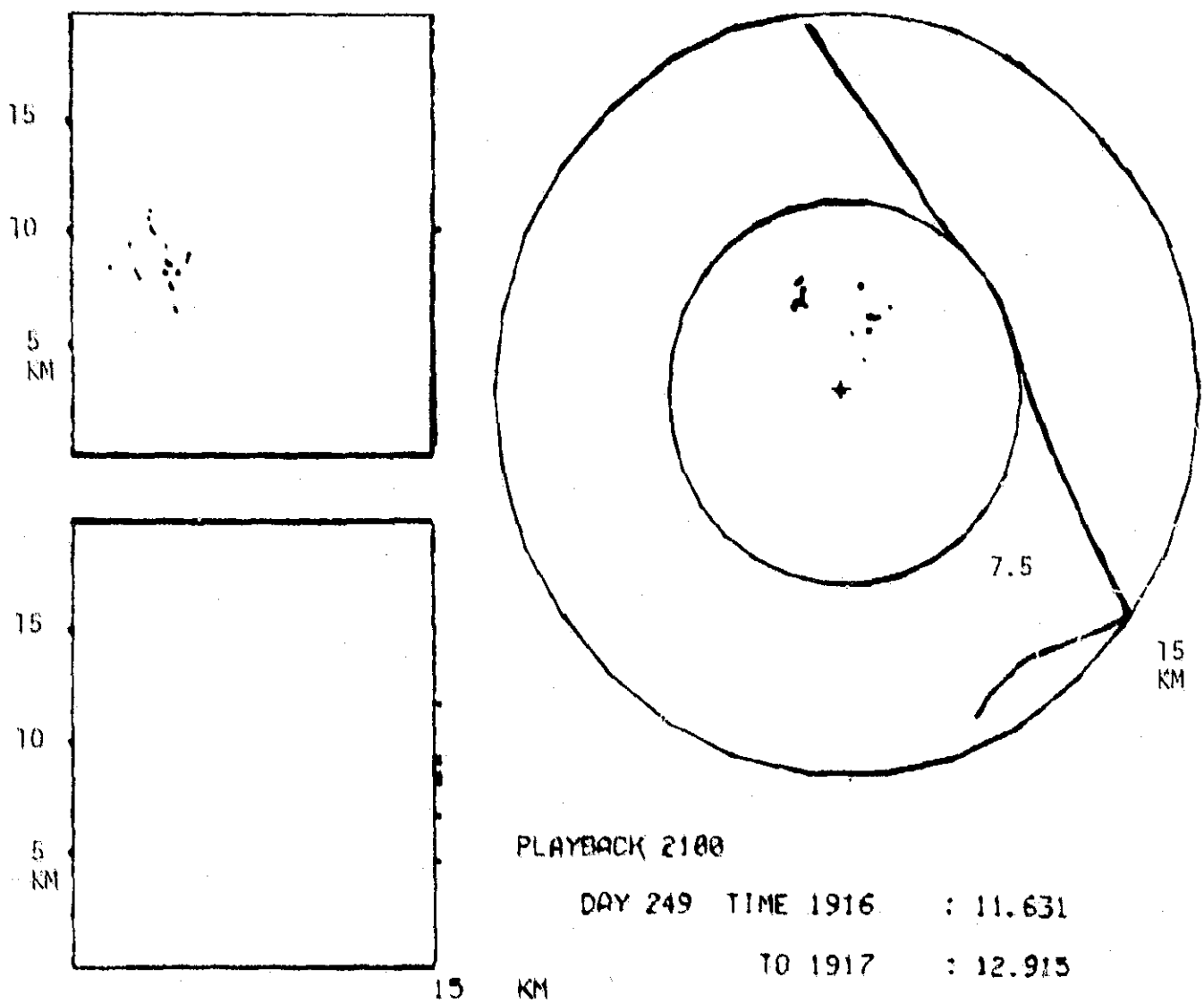

FIG. 58 LDAR PLOT, JUST AFTER GROUND STRIKE
AT 1916:11.625 GMT

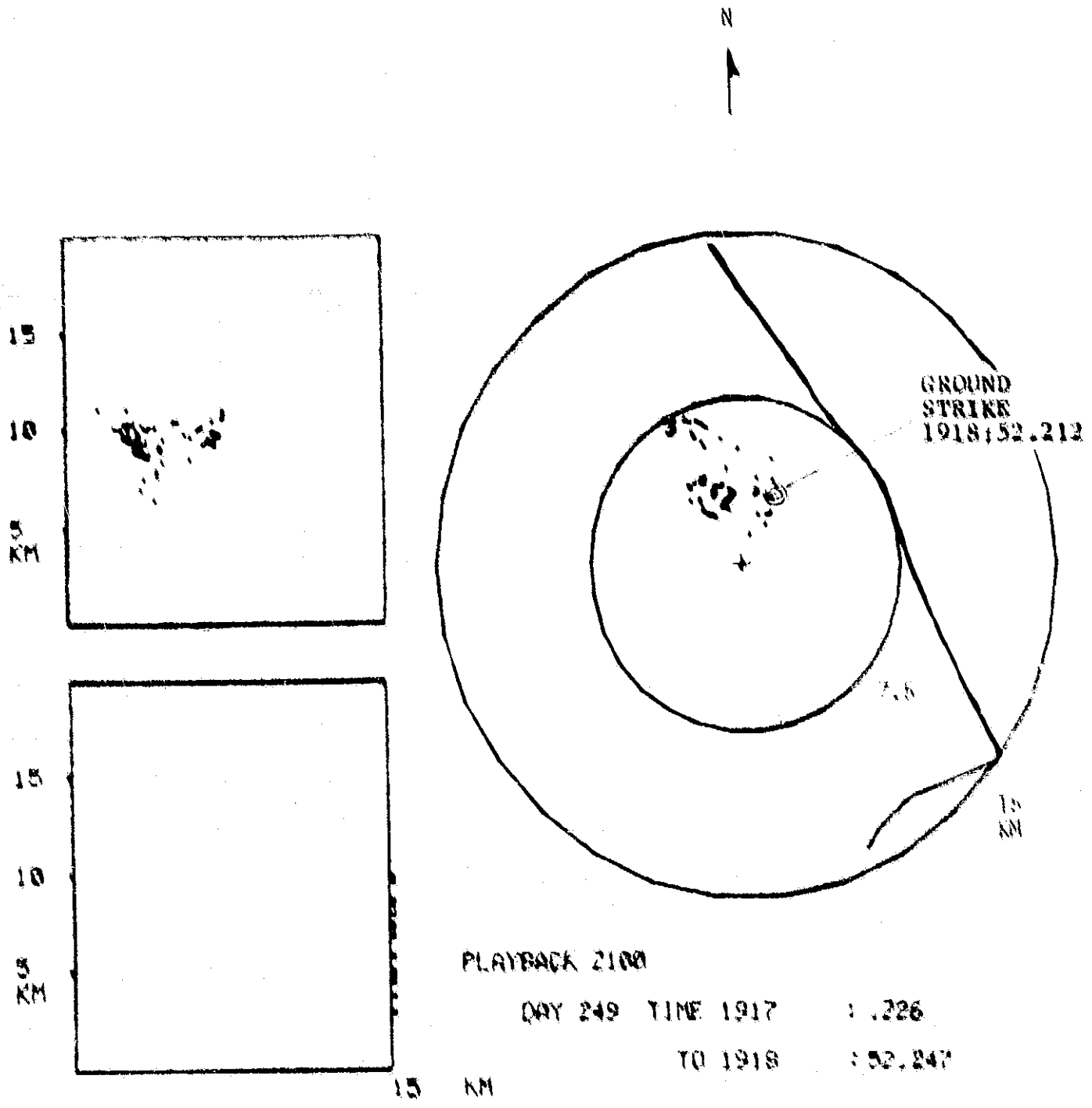

FIG. 59 LDAR PLOT, JUST BEFORE GROUND STRIKE
AT 1918:52.212 GMT

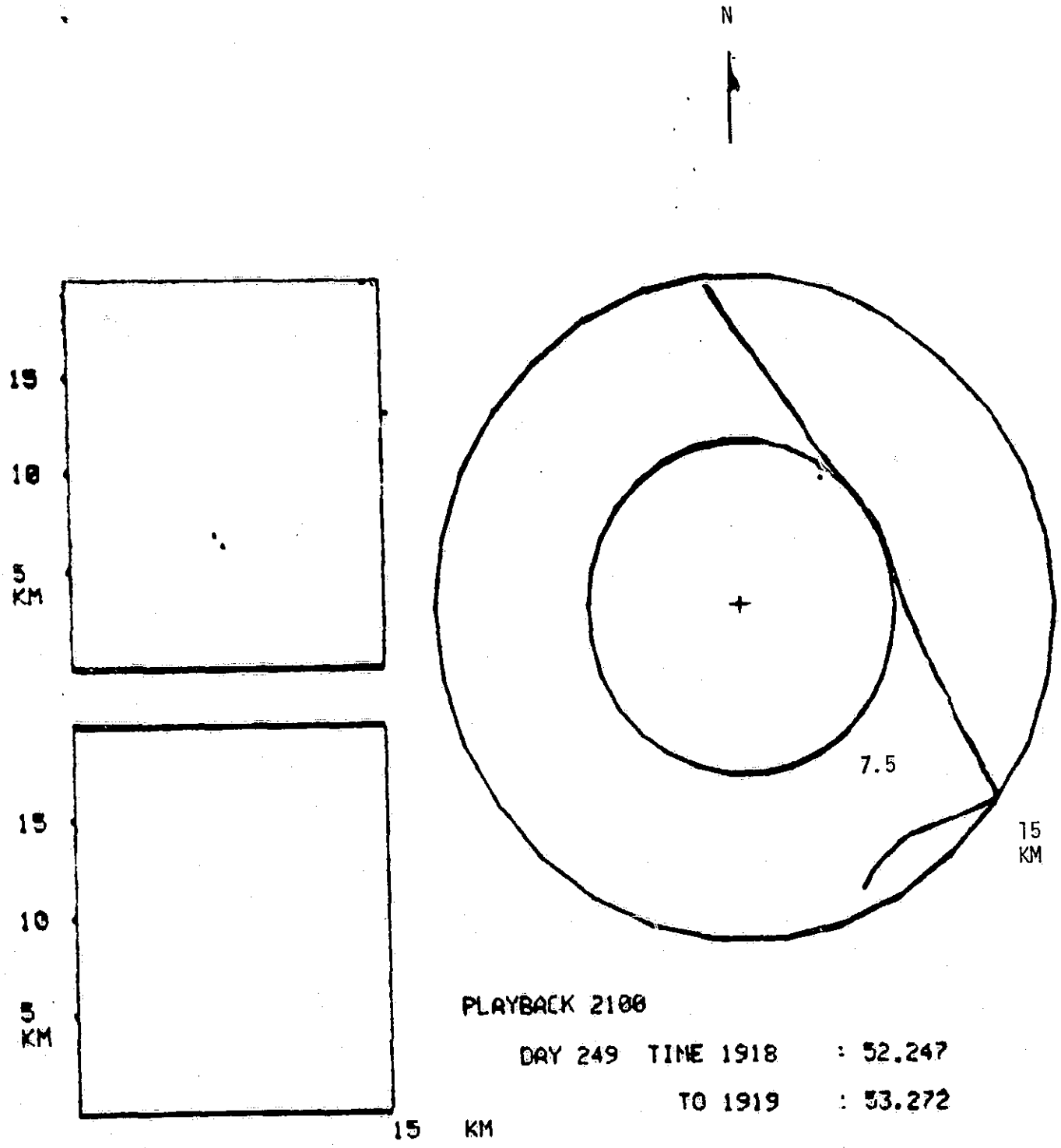

FIG. 60 LDAR PLOT, JUST AFTER GROUND STRIKE
AT 1918:52.212 GMT

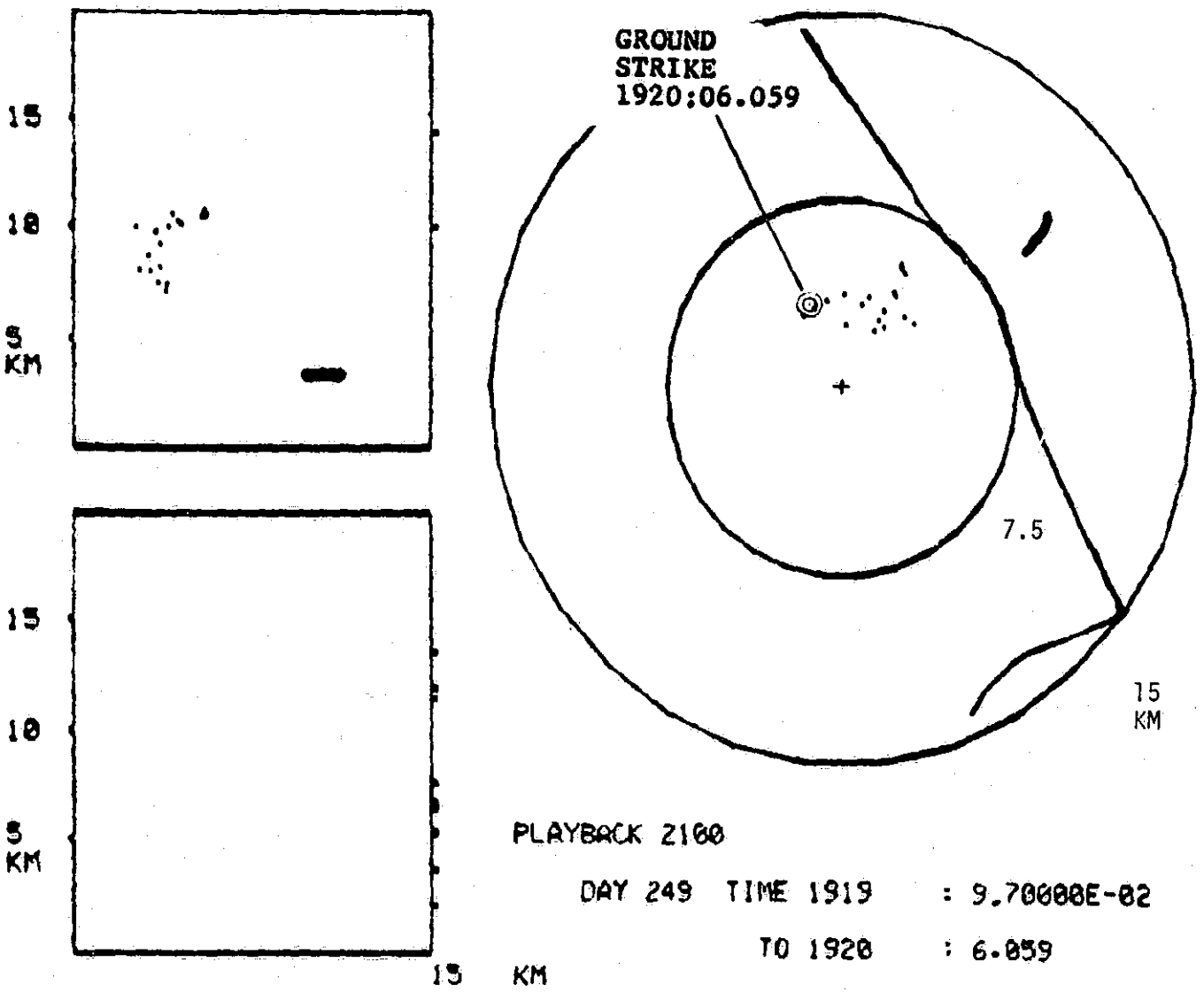

FIG. 61 LDAR PLOT, JUST BEFORE GROUND STRIKE
AT 1920:06.059 GMT

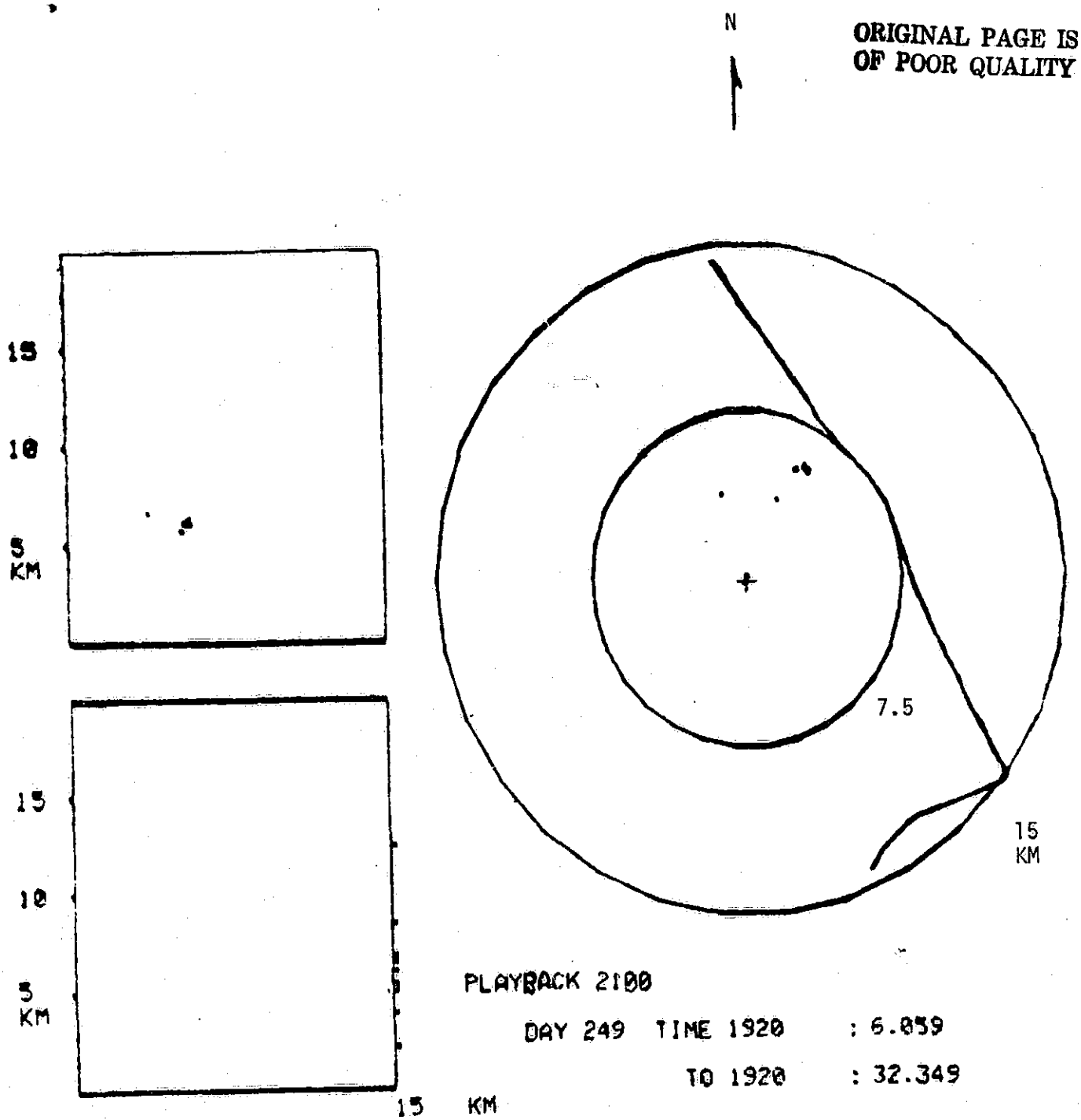

FIG. 62 LDAR PLOT, JUST AFTER GROUND STRIKE
AT 1920:06.059 GMT

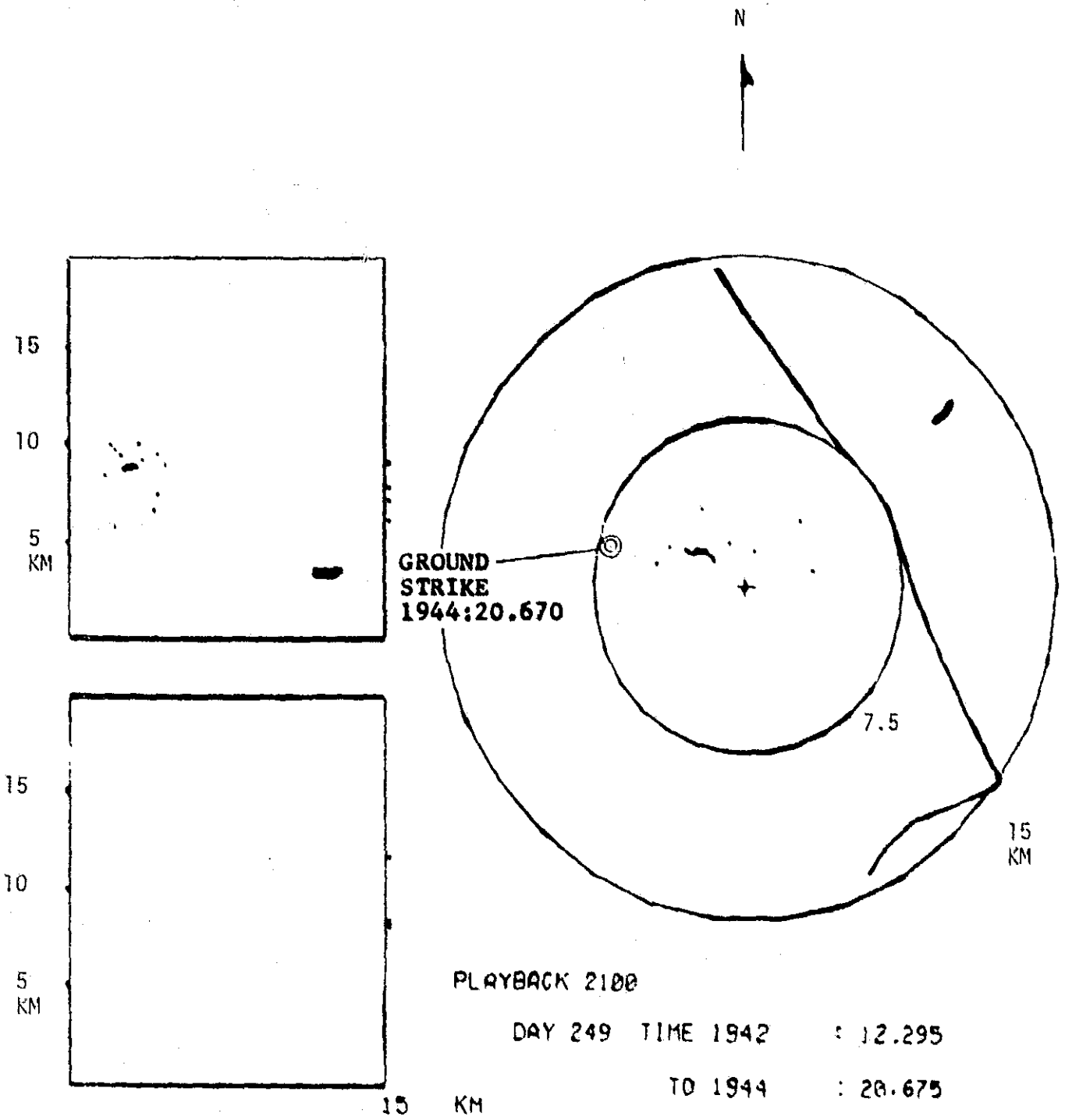

FIG. 63 LDAR PLOT, JUST BEFORE GROUND STRIKE
AT 1944:20.670

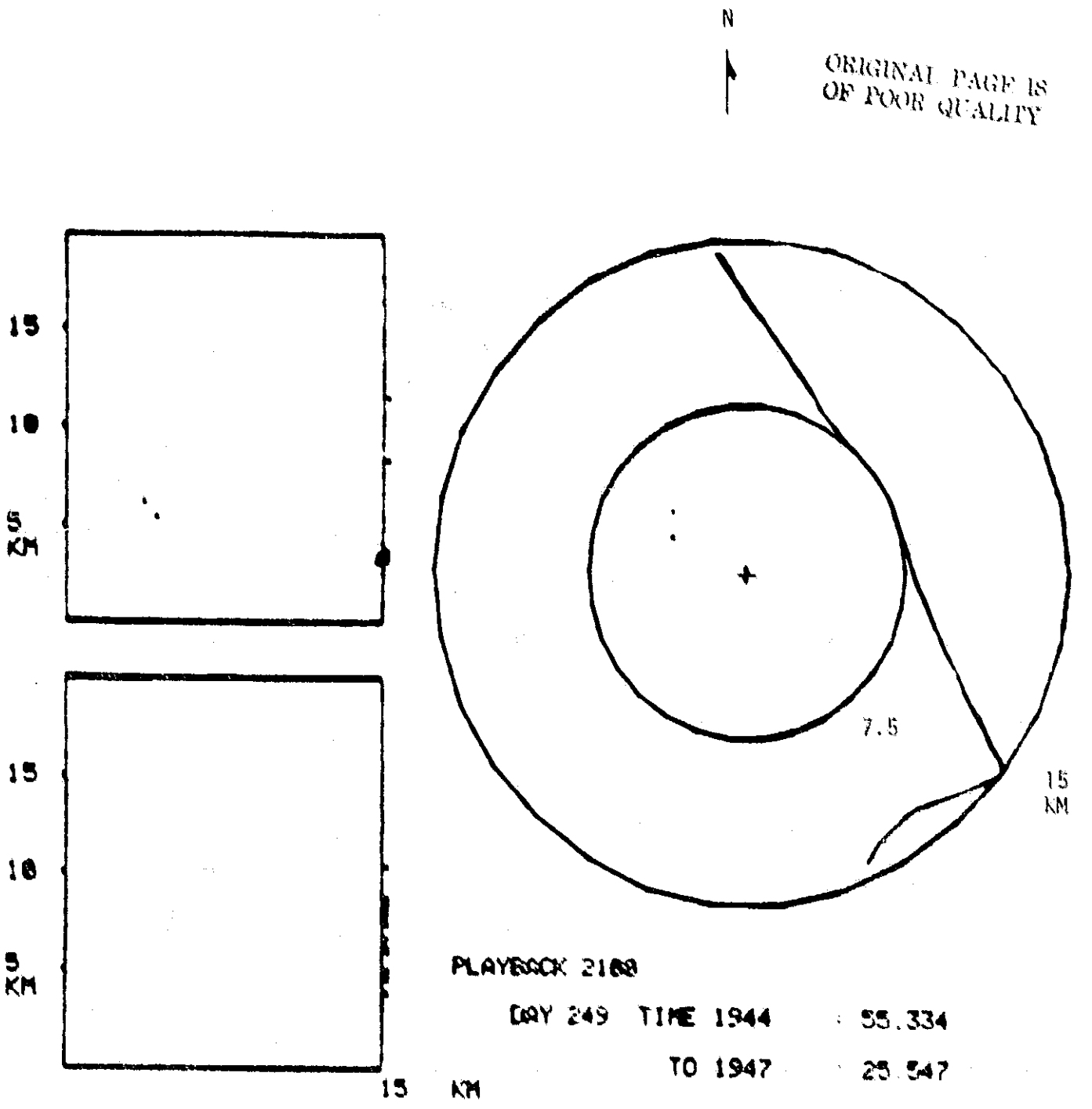

FIG. 64 LDAR PLOT, JUST AFTER GROUND STRIKE AT 1944:20.670

III G. AIRBORNE FIELD MILL READINGS ALONG FLIGHT PATH, AND CORRELATION OF DISTANCE TO LDAR DISCHARGES WITH OBSERVED AIRBORNE FIELD STRENGTH

Data for six airplane passes (Runs #13, 14, 15, 16, 17, and 18) along the thunderstorm cloud during the peak (1903 to 1947 GMT) of the thunderstorm are presented. The airplane's path has been sketched onto the LDAR plot, the times at the beginning and end of the run are noted, and airborne field-strength levels measured by NASA-6 along selected portions of the flight path have been marked. For futher information, the position of the ground strikes, as determined by the Ground Strike Location System (GSLS) have been added. The airplane's path during the time period of the LDAR plot is indicated by a solid line. The remainder of the run is indicated by a dotted line. The airborne field along selected portions of the solid line part of the run is indicated, as well as the maximum airborne field encountered during the entire run. The airplane's elevation was 10,500 feet.

LDAR plots for the intervals

1915:20.237	to	1916:11.471 GMT	Run # 13
1922:32.212	to	1924:19.353 GMT	Run # 14
1927:55.653	to	1929:41.585 GMT	Run # 15
1933:43.244	to	1934:45.455 GMT	Run # 16
1939:42.883	to	1941:31.355 GMT	Run # 17
1941:31.358	to	1942:20.965 GMT	Run # 17
1946:01.621	to	1946:19.701 GMT	Run # 18
1946:31.746	to	1947:31.859 GMT	Run # 18

and 1947:30.072 to 1948:50.133 GMT Run # 18 are presented in Figures 65 to 73.

Where numerous LDAR data points overlap, it is not possible to show more than one in the LDAR plot. To illustrate this matter, on several of the plots we have added the GMT time and the number of LDAR data points

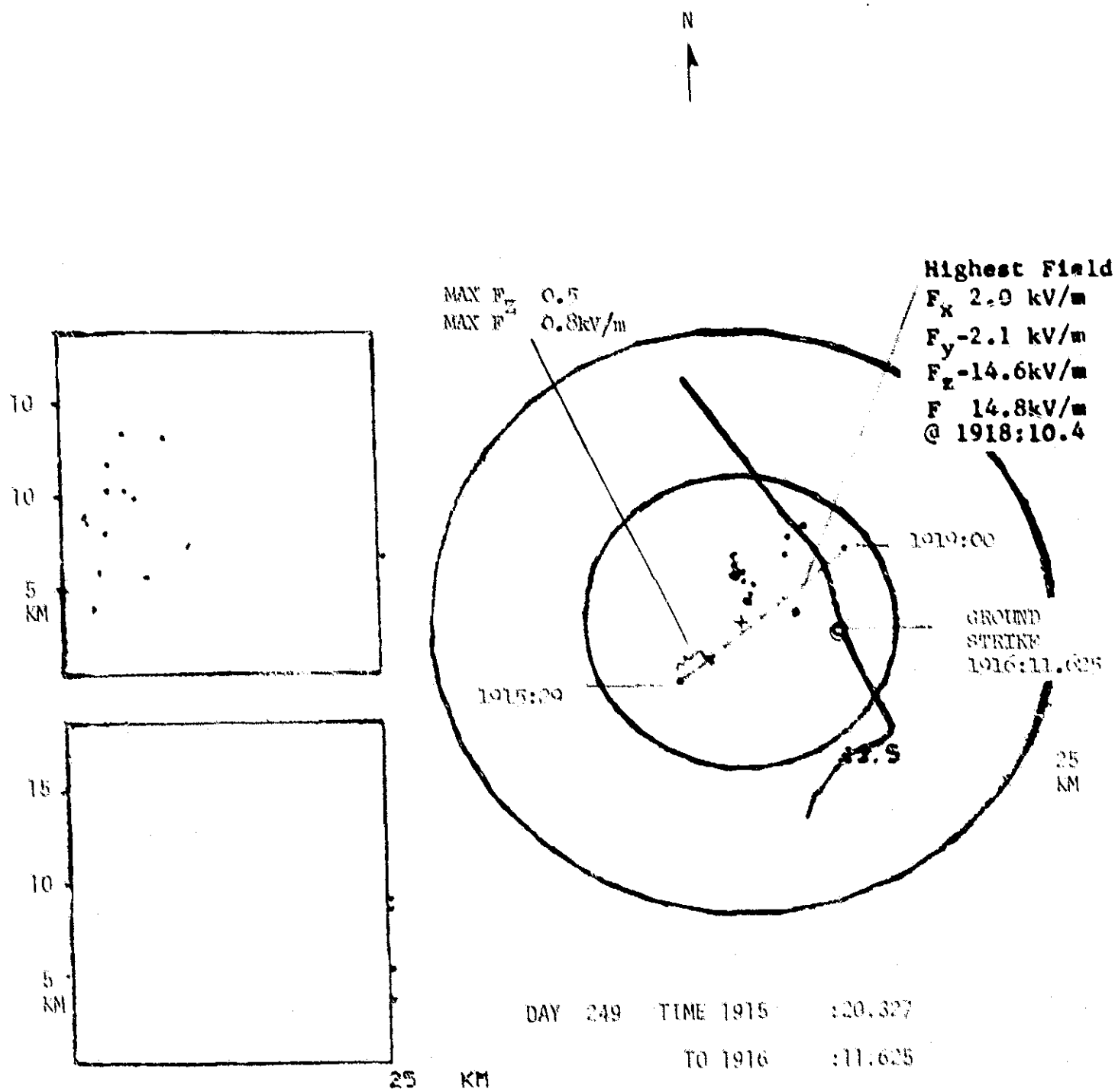

FIG. 65 LDAR PLOT OF 1915:20.327 TO 1916:11.451 GMT
WITH SUPERIMPOSED NASA-6 TRACK (RUN #13)
GROUND STRIKE AT 1916:11.625 GMT (7.5,-0.7)km

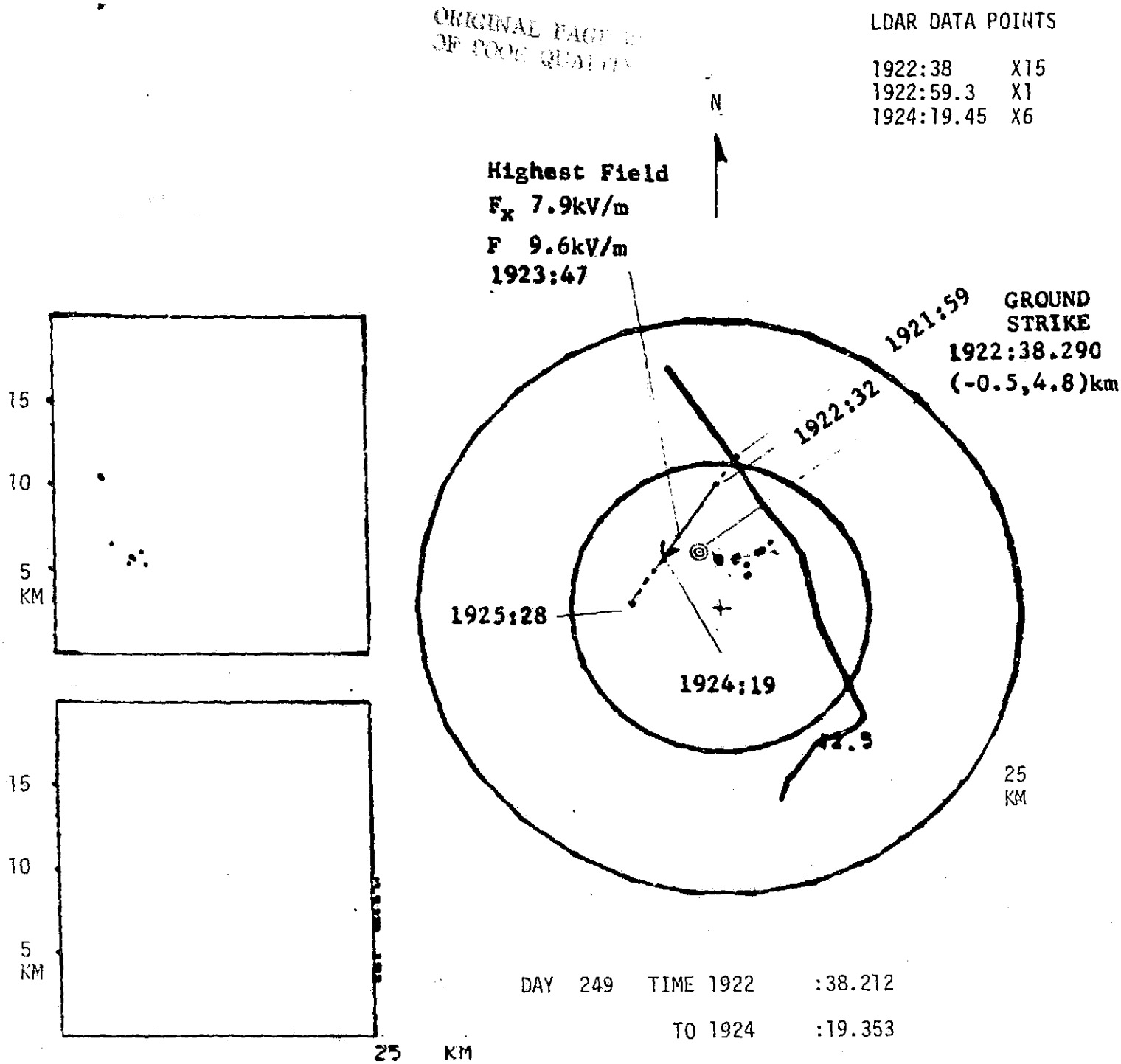

FIG. 66 LDAR PLOT OF 1922:38.212 TO 1924:19.353 GMT, WITH SUPERIMPOSED NASA-6 TRACK (RUN #14), AND AIRBORNE FIELD STRENGTH

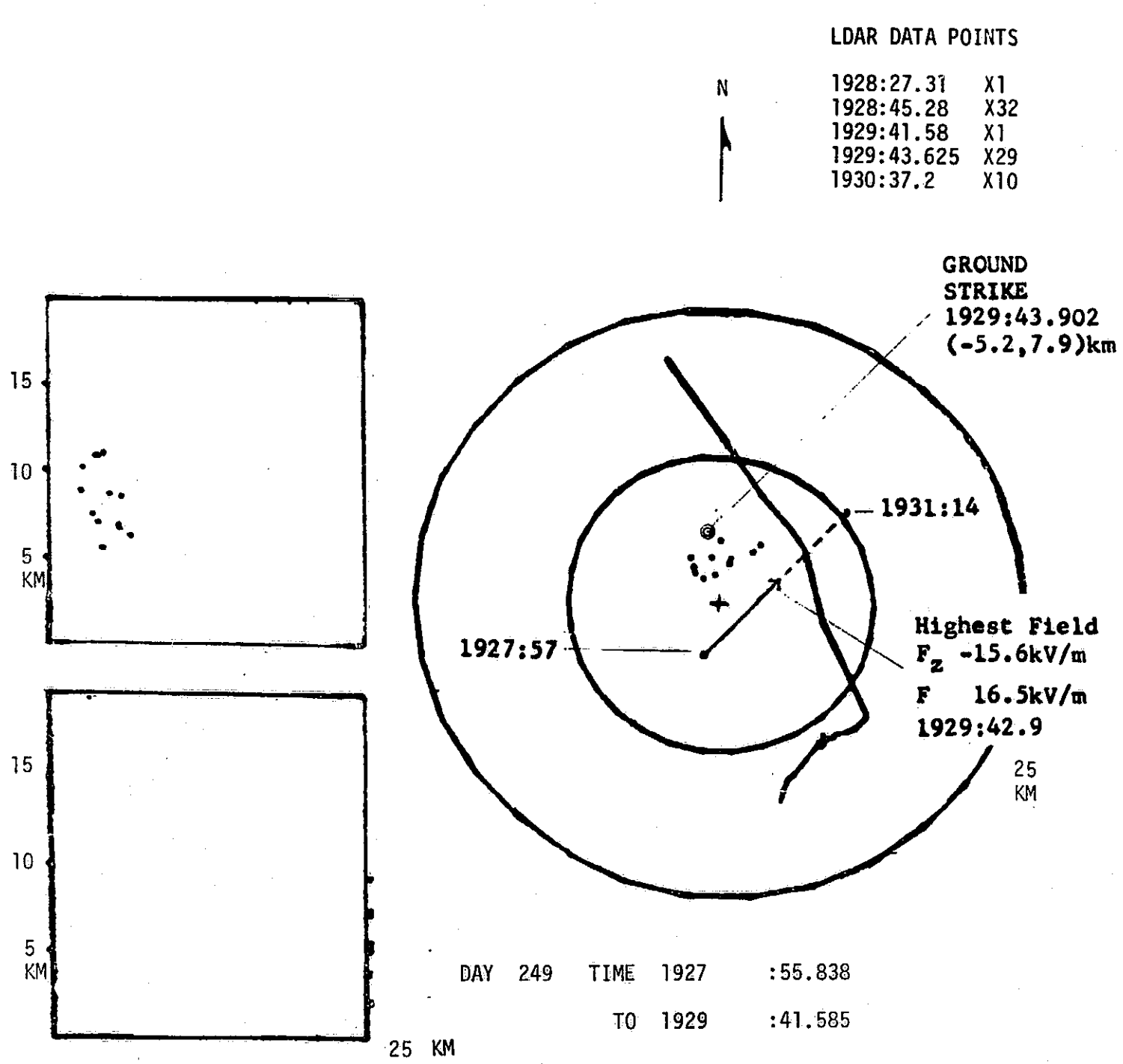

FIG. 67 LDAR PLOT OF 1927:55.838 TO 1929:41.585 GMT, WITH SUPERIMPOSED NASA-6 TRACK (RUN #15), AND AIRBORNE FIELD STRENGTH

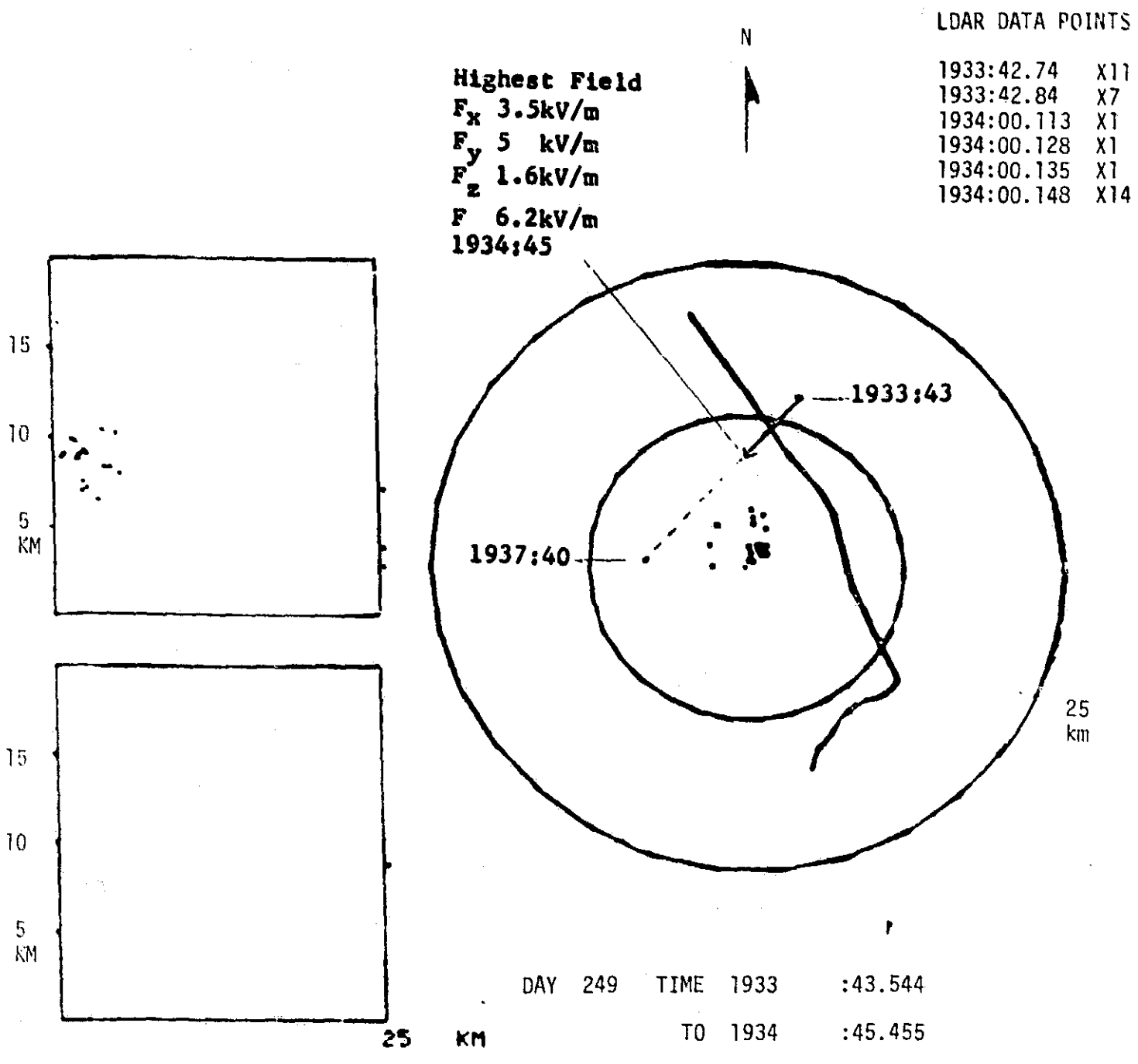

FIG. 68 LDAR PLOT OF 1933:43.544 TO 1934:45.455 GMT, WITH SUPERIMPOSED NASA-6 TRACK (RUN #16), AND AIRBORNE FIELD STRENGTH

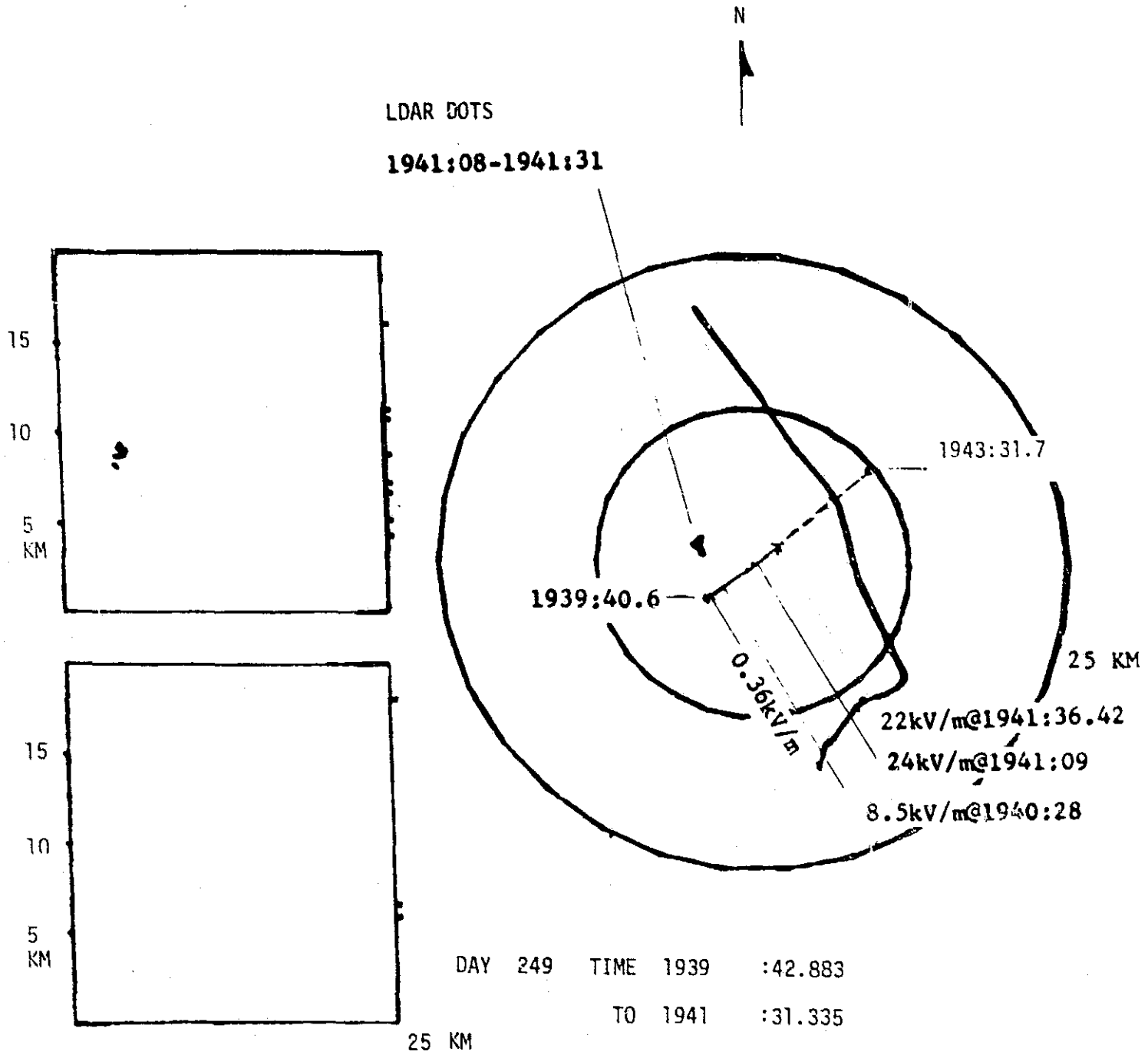

FIG. 69 LDAR PLOT OF 1939:42.883 TO 1941:31.335 GMT, WITH SUPERIMPOSED NASA-6 TRACK (RUN #17), AND AIRBORNE FIELD STRENGTH

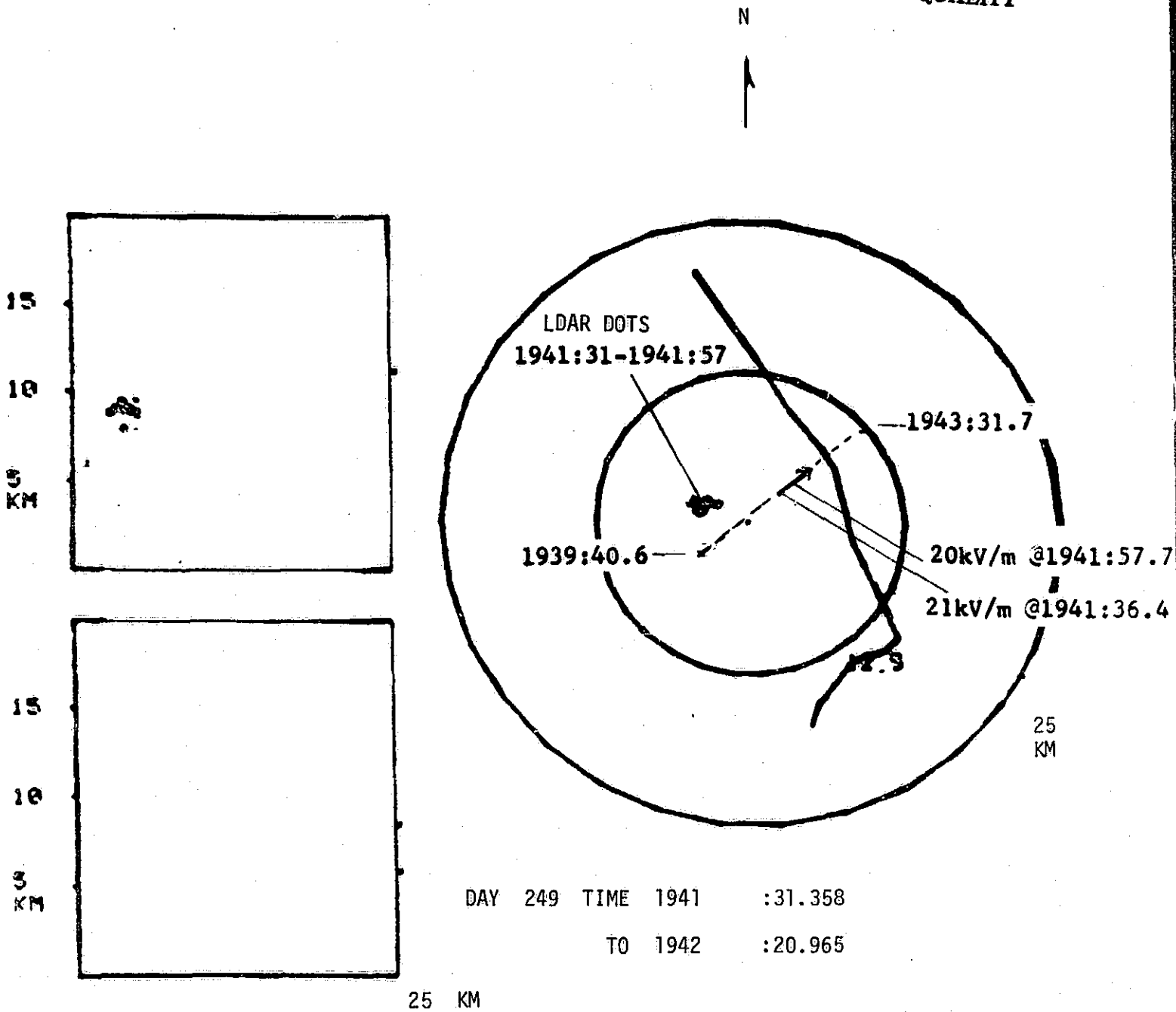

FIG. 70 LDAR PLOT OF 1941:31.358 TO 1942:20.965 GMT, WITH SUPERIMPOSED NASA-6 TRACK (RUN #17), AND AIRBORNE FIELD STRENGTH

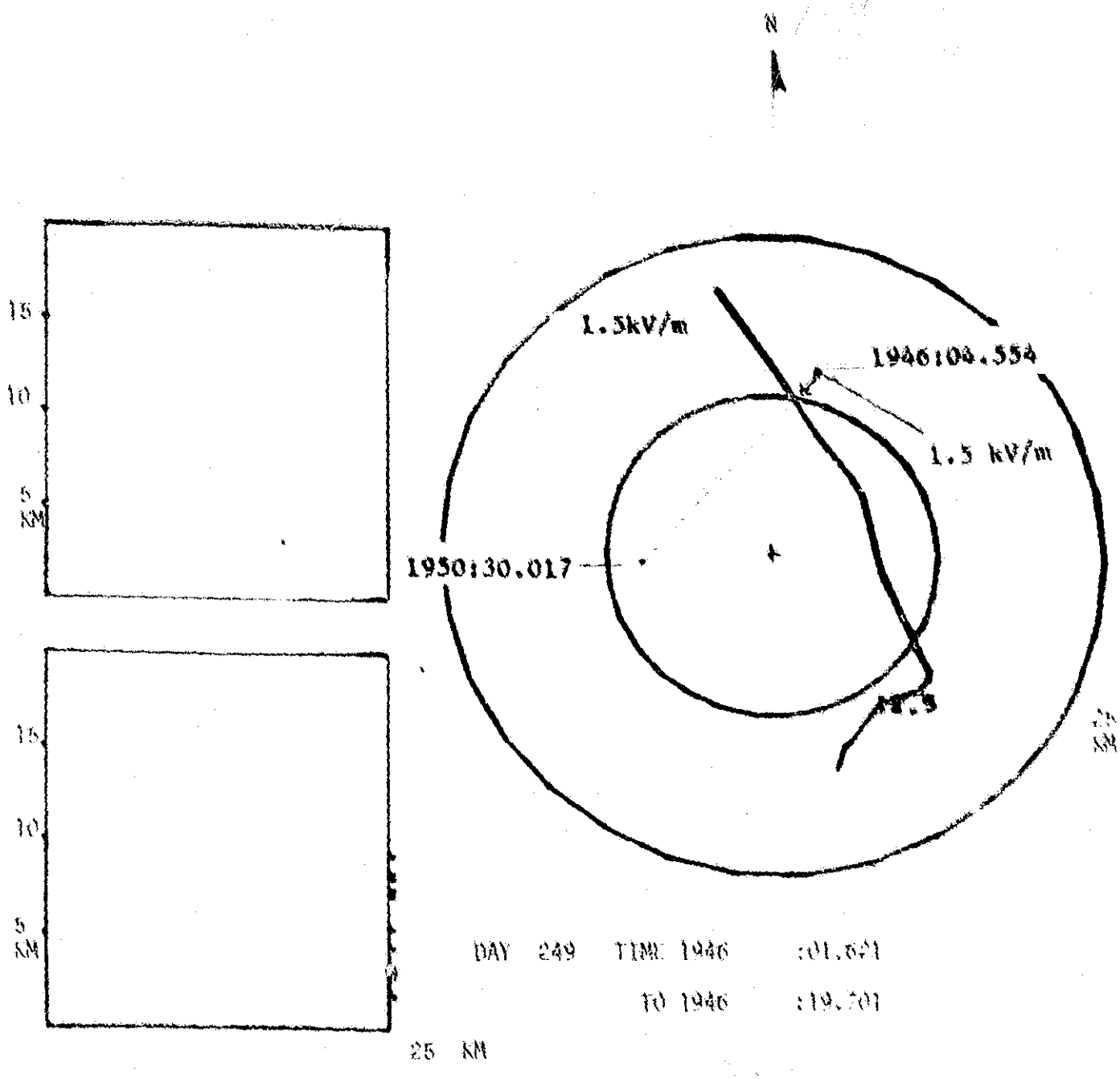

FIG. 71 LDAR PLOT OF 1946:01.621 TO 1946:19.701 GMT, WITH SUPERIMPOSED NASA-6 TRACK (RUN #18), AND AIRBORNE FIELD STRENGTH

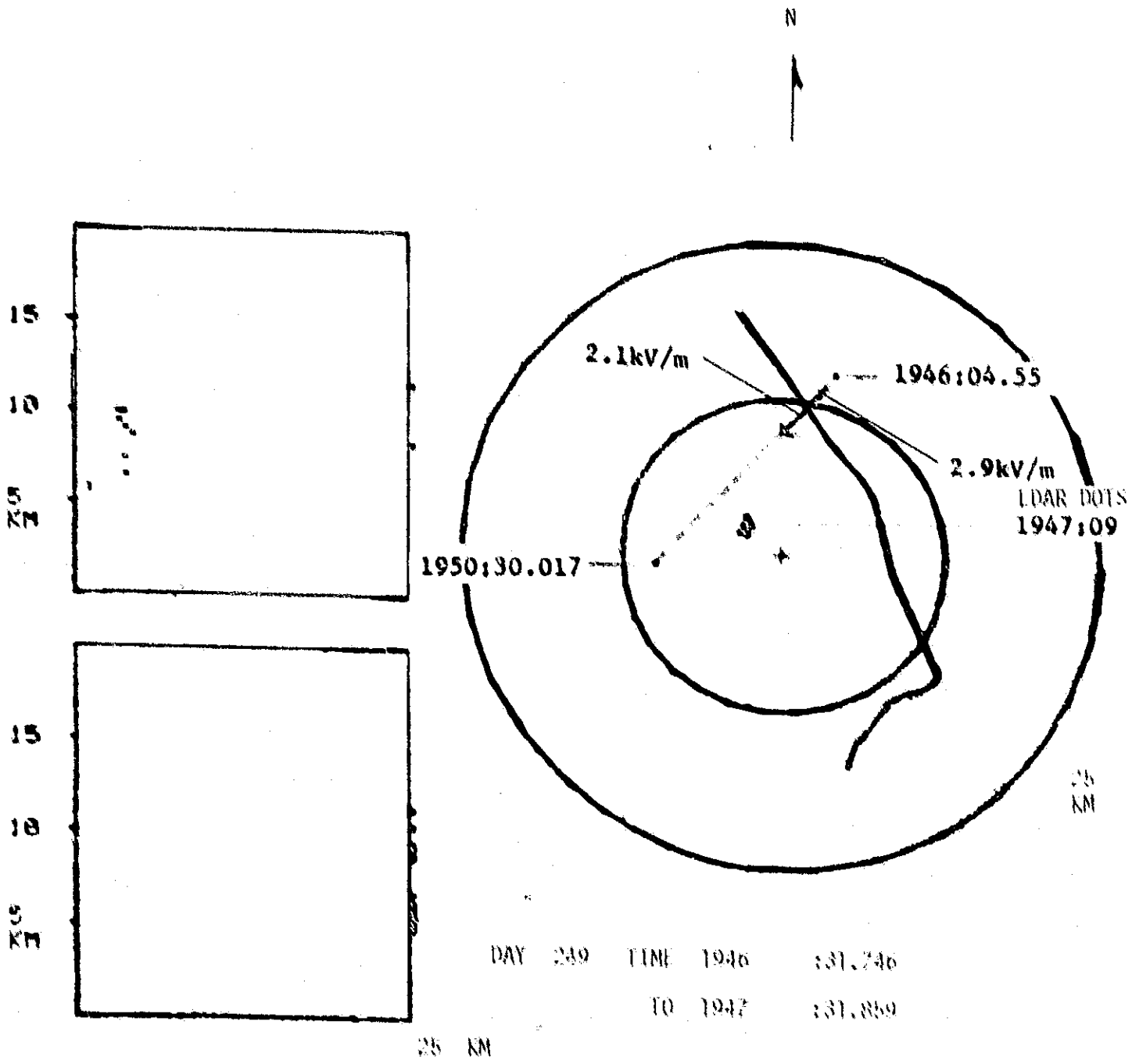

FIG. 42 LDAR PLOT OF 1946:31.246 TO 1947:31.859 GMT, WITH SUPERIMPOSED NASA-6 TRACK (RUN #18), AND AIRBORNE FIELD STRENGTH

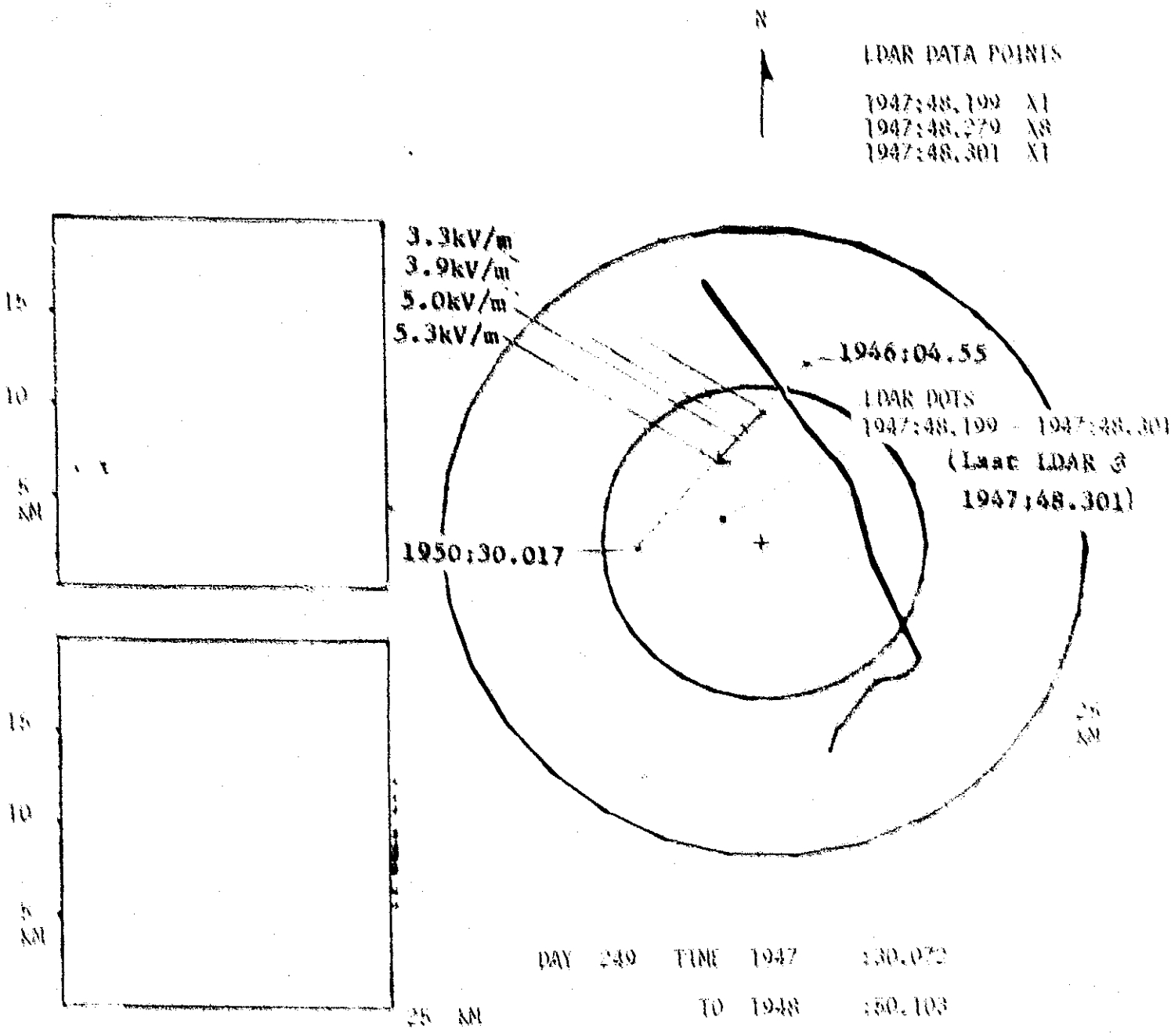

FIG. 73 LDAR PLOT OF 1947:30.072 TO 1948:50.103 GMT, WITH SUPERIMPOSED NASA-6 TRACK (RUN #18), AND AIRBORNE FIELD STRENGTH

that occur in a 50 to 100 millisecond sequence. Note, for example that in Figure 67, thirty-four data points occurred in the time span covered by the LDAR plot. However, only fourteen appear on the plot. The other twenty-three were so close together that they overlapped.

LDAR discharges occur in closely spaced sequences. For example, in Figure 67, at 1928:45.28 GMT there were some 32 LDAR data points separated in time by 10 milliseconds (on the average), and spaced by 1 km (on the average). The bunching of the LDAR data points in space and time is typical of the LDAR data, and has already been illustrated and discussed in connection with Figure 9.

The Higest Airborne Field

The highest airborne field recorded in the plots was 22 kV/m. Higher readings were not obtained since NASA-6 is not permitted to fly too close to the center of the storm. The closest approach here was approximately 5 km. To solve the problem one needs a more rugged airplane, designed to fly through the center of thunderstorms. Such airplanes exist, but were not available to us. The problem could also be solved by instrumented rockets that are launched through the center of the thunderstorm.

Correlation of Airborne Field Mill Reading with Distance to Nearest LDAR Point

Airborne field mill readings have been correlated with the nearest LDAR discharge point, in both distance and time. The results are shown plotted in Figure 74. Unfortunately the data is too scattered to form a basis for predicting airborne field strength at various distances from an LDAR discharge point. However, the data does indicate that the electric field strength at an LDAR discharge point is in excess of 200 kV/m.

FIG. 74 RELATION BETWEEN THE MEASURED ELECTRIC FIELD AND THE DISTANCE TO THE NEAREST LDAR DATA POINT

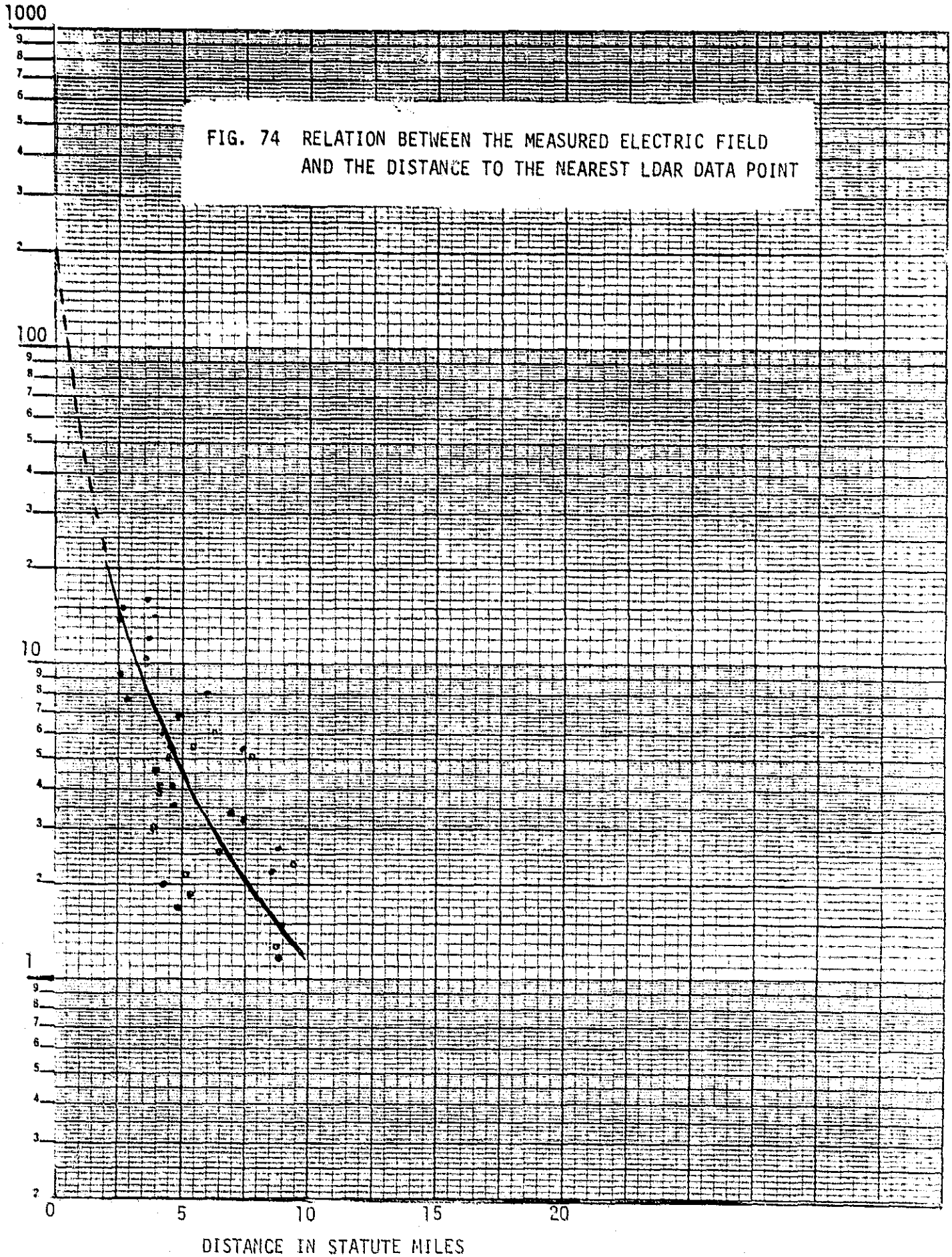

H. GROUND-BASED FIELD MILLS VS AIRBORNE FIELD MILLS

Airborne field mill measurements were correlated with concurrent ground-based field mill measurements at points directly beneath the airplane. For eight of the airplane runs (Runs #11-18) during the peak of the storm, and for one run (Run #19) during the decaying portion of the storm, the airplane's track was superimposed on the field mill contour plots, as shown in Figures 75 to 83.

Figure 75	Run #11	1903:47	to	1907:17 GMT
76	Run #12	1910:36	to	1913:09 GMT
77	Run #13	1915:29	to	1919:00 GMT
78	Run #14	1921:59	to	1925:28 GMT
79	Run #15	1927:57	to	1931:14 GMT
80	Run #16	1933:41	to	1937:40 GMT
81	Run #17	1946:04	to	1950:30 GMT
82	Run #18	1952:09	to	1955:56 GMT
83	Run #19	1939:41	to	1943:32 GMT

The position of the airplane at the instant represented by the field mill contour plot was derived by extrapolation from the airplane's known position and time at the end points, on the assumption of constant speed, for points in between The height was 10,500 feet. The position of the airplane is shown on each plot, as well as the measured values of the airborne field-strength components F_X, F_Y, F_Z, and F ($= \sqrt{F_X^2 + F_Y^2 + F_Z^2}$).

The parameter of interest is the ratio of the airborne to the ground-based field mill reading. In keeping with Kasemir's nomenclature, we shall call this ratio the multiplication factor, and determine this for the

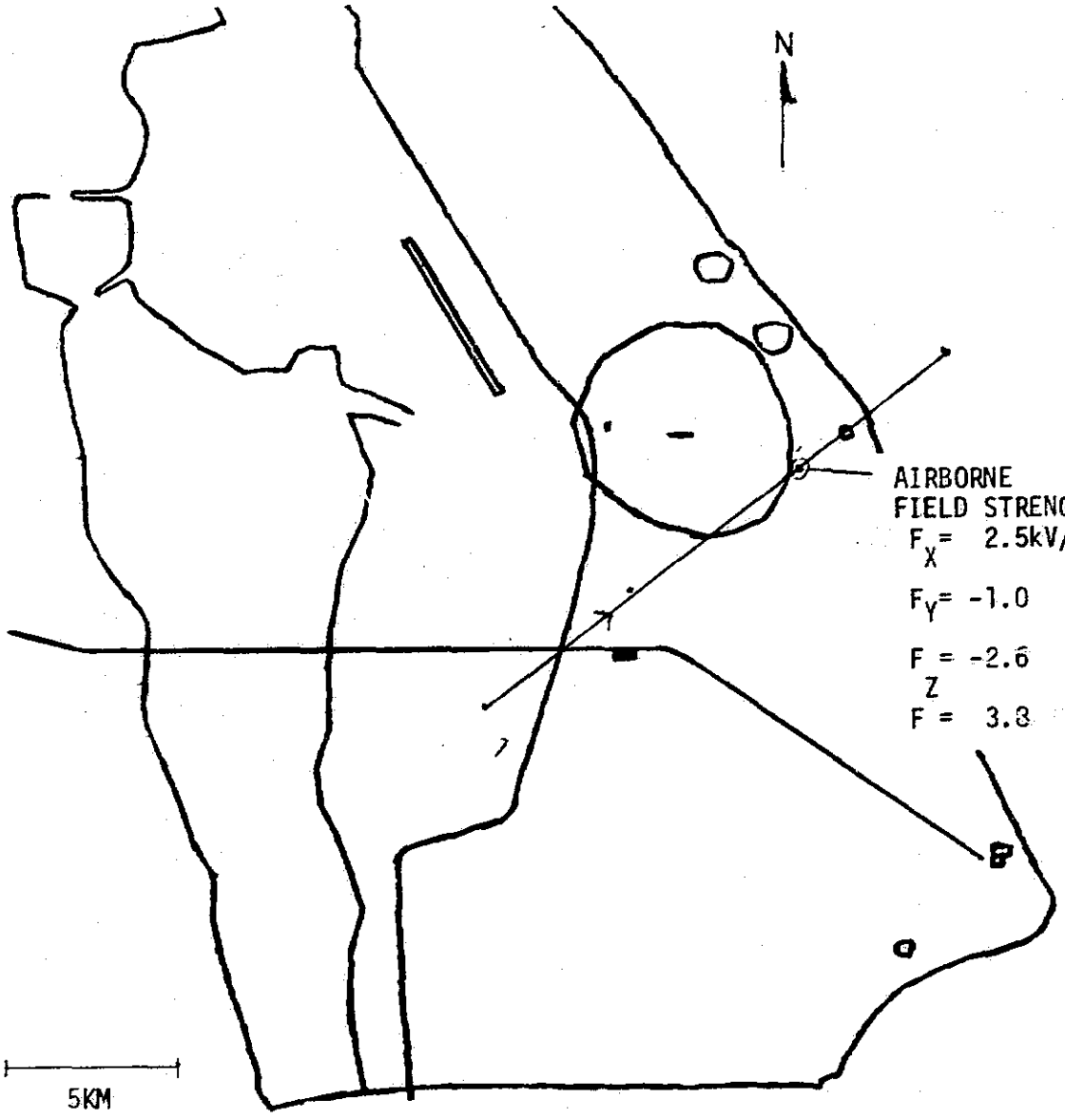

KSC EQUIPOTENTIAL
GRADIENT CONTOURS

09/06/77 1906:09.138 GMT

Line Scale - 1000 V/M

Site #	Volts/Meter
1	-47
2	261
3	169
4	199
5	107
6	-108
7	261
8	-416
9	-693
10	230
11	-508
12	-1216
13	-570
14	-1277
15	-1370
16	-293
17	-416
18	76
19	-785
20	-262
21	-201
22	199
23	261

FIG. 75 FIELD MILL CONTOUR PLOT OF 1906:09.138 GMT, WITH SUPERIMPOSED FLIGHT PATH (RUN #11), AND AIRBORNE FIELD MILL READINGS

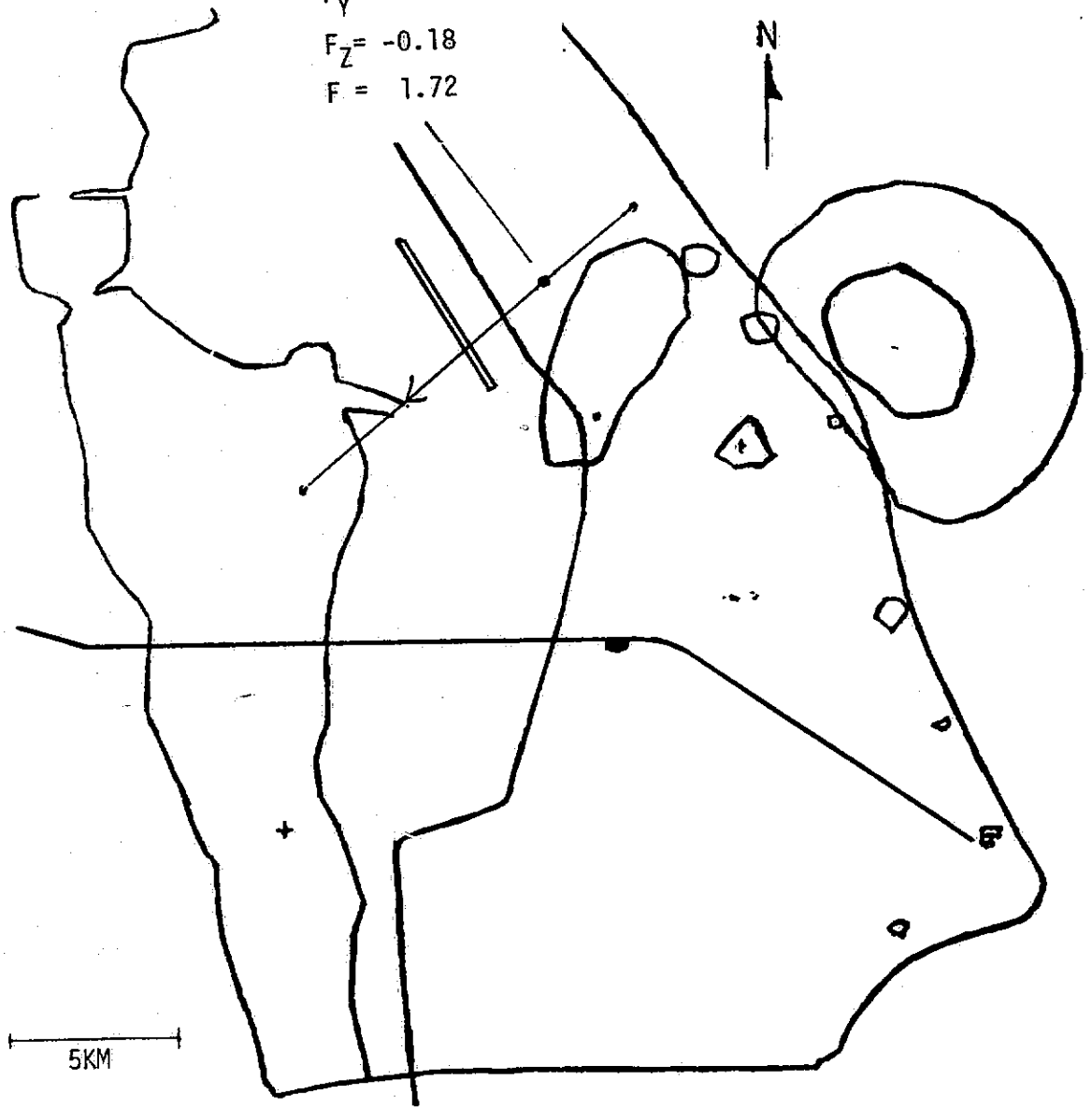

KSC EQUIPOTENTIAL
GRADIENT CONTOURS

09/06/77 1911:16.242 GMT

Line Scale - 1000 V/M

Site #	Volts/Meter
1	-416
2	169
3	46
4	138
5	-16
6	-385
7	169
8	-785
9	-908
10	138
11	-447
12	-1431
13	-1647
14	1369
15	-785
16	-1154
17	-693
18	-16
19	-847
20	-416
21	-601
22	76
23	138
24	138

FIG. 76 FIELD MILL CONTOUR PLOT OF 1911:16.242 GMT, WITH SUPERIMPOSED FLIGHT PATH (RUN #12), AND AIRBORNE FIELD MILL READINGS

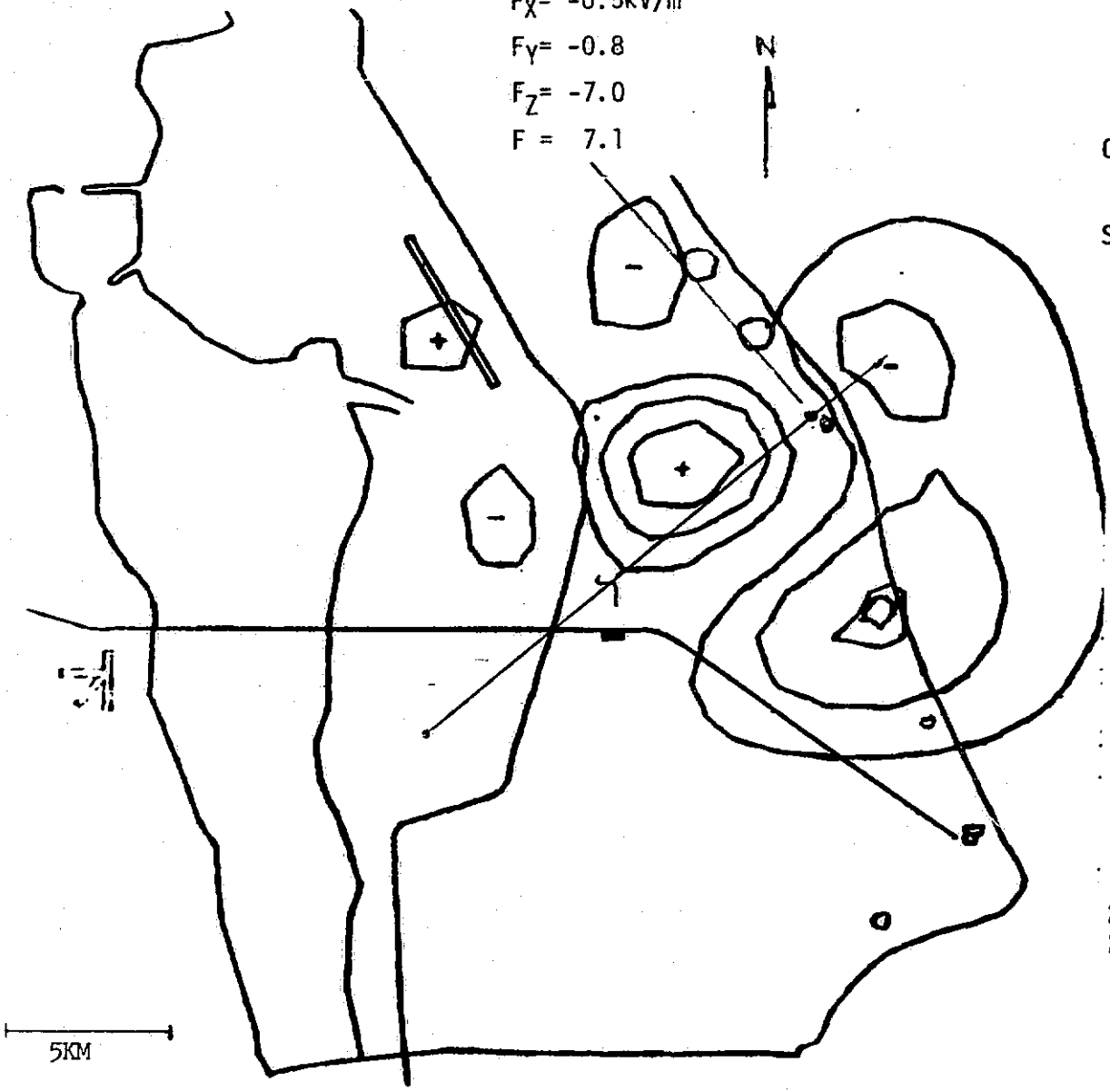

KSC EQUIPOTENTIAL
GRADIENT CONTOURS

09/06/77 1918:26.197 GMT

Line Scale - 1000 V.M

Site #	Volts/Meter
1	-3216
2	76
3	-324
4	-201
5	-262
6	-477
7	-16
8	-785
9	-570
10	-139
11	661
12	-385
13	-1370
14	2938
15	2846
16	-1216
17	-1216
18	-139
19	1399
20	969
21	-785
22	-262
23	-139
24	-47

FIG. 77 FIELD MILL CONTOUR PLOT OF 1918:26.197 GMT, WITH SUPERIMPOSED FLIGHT PATH (RUN #13), AND AIRBORNE FIELD MILL READINGS

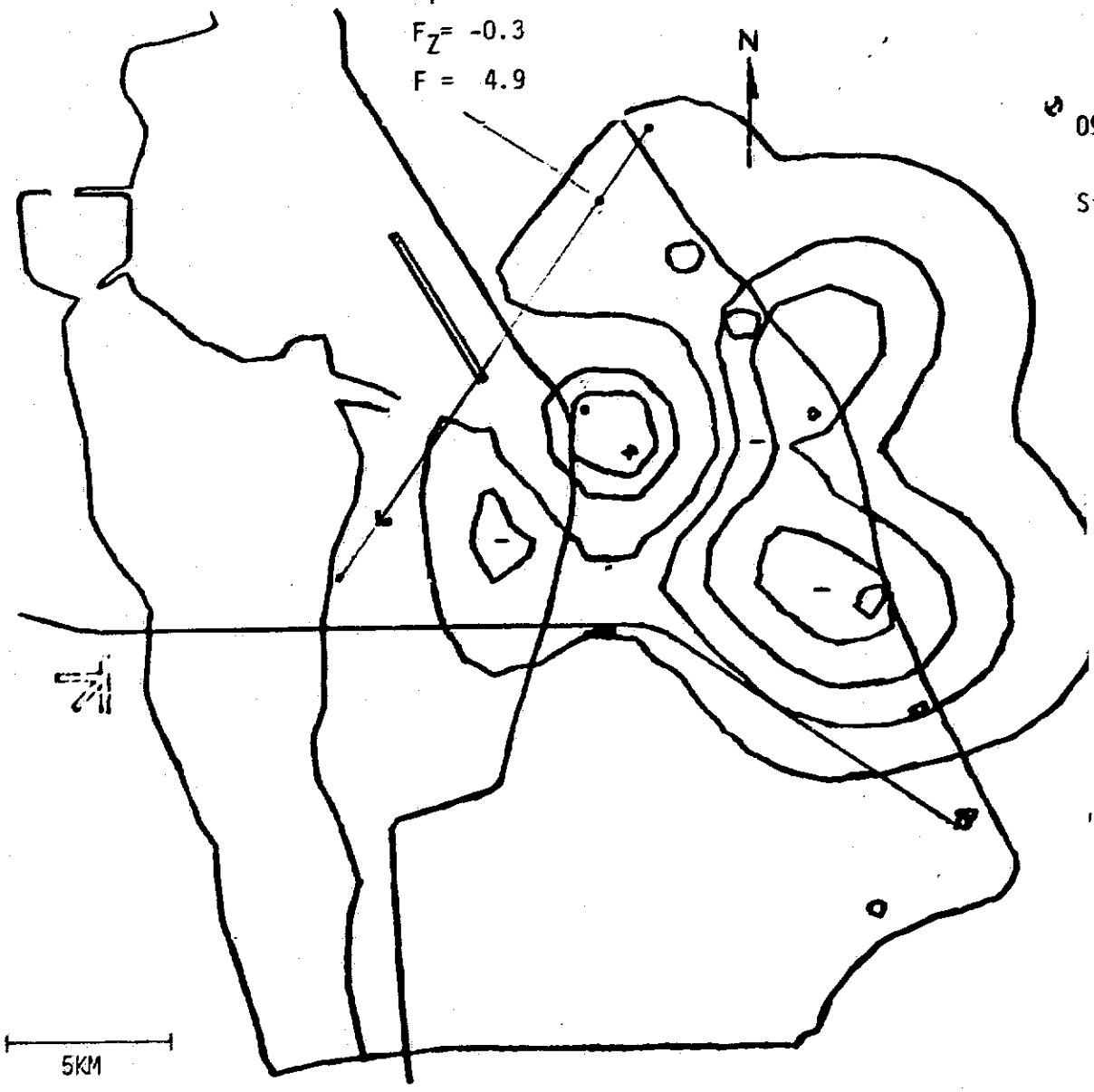

KSC EQUIPOTENTIAL
GRADIENT CONTOURS

09/06/77 1922:31.873 GMT

Line Scale - 1000 V/M

Site #	Volts/Meter
1	-4447
2	-16
3	-785
4	-539
5	-508
6	-877
7	-139
8	-1401
9	-1616
10	-447
11	-724
12	138
13	-3954
14	-1677
15	3338
16	-2508
17	-1616
18	-724
19	-2385
20	-1154
21	-1893
22	-785
23	-324
24	-231

FIG. 78 FIELD MILL CONTOUR PLOT OF 1922:31.873 GMT, WITH SUPERIMPOSED FLIGHT PATH (RUN #14), AND AIRBORNE FIELD MILL READINGS

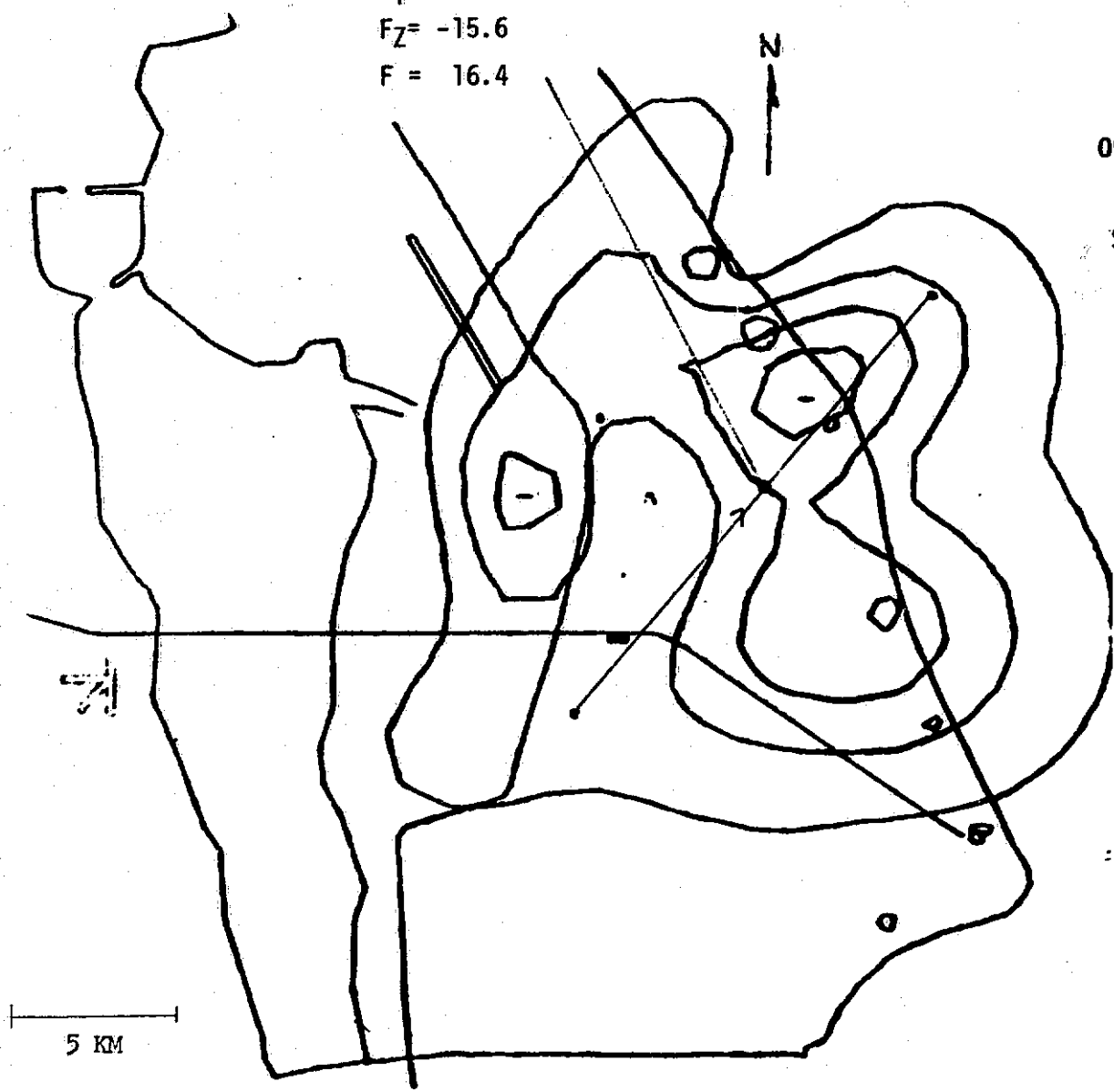

KSC EQUIPOTENTIAL
GRADIENT CONTOURS

09/96/77 1929:41.712 GMT

Line Scale - 1000 V/M

Site #	Volts/Meter
1	-3800
2	-108
3	-1185
4	-1000
5	-570
6	-1000
7	-539
8	-1124
9	-1124
10	-785
11	-1924
12	-2939
13	-4354
14	-3454
15	-1370
16	-2816
17	-3431
18	-508
19	-1800
20	-1247
21	-2354
22	-1431
23	-539
24	-416

FIG. 79 FIELD MILL CONTOUR PLOT OF 1929:41.712 GMT, WITH SUPERIMPOSED FLIGHT PATH (RUN #15), AND AIRBORNE FIELD MILL READINGS

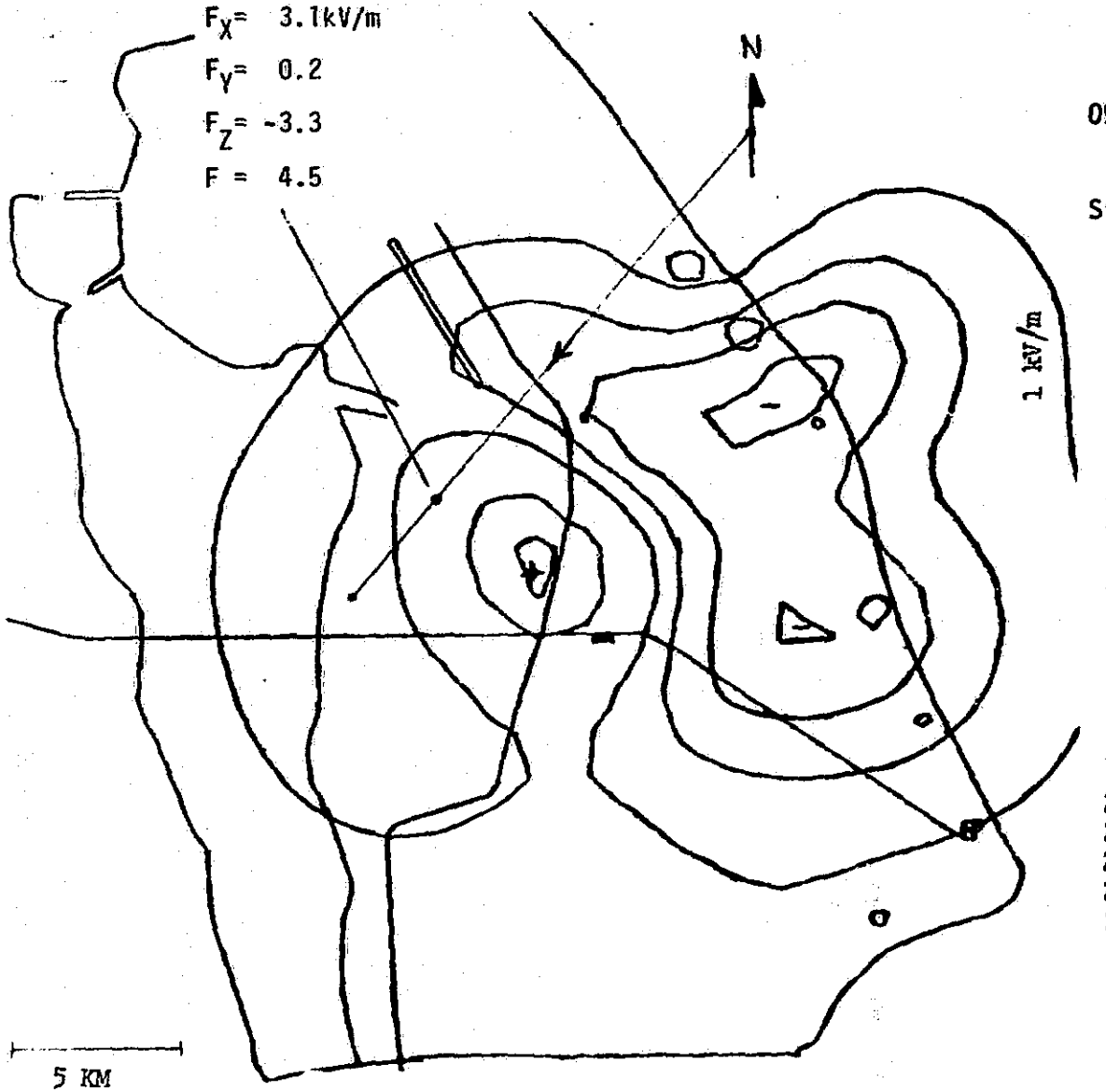

KSC EQUIPOTENTIAL
GRADIENT CONTOURS

09/06/77 1936:51.581 GMT

Line Scale - 1000 V/M

Site #	Volts/M
1	-3800
2	46
3	-1677
4	-1370
5	-16
6	-601
7	-139
8	-447
9	-1124
10	-1093
11	-2477
12	-2785
13	-4108
14	-4077
15	-2785
16	-3000
17	1399
18	-631
19	-2416
20	1061
21	-2416
22	-1462
23	-570
24	-631

FIG. 80 FIELD MILL CONTOUR PLOT OF 1936:51.581 GMT, WITH SUPERIMPOSED FLIGHT PATH (RUN #16), AND AIRBORNE FIELD MILL READINGS

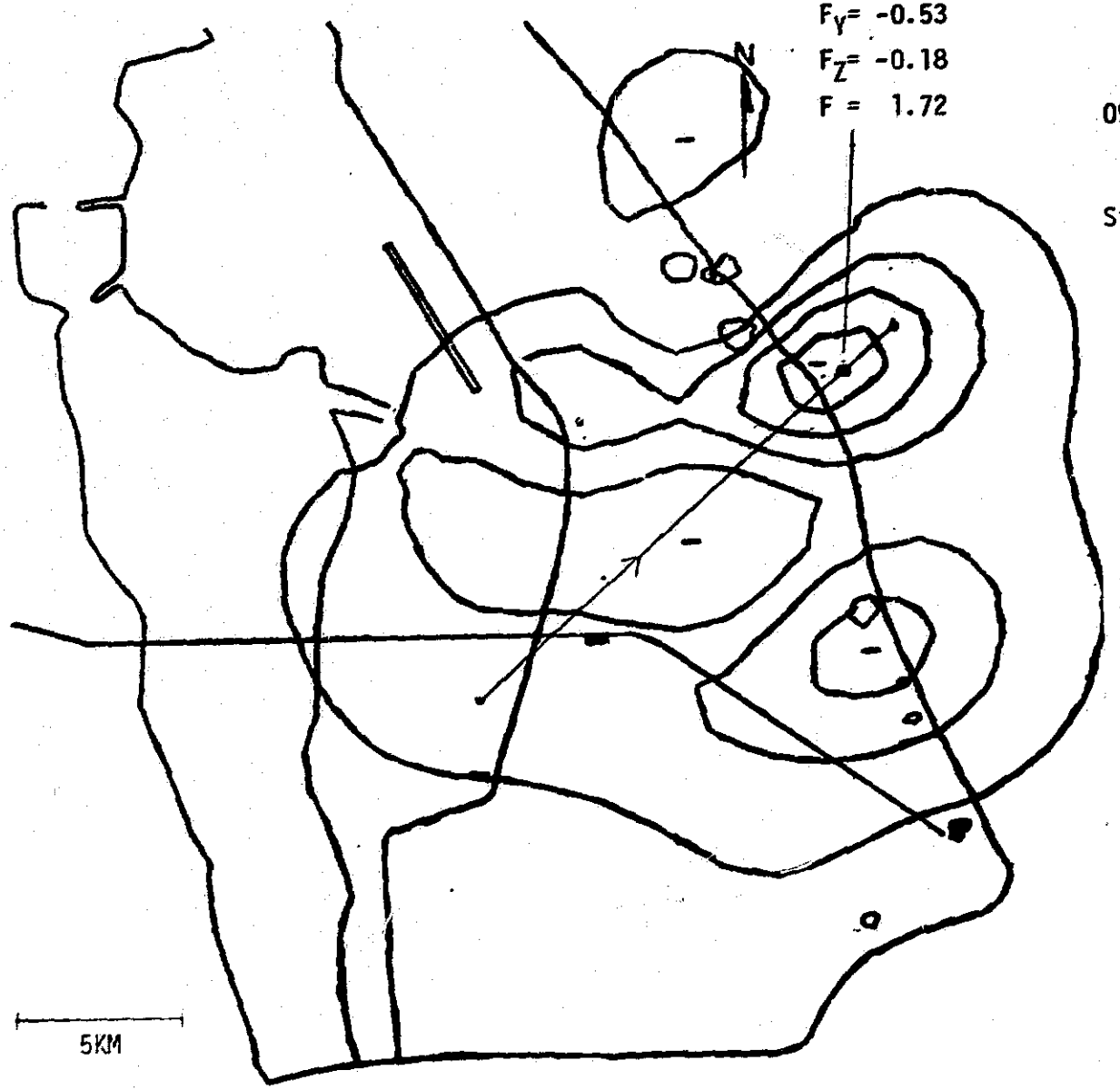

KSC EQUIPOTENTIAL
GRADIENT CONTOURS

09/06/77 1943:01.110 GMT

Line Scale - 1000 V/M

Site #	Volts/Meter
1	-3308
2	323
3	-1462
4	-1124
5	507
6	353
7	538
8	-385
9	1123
10	-1000
11	-1708
12	-1985
13	-4170
14	-1800
15	-1985
16	-2262
17	-508
18	-1062
19	846
20	-385
21	-1124
22	-1308
23	-508
24	-601

FIG. 81 FIELD MILL CONTOUR PLOT OF 1943:01.110 GMT, WITH SUPERIMPOSED FLIGHT PATH (RUN #17), AND AIRBORNE FIELD MILL READINGS

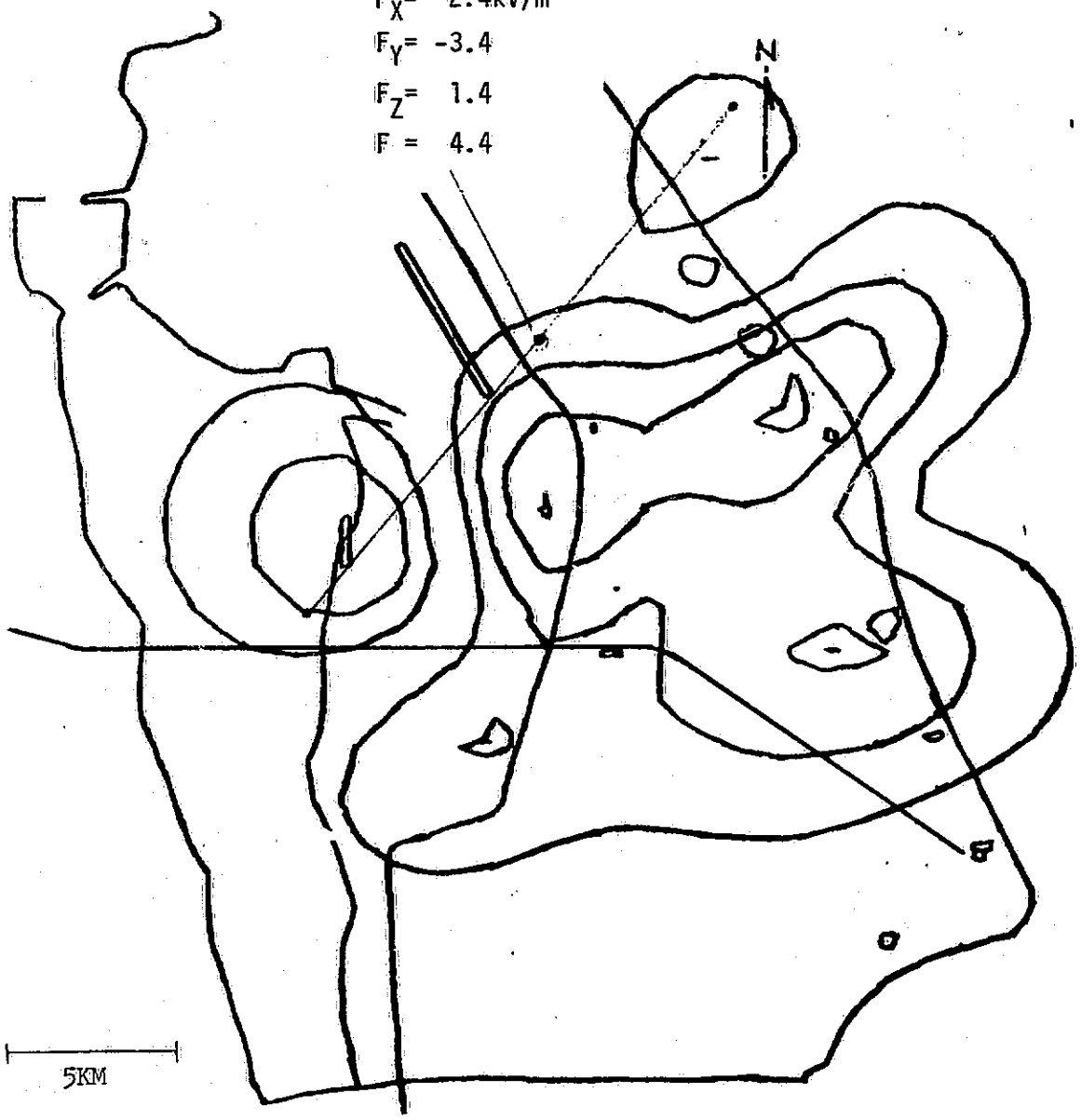

KSC EQUIPOTENTIAL
GRADIENT CONTOURS

09/06/77 1948:07.021 GMT

Line Scale - 1000 V/M

Site #	Volts/Meter
1	-3031
2	681
3	-1124
4	-662
5	199
6	199
7	323
8	-1000
9	-601
10	-601
11	-1524
12	-1985
13	-3954
14	-3800
15	-3370
16	-1924
17	-3770
18	1799
19	-2293
20	-2201
21	-2231
22	-1831
23	-631
24	-416

FIG. 82 FIELD MILL CONTOUR PLOT OF 1948:07.021 GMT, WITH SUPERIMPOSED FLIGHT PATH (RUN #18), AND AIRBORNE FIELD MILL READINGS

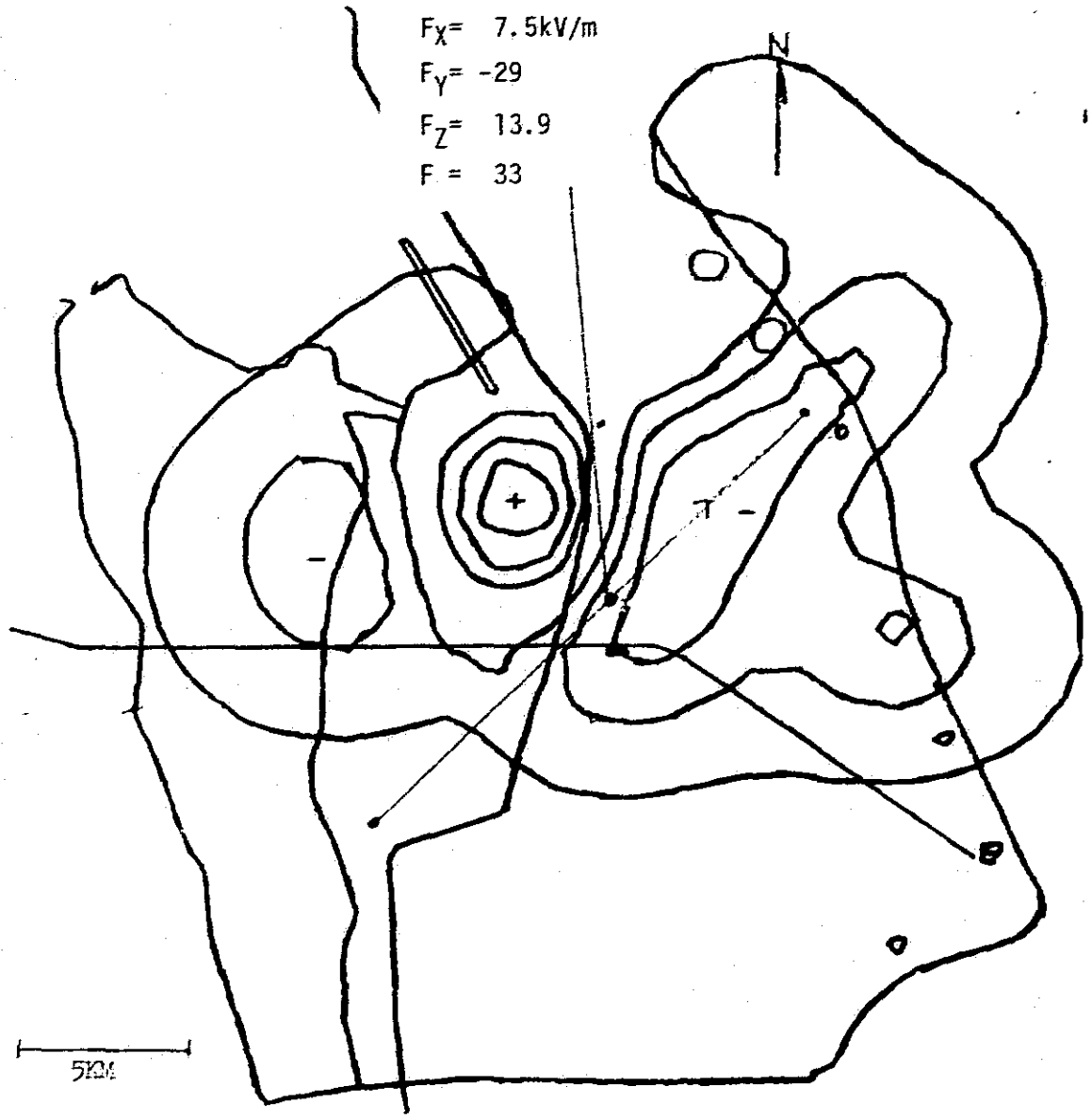

KSC EQUIPOTENTIAL
GRADIENT CONTOURS

09/06/77 1954:15.433 GMT

Line Scale - 1000 V/M

Site #	Volts/Meter
1	-2539
2	800
3	-601
4	-477
5	169
6	199
7	199
8	-847
9	-389
10	-324
11	-754
12	415
13	-3093
14	-3524
15	-1616
16	-1893
17	3953
18	-539
19	-3585
20	-3031
21	-2816
22	-1000
23	-447

FIG. 83 FIELD MILL CONTOUR PLOT OF 1954:15.433 GMT, WITH SUPERIMPOSED FLIGHT PATH (RUN #19), AND AIRBORNE FIELD MILL READINGS

ratios F_Z/F_G and for the ratios F/F_G, where F_G is the ground-based field mill reading, and where negative signs have been disregarded.

The mean, standard deviation, and the median values of the multiplication factors have been calculated, and are shown together with the data in Table VI.

For comparison we cite the multiplication factors calculated by Kasemir et al[4]. For a model of a simple bipolar thunderstorm they found the multiplication factor to range from 2.4 to 5 for the vertical component and from 1.8 to 5.4 for the horizontal component of the maximum airborne fields above ground-based fields of 1 and 5 kV/m, respectively.

TABLE VI

RATIO OF AIRBORNE TO GROUND-BASED FIELD MILL READINGS

	AIRBORNE		GROUND-BASED	RATIO	RATIO
	F_Z	F	F_G	F_Z/F_G	F/F_G
GMT	kV/m	kV/m	kV/m	(MULTIPLICATION FACTOR)	(MULTIPLICATION FACTOR)
1906	-2.6	3.8	1.0	2.6	3.8
1911	-.18	1.72	0.9	0.2	1.9
1918	-7	7.1	0.9	7.8	7.9
1922	-0.28	4.0	1.3	0.2	3.8
1929	-15.6	16.4	2	7.8	8.2
1936	-3.3	4.5	1.5	2.2	3
1943	-16	18	4.2	3.8	4.2
1948	+1.4	4.4	1.3	1.1	3.4
1954	+13.9	33	2.4	5.8	14
			Mean	3.5	5.6
			Std. Dev.	3.0	3.8
			Median	2.8	3.6

Detailed analysis of the thermal thunderstorm of September 6, 1977 shows:

1. Ground strikes generally occur near* the edge of the radar precipitation echo.

2. Ground strikes generally occur within 2 km of the center of the LDAR discharge points.

3. LDAR cloud discharge data points generally do not occur until the radar tops exceed 30,000 feet.

4. The use of an on-board lightning simulator is a feasible, and a very accurate, way to determine the position of an airplane within the LDAR System, expecially in the investigation of thunderstorms.

5. A high field-mill reading cannot be relied upon as a necessary criterion for an impending ground strike. In our test, a ground strike took place within the field mill network at a time when the maximum field mill reading in the field mill network was no higher than 0.91 kV/m.

6. A ground strike clears the cloud of high field gradients, at least for a minute or two, as determined from the decrease and the scattering of the LDAR discharge data points.

7. The estimated value of the electric field at an LDAR discharge point in the cloud is in excess of 200 kV/m.

8. The new Ground Strike Location System, GSLS, was successfully employed to locate the position of ground strikes. The estimated precision of the ground strike measurement is 2%.

9. The ground strike positions determined by the GSLS System were in excellent agreement with the locations of the charge removed, determined by the flash (or dynamic) field mill contour plots.

10. Field mill contour plots are useful in telling that a disturbed condition exists, but are of limited value in telling where a ground strike is likely to take place.

11. The data shows LDAR to be useful as a warning system of impending ground strikes.

---

*Some inside, an approximately equal number outside the precipitation echo, with mean distances from the edge of 2 km for those inside, and 2 km for those outside.

V. REFERENCES

1. Poehler, H. A., "Measured Electrical Field Intensities Near Electrical Cloud Discharges Detected by the Kennedy Space Center's Lightning Detection and Ranging System, LDAR," FEC 720-7154, February 1977, Federal Electric Corporation, Kennedy Space Center, Florida, 32899.

2. Poehler, H. A., "S-Band Radar Calibration Test of the Lightning Detection and Ranging System, LDAR," RCA 620-5001, June 1, 1978, NASA Contractor Report No. 154627 Radio Corporation of America, Kennedy Space Center, Florida, 32899.

3. Nicholson, J., "On Thunderstorms at KSC," American Geophysical Union, 1975 Fall Meeting, San Francisco, December 1975.

4. Kasemir, W, Rust, W. D., and Holitza, F. J., "Final Report to KSC Contract No. CC-59753", June 1976, Atmospheric Physics and Chemistry Laboratory, National Oceanic and Atmospheric Administration, Boulder, Colorado.

5. Uman, M. A. et al, "An Unusual Lightning Flash at the Kennedy Space Center," Science, 7 July 1978, vol.201, pp.9-16.

6. Latham, R, "Aircraft Positioning with Multiple DME," Navigation, Journal of the Institute of Navigation, Vol. 21, No. 2, Summer 1974, pp.150-158.

7. Poehler, H. A., "An Accuracy Analysis of the LDAR System," FEC-7146, 8 March 1977, Federal Electric Corporation, Kennedy Space Center, Florida, 32899.

8. Poehler, H. A., "LDAR III, System Description and Performance Objectives," FEC 720-7157, 26 April 1977, Federal Electric Corporation, Kennedy Space Center, Florida, 32899.

AIRBORNE FIELD MILL SYSTEM

The airborne field mill system consists of two cylindrical field mills mounted on the NASA-6 airplane. One field mill is mounted on the nose, with its axis of rotation horizontal, and pointed forward. The other field mill is mounted on the top of the plane, approximately in line with the wings, with its axis of rotation pointing up and perpendicular to the axis of the nose-mounted field mill.

The airborne cylindrical field mills are similar in principle to the ground-based field mills, but they differ in that they have a rotating cylinder in place of a rotating segmented rotor. They also differ in that the rotating cylinder is not grounded, but consists of two half cylinders that are able to take on charge. The rotating cylindrical field mill responds to electrostatic fields perpendicular to its axis of rotation. Phasing signals from an a-c generator, mounted on the same shaft as the cylindrical rotor of the field mill, permits one to decompose the electrostatic field perpendicular to the axis of rotation into its two components. Designating the upward direction of the rotational azis of the top-mounted cylindrical field mill by Z, when proper phasing signals are applied, this field mill provides an output proportional to F_X and F_Y. In a similar manner, the nose-mounted field mill supplies an output proportional to F_Z and F_X. Positive F_X, F_Y and F_Z field readings indicate positive field vectors directed from the left to the right wing tip, from the tail to the nose, and from the lower to the upper side of the airplane, respectively. When suitably calibrated, the airborne field mills provide measurement of the X, Y, and Z components of the ambient electrostatic field over the range 0.001 to 500 kV/meter.

APPENDIX B

GROUND-BASED FIELD MILL NETWORK

The vertical component of the electrostatic field at the ground is measured by a network of 25 field mills, strategically placed around the Kennedy Space Center, as shown in Figure 1A. The field mill is a capacitively coupled electric field pickup sensor that consists of an insulated, segmented stator, each sector of which is alternately covered and uncovered by a grounded four-segment rotor that revolves at 1800 rpm. When not covered by the grounded rotor segments, the stator segments assume the potential of the ambient electrostatic field. When covered, the potential of the insulated stator goes to zero. Hence the potential of the stator alternately jumps from the potential of the ambient field (either positive or negative) to zero. As an output we therefore have an voltage that alternates between zero and the voltage of the ambient field.

The output of the field mill is filtered to remove the high-frequency components, then amplified and rectified by a synchronous sample-and-hold circuit. A second low pass filter provides us with a bi-polar voltage proportional to amplitude, having a time constant of 0.1 second. Properly calibrated, the field mills provide us with a measure of the vertical component of the electrostatic field, from -15 kV/meter to +15 kV/meter, with a resolution of 0.05 kV/meter.

The output of the 25 field mills is digitized for transmission to the central processing facility. There the data is sampled once a minute for input to a computer. An especially-designed isocontour plotting program generates an isocontoured map of the electric field strength at KSC, as shown in Figure 2A. These field maps are used to identify areas where the

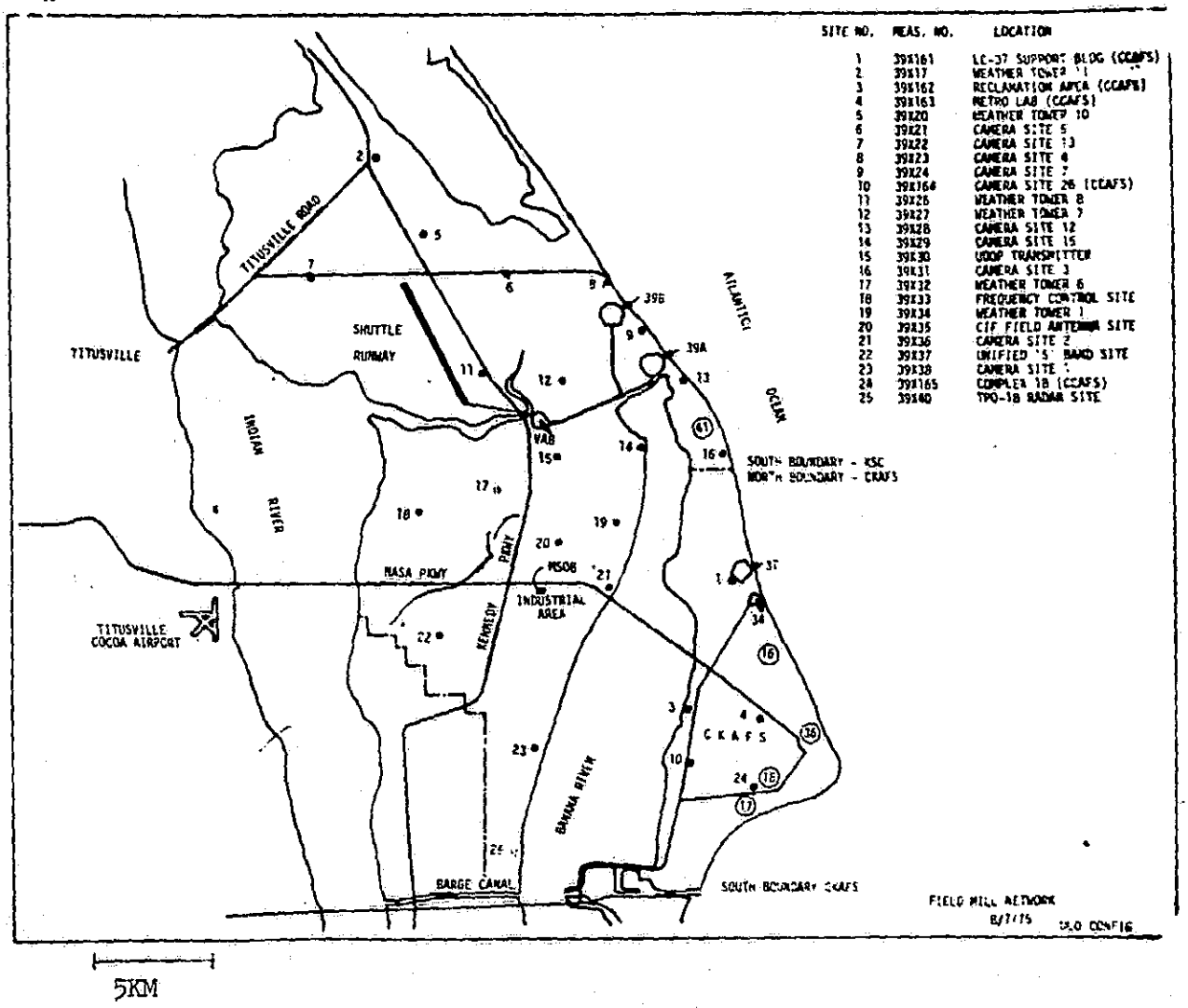

FIG. 1A FIELD MILL NETWORK
LOCATION OF FIELD MILL SENSORS

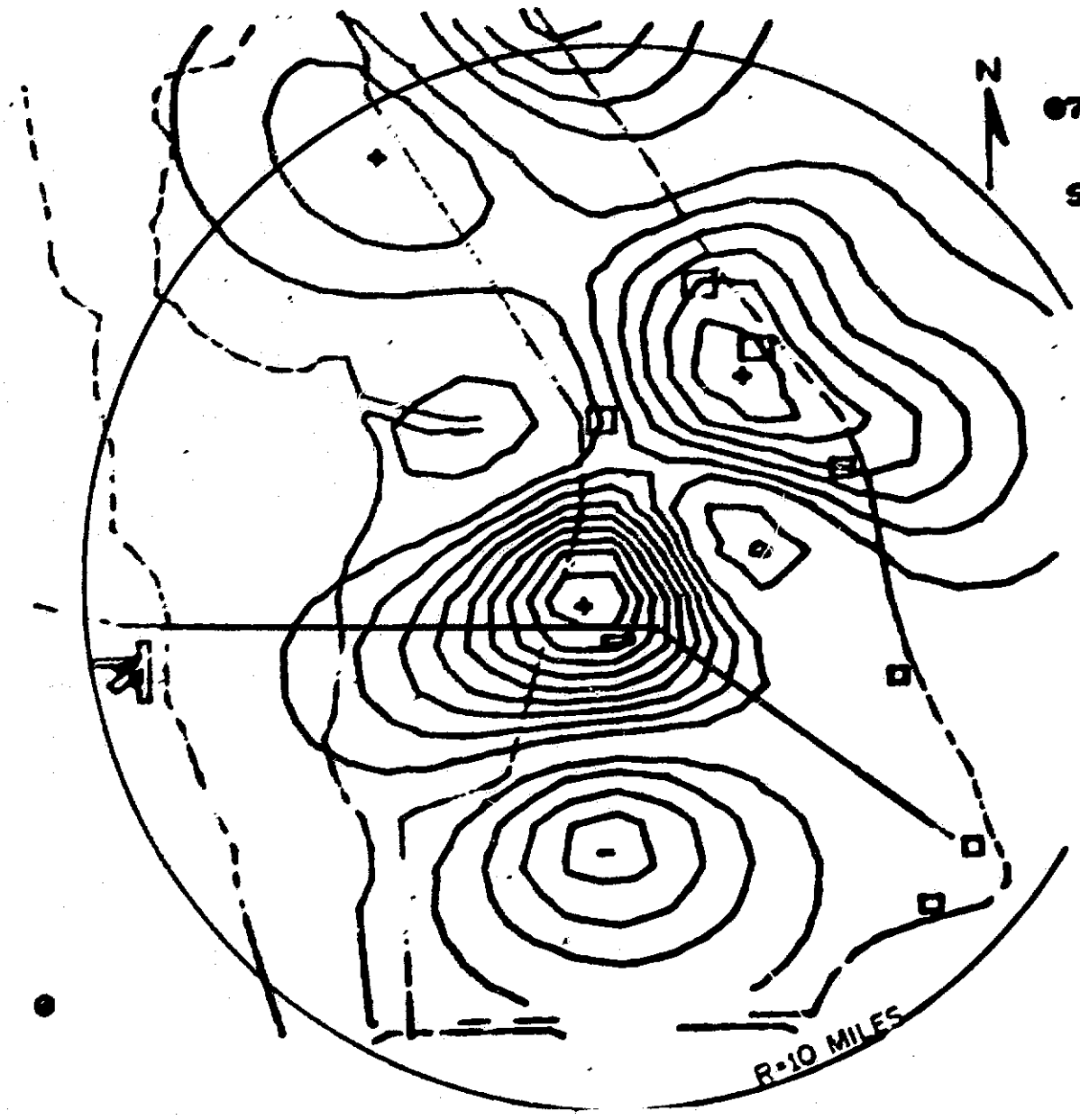

KSC EQUIPOTENTIAL
GRADIENT LINES

07/09/75 GMT 2145:46.747

LINE SCALE = 1000

SITE #	VOLTS/METER
1	-4369
2	2037
3	INVALID DATA
4	INVALID DATA
5	2780
6	1355
7	1526
8	2274
9	5236
10	INVALID DATA
11	17
12	3249
13	4853
14	5426
15	1662
16	5204
17	1321
18	51
19	-876
20	7706
21	3481
22	4368
23	-4239
24	-3283
25	-2207

ORIGINAL PAGE IS
OF POOR QUALITY

FIG. 2A FIELD MILL CONTOUR PLOT

field strength is above a level considered to be safe from impending ground strikes, and also used to track the movement of charged clouds across KSC, as thunderstorms develop.

A second, recently-completed, isocontoured mapping program generates isocontours of step changes in the electric field. These contours are helpful in locating the position of ground strikes. We shall call these contours Dynamic Field Mill Contours, to distinguish them from the more usual Field Mill Contours. They are also know as "Flash Contours", or "Delta Contours", and were developed for use at the Kennedy Space Center by Dr. E. Philip Krider of the Institute of Atmospheric Physics, University of Arizona, Tucson, Airzona.

APPENDIX C

LIGHTNING DETECTION AND RANGING SYSTEM, LDAR

The LDAR System consists of two independent, four-station, hyperbolic time-of-arrival networks of the 120°-Y configuration, as described in "An Accuracy Analysis of the LDAR System"[7]. The central station of the two networks is common, hence we have a total of seven stations.

LDAR detects electrical discharges in the cloud from their pulsed emission in the 30-50 MHz band.

The LDAR System determines position from the differences in the time of arrival of the detected envelope at four stations, having a baseline length of approximately 10 km. In operation the relative times of arrival are recorded, as well as the computed position in space (X, Y, Z) from which the pulse originates. The configuration and its location at the Kennedy Space Center is shown in Figure 3A.

The second, independent network of stations is used to provide a check against false data points. In operation, data is not accepted unless the measurements of the two independent sets of stations agree within 10%. Actually, the agreement is much better than that. Less than 5% for distances out to two times the baseline length, that is out to 20 km. Within the baseline of the system, that is within 10 km, the agreement is more line 2%.

The difference between the two systems has been observed to be a fairly good measurement of the random error of the measurement.

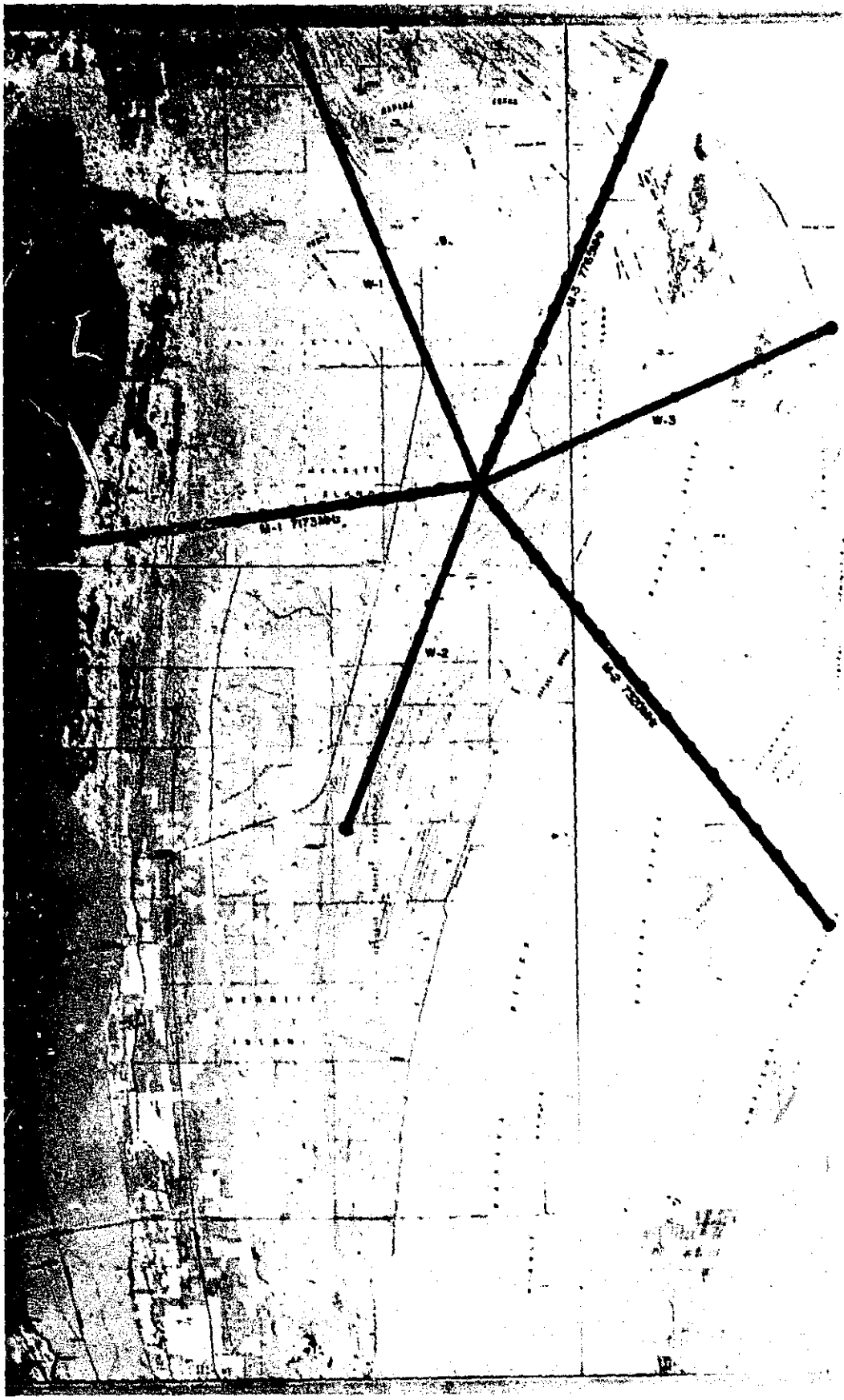

FIG. 3A **LDAR RECEIVER SITES**

APPENDIX D

GROUND STRIKE LOCATION SYSTEM, GSLS

In order to detect ground strikes, use is made of the fact that electromagnetic radiation associated with ground strikes is centerd at a frequency considerably lower than electromagnetic radiation associated with electrical discharges in the clouds. In the Ground Strike Location System, ground strike phenomena is isolated by looking for electromagnetic radiation below 1.5 MHz. Cloud discharge phenomena is isolated by looking in the frequency range 30-50 MHz, as is done in LDAR.

The Ground Strike Location System detects ground strikes by their electromagnetic radiation in the frequency range 0-1.5 MHz, and determines their location by the times-of-arrival at E-field sensors. The use of the time-of-arrival of ground strike radiation at E-field sensors to determine the location of the ground strikes is a new concept that has not previously appeared in the public literature, although the concept has previously been described in an internal Kennedy Space Center Document, "LDAR-III System Description and Performance Objectives"[8].

Credit for the conception, and for the successful implementation of the new system belongs to Carl L. Lennon, Chief Electromagnetic Analysis Section, National Space Aeronautics and Space Administration, Kennedy Space Center.

The Ground Strike Location System consists of seven electric field sensors located within a few meters of the LDAR receiving sites already shown in Figure 3A. The time-of-arrival signals are transmitted along the same wideband cable and microwave links (3 wideband cables and 3 microwave

links) that are used to transmit the LDAR signals.

The electric field sensors consist of a 19.68" diameter, 1 3/16" aluminum disk insulator-mounted within a grounded plate 36X36", as shown in Figure 4A , some 36" off the ground. Before transmission to the central site, the electric field signals are sent through a bi-polar logarithmic amplifier. The use of a logarithmic amplifier is necessary to achieve the required dynamic range.

Figure 5A shows the data flow from the electric field sensor to the central station. Starting at the sensing plate A-1, the output of the sensing plate feeds an unbalanced/balanced matching transformer A-2 of impedance ratio 600/124 ohms having a bandwidth 1 kHz to 20 MHz, the input of which is loaded with a 600 ohm resistor to match impedance, and with a diode to select the proper polarity. Output of the matching transformer feeds a 300 foot 124 ohm balanced cable, which is terminated by a 124/75 ohm balanced/unbalanced, 1 kHz to 20 MHz matching transformer A-3 which in turn passes the signal to a bi-polar logarithmic amplifier A-4. From there the signal passes through a 1.5 MHz low-pass filter A-5 and through a line-driver amplifier A-6 for transmission over the 5 MHz lines to the central station.

Ground strike location can be determined from the time-of-arrival at any four stations. The best GDOP characteristics (minium error over the maximum area) are achieved when the stations are located in a symmetrical 120 degree Y-configuration. However, a 120 degree Y-configuration is only the best method if usable signals are available from the four stations of a 120 degree Y-configuration, that is from Ø-1-3-5 or Ø-2-4-6, where Ø is the central station and 1, 2, 3, 4, 5, 6 are the outlying stations shown in Figure 6A , taken counterclockwise.

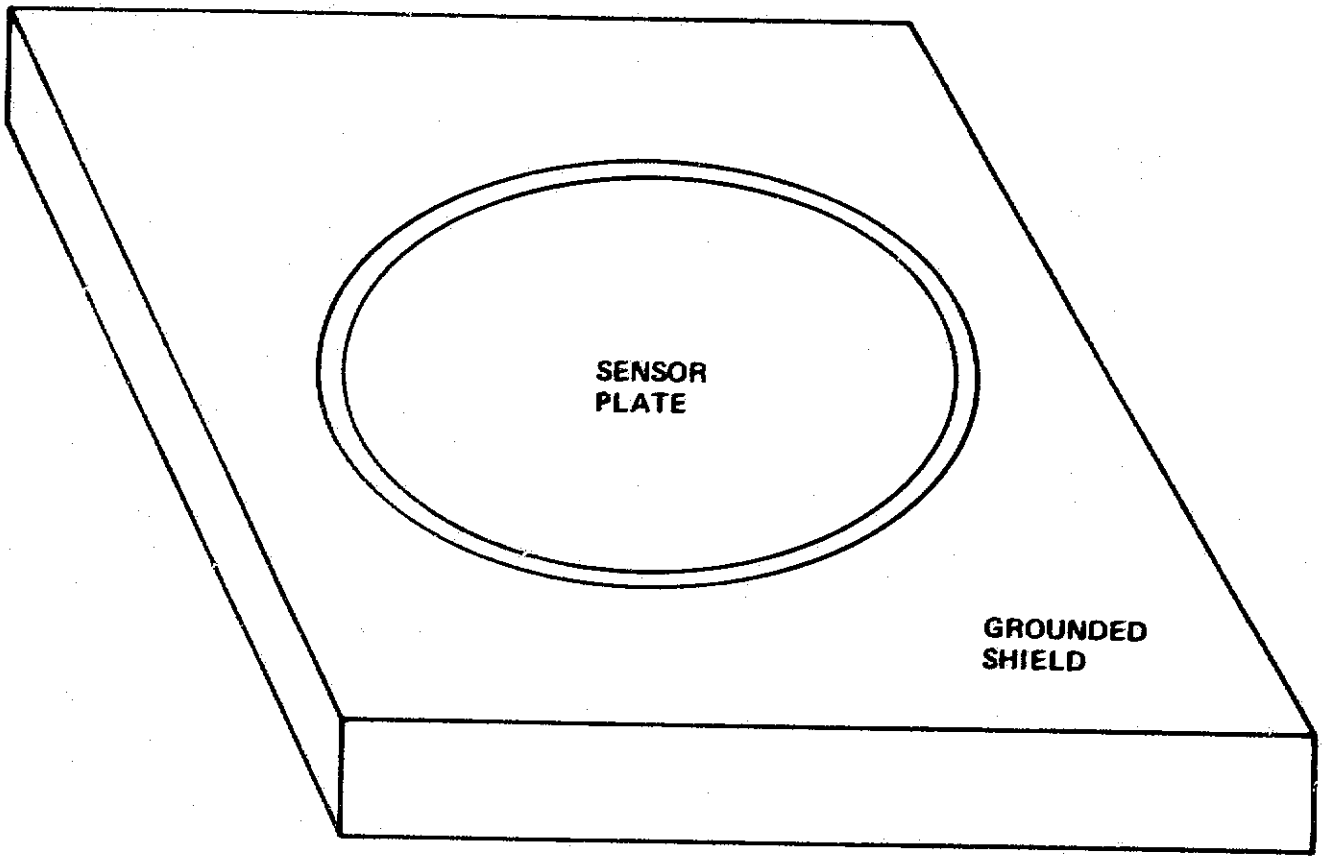

FIGURE 4A. ELECTRIC FIELD SENSOR

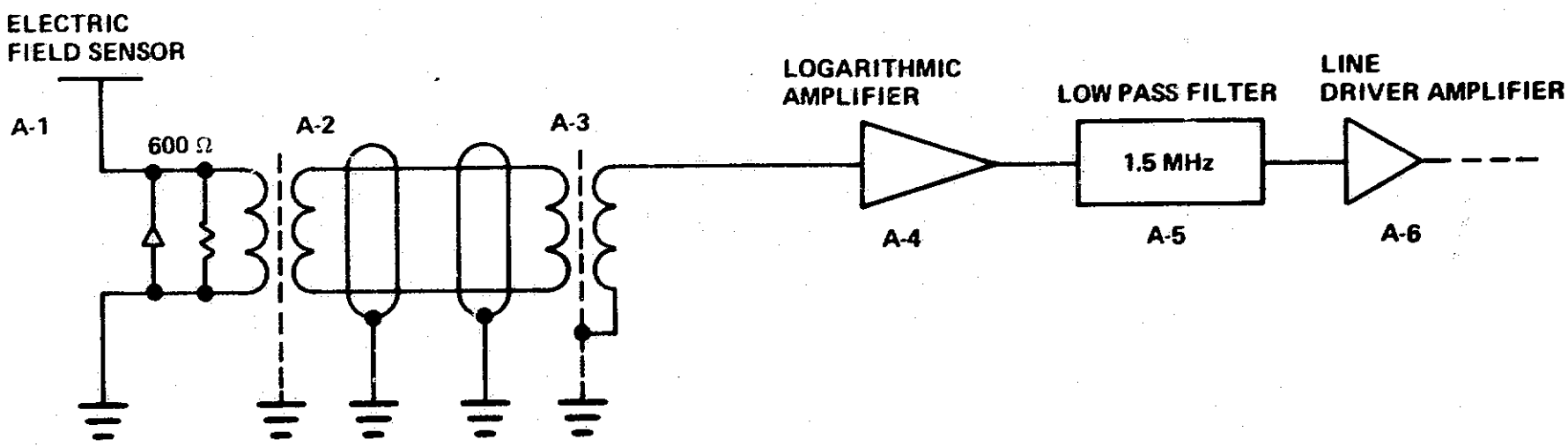

FIGURE 5A. ELECTRIC FIELD SENSOR DATA FLOW

The approach taken in the ground-strike location for the Ground Strike Location System is to use all possible combinations of the six outlying stations, three-at-a-time. Twenty combinations three-at-a-time are possible from six stations. Three of these combinations are shown in Figure 6A.

We use all twenty combinations in the calculation of the ground strike location. Poor signals and/or poor geometry (GDOPS) will lead to poor, or incorrect, solutions for some of these combinations. However, for most combinations the solutions will agree closely, providing the ground strike location that we seek. A typical 20-combination solution is shown in Table IA. Note the close agreement for 13 of the 20 combinations. Since the solutions are all independent, the only way that agreement could be obtained is if all the signals involved originated from the same event. Data from a number of independent configurations not only lends validity to the measurement but its dispersion provides us with a measure of the accuracy of the ground-strike location.

Ground Strike Location System signals are illustrated in Figures 7A and 8A. Here we show the ground-strike signals of four outlying electric field sensors (processed as described earlier) as they appear at the central site on a microsecond scale. All records are synchronous, and were recorded by analogue-to-digital converter units (Biomation) on receipt of a common trigger. The trigger is generated at the central site, when the received electric field signal exceeds a prescribed threshold. Since the analogue-to-digital converters store and discard data in a continuous stream, the records contain data prior to the trigger. The data span is 100 microseconds, the digitization interval is 0.05 microseconds. Hence we have 2000 data points in one 100 microsecond span of data.

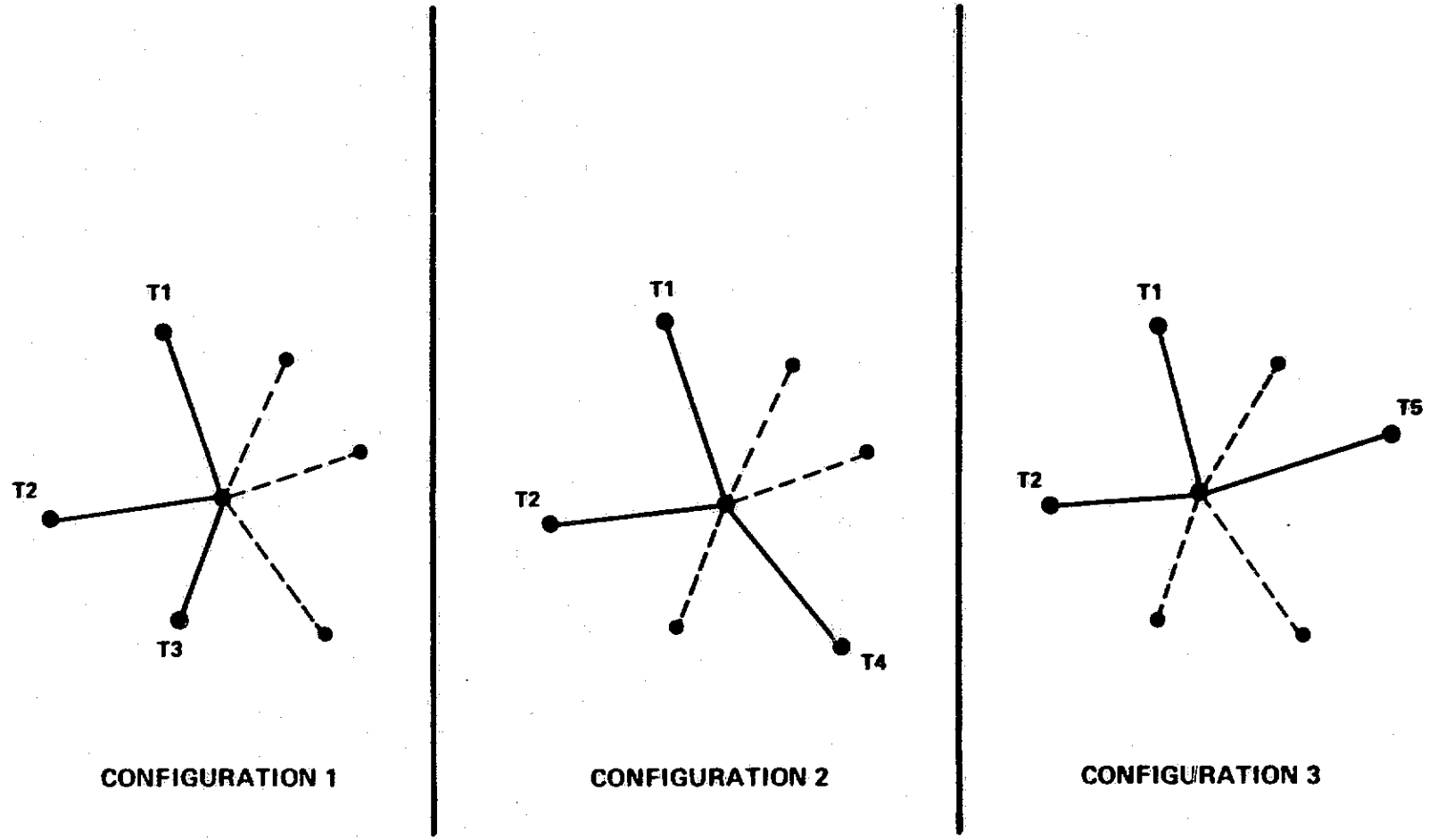

FIGURE 6A. STATION CONFIGURATIONS USED IN GROUND STRIKE LOCATION SYSTEM SOLUTION (THREE OF A POSSIBLE TWENTY)

TABLE 1A TWENTY-CONFIGURATION SOLUTION FOR A GROUND STRIKE AT 2136:15.503 GMT

LDAR COORDINATES		STATIONS USED
X	Y	
Meters	Meters	
8789	-5057	1-2-3
10424	-6040	1-2-4
10713	-6214	1-2-5
11699	-6807	1-2-6
10536	-5488	1-3-4
9926	-5337	1-3-5
10627	-5510	1-3-6
10449	-5919	1-4-5
10550	-5417	1-4-6
16973	-13188	1-5-6
68759	-14612	2-3-4
10139	-5272	2-3-5
9935	-5239	2-3-6
10625	-6070	2-4-5
10917	-6113	2-4-6
10337	-5597	2-5-6
9807	-5373	3-4-5
10592	-5496	3-4-6
10071	-5293	3-5-6
11116	-6487	4-5-6

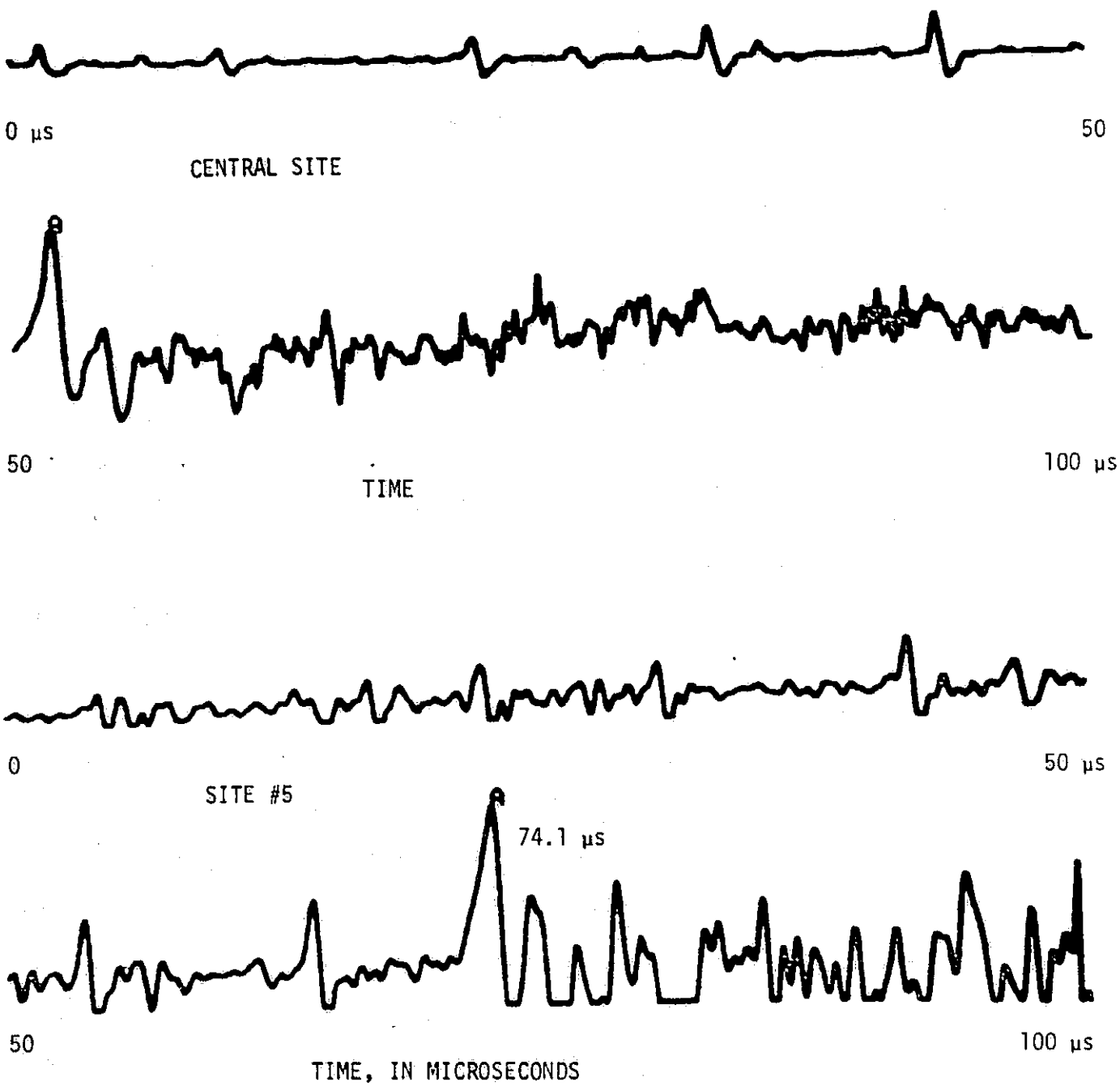

FIG. 7A TYPICAL, GROUND-STRIKE E-FIELD SENSOR SIGNALS
DAY 262, 1977, 1800:07 GMT

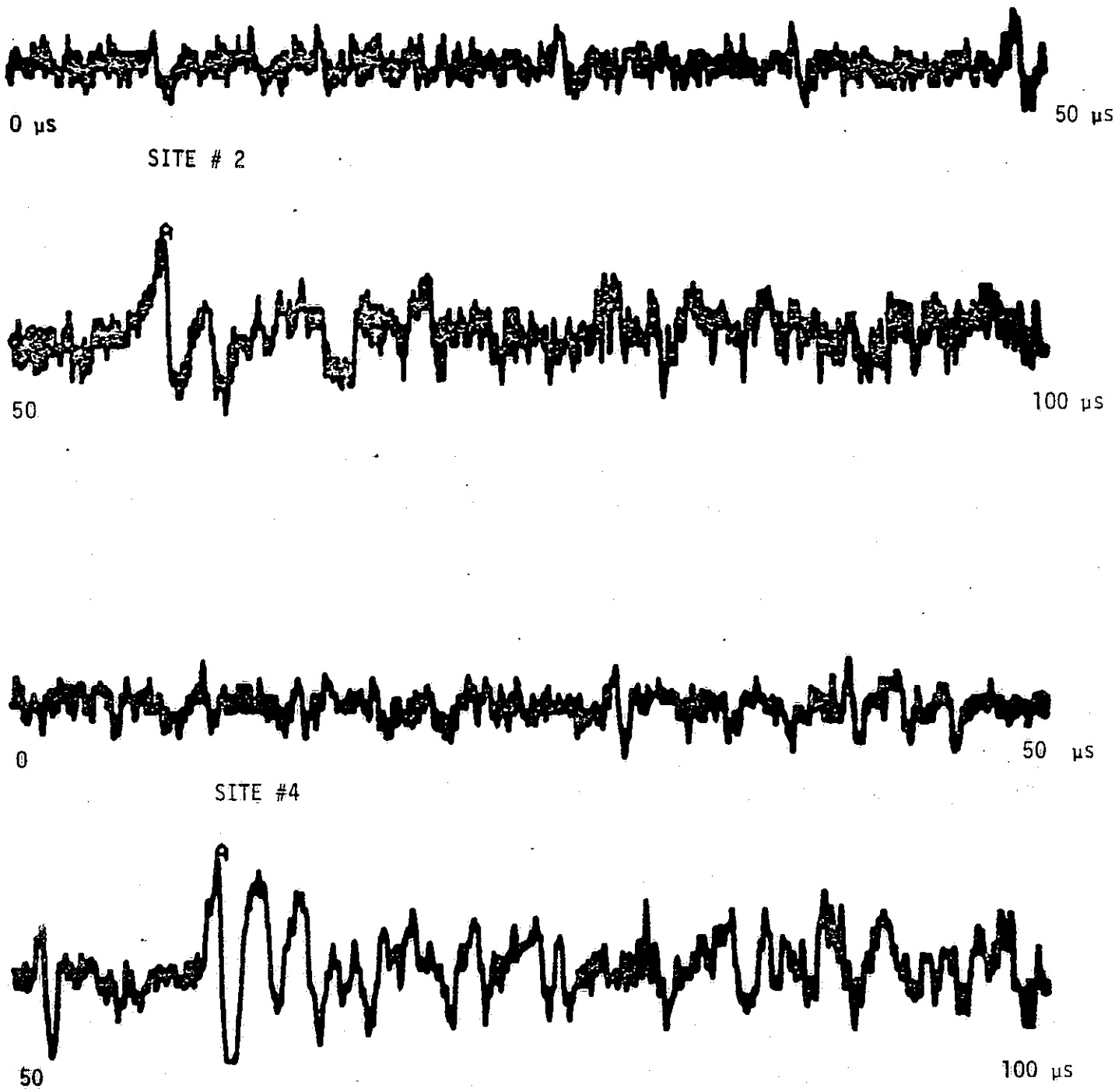

FIG. 8A GROUND-STRIKE, E-FIELD SENSOR SIGNALS

The signals from all the stations present a similar pattern. The peak of interest is generally the largest peak. The pulses that appear prior to the main pulse are spaced at approximately 10 μs, and are attributed to the stepped leader. The incoming data is stored on tape.

Data analysis is conducted post test. The computer permits readout of time delays associated with each peak. Generally the largest peak is used in the analysis. A typical twenty-configuration solution for a ground strike was shown in Table IA . Note the remarkable agreement between the independent solutions.

APPENDIX E

KSC WEATHER RADAR

The weather radar used by the KSC Weather Office is a WSR-72X Meteorological Radar System, manufactured by the Enterprise Electronics Corporation, of Enterprise, Alabama. It operates at 3.2 cm (9375 MHz) with a pulse power of 90 kw, at 0.6 microseconds, and at a repetition frequency of 983 pulses per second. The antenna has a gain of 39 db, with a beamwidth of 1.8 $\pm$ 0.1 degree. A choice of linear (26 db) or logarithmic (80 db) response is provided. The range of the radar is 48 km (29.8 miles).

The weather radar provides constant-elevation and constant-azimuth scans, at about 20 second intervals, with the conventional PPI and RHI displays. The radar display is routinely recorded by a 35 mm motion picture camera. Provisions permit selected Polaroid pictures to be taken when the data warrants. The isocontouring feature provided for in the original design was redesigned at KSC to provide for a more satisfactory performance.